Improved Cryopreservation of Induced Pluripotent Stem Cells Using *N*-aryl Glycosidic Small Molecule Ice Recrystallization Inhibitors

Karishma Chopra

H.BSc. Biopharmaceutical Science

(Medicinal Chemistry)

A thesis submitted in partial fulfillment of the requirements for the
Master's degree in Chemistry

Department of Chemistry and Biomolecular Sciences
Faculty of Science
University of Ottawa

Dedicated to my family

My Mother – Lakshmi Chopra

My Brother – Kaushik Chopra

"Nothing in life is to be feared, it is only to be understood"

- Marie Curie

Acknowledgments

I would like to acknowledge various individuals from University of Ottawa and at the National Research Council of Canada (NRC) for their continuous support and encouragement throughout my master's program. First, I would like to convey my sincere thanks to Dr. Robert Ben, my principle investigator, and Dr. Anna Jezierski from NRC, for being my mentors throughout my research. I am very grateful for all the experiences and opportunities which have cherished my love and passion for biochemistry research.

I would like to acknowledge all the Ben lab members – Salma, Anna, Jatinder, Leah, Maddy, Marcus, Julia, and Thomas, for their group discussions and support in group meetings, seminar presentations, and graduate classes. I owe a big thanks to Salma Alasmar for her efforts with editing my thesis and being the best lab-partner ever! We have shared many sweet memories from travelling to NRC together and TA-ing for the same undergraduate classes.

Additionally, I would like to thank Junzhuo Huang (Jez), for always lending a helpful hand at NRC facility and training me with all my acquired biochemistry and molecular biology techniques such as cell culture techniques, working in a CL2 lab facility, setting up flow cytometry experiments, analyzing and generating statistical data. I would also like to extend my thank you to Ewa Baumann for guiding me in the techniques and protocols unique to the facility. Ewa was always very patient and helpful with changing the media for cell culture plates when I was occupied with experiments at uOttawa campus.

Anna Jezierski's team at the NRC was very supportive and encouraging with all new techniques such as iPSC culture and maintenance, cryopreservation (Jez and Ewa) as well as training on Flow Cytometry and IncuCyte analysis (Jez). Thank you, Caroline, for the immunostaining of the pluripotency markers. Thank you for all the great lunch time gatherings and for exciting discussions at group meetings – Jez, Ewa, Caroline, Marina, Betty, Claudie, Yonghong and Will.

I would like to acknowledge the following members for performing the “gold standard” in vivo teratoma assay and the immunohistochemistry analysis – Scott McMomb, Risini Weeratna, Jagdeep Sandhu, Junzhuo Huang, Melissa Hewitt and Junzhuo Huang (Jez).

Thank you to Scott McComb for always answering questions about the IncuCyte live cell imaging system and FACs studies. Thank you, kindly Scott, for all your help in troubleshooting minor problems with the IncuCyte software and for all your support during the research. I would also like to sincerely thank Ahmed Zafar and Rob Pon for giving me access to using their flow cytometry equipment.

Lastly, I would like to thank my family members for their love and support throughout my undergraduate and graduate studies.

Contributions to thesis

- Immunohistochemical Staining was performed by Caroline Sodja
- The teratoma assay experiment was performed by Junzhuo Huang, Ewa Baumann, Risini Weeratna, Scott McComb, Shawn Makinen, Melissa Hewitt, and Jagdeep Sandhu from the NRC.
- Data Acquisition of Statistical analysis from IncuCyte Cell Imaging System by Junzhuo Huang.

Abstract

Induced pluripotent stem cells (iPSCs) are an attractive cell source for various applications in regenerative medicine and cell-based therapies given their unique capability to differentiate into any cell type of the human body. However, human iPSCs are highly vulnerable to cryopreservation with post-thaw survival rates of 40-60%; this is due to cryoinjury resulting from ice recrystallization when using conventional slow cooling protocols.

Ice recrystallization is a process where the growth of large ice crystals occurs at the expense of small ice crystals. Ice recrystallization inhibitors (IRIs) are designed to inhibit the growth of intracellular ice crystals, increasing post-thaw viability. In this study, we tested a panel of four IRIs to determine if the inhibition of ice recrystallization can decrease cellular damage during freezing and improve viability post-thaw of iPSC colonies. We supplemented commercially available and serum-free cryopreservation medium mFreSR, routinely used for the cryopreservation of iPSCs, with a class of *N*-aryl-D-ß-gluconamide IRIs. A 2-fold increase in post-thaw viability was observed, in a dose dependent response, for *N*-(4-methoxyphenyl)-D-gluconamide (PMA) at 15 mM, *N*-(2-fluorophenyl)-D-gluconamide (2FA) at 10 mM, and *N*-(4-chlorophenyl)-D-gluconamide (4ClA) at 0.5 mM over mFreSR controls. After testing the panel of four IRIs, 2FA frozen iPSCs showed an increase in cell viability, proliferation, and recovery. The addition of ROCK inhibitor (RI), commonly used to increase iPSC viability post thaw, further enhanced the survival of the iPSCs frozen in the presence of 2FA and is used routinely in research. This additive effect increased cell recovery and colony formation post thaw, resulting in increased proliferation with no adverse effects on iPSC pluripotency or differentiation capabilities.

The development of improved cryopreservation strategies for iPSCs is key to establishing master clonal cell banks and limiting cell selection pressures, all while maintaining high post-thaw viability and function. This will help ensure sufficient supplies of high-quality iPSC required to meet the cell demands for cell and regenerative based therapies. Since iPSCs hold promise as a potentially unlimited cell source

for a plethora of cell-based therapies, improving cryopreservation is essential to the successful deployment of iPSC-derived therapeutic cell products in the future.

Table of Contents

List of Figures

Chapter 1

Chapter 3

List of Schemes

List of Reactions

Chapter 2

List of Tables

List of Abbreviations

% MGS	Mean grain size
2,6-DFB	*N*-(2,6-diflurobenzyl)-D-gluconamide
2FA	*N*-(2-fluorophenyl)-D-gluconamide
4ClA	*N*-(4-chlorophenyl)-D-gluconamide
AF-iPSCs	Amniotic fluid derived cells
AFGPs	Antifreeze glycoproteins
AFPs	Antifreeze proteins
br	Broad
CPAs	Cryoprotective agents
CS10	Cryostore 10
d	Doublet
DMSO	Dimethyl sulfoxide
ESCs	Embryonic stem cells
ESI	Electrospray ionization
FACs	Fluorescence activated cell sorting
FBS	Fetal Bovine Serum
FITC	Fluorescein isothiocyanate
HAFs	Human amniotic fluid cells
HBMEC	Human brain microvascular endothelial cells
$HEPG_2$	Human liver cancer cell line
HES	Hydroxyethyl Starch
hiPSCs	Human induced pluripotent stem cells
HSCs	Hematopoietic stem cells
HSPCs	Hematopoietic stem and progenitor stem cells
I_h	Hexagonal ice

IIF	Intercellular ice formation
iPSCs	Induce Pluripotent Stem cells
IRI	Ice recrystallization inhibitor
K_{norm}	Normalized rate constant
LRMS	Low resolution mass spectrometry
m	Multiplet
MSCs	Mesenchymal stem cells
Myc	C-Myc oncoprotein
PBS	Phosphate-buffered solution
PEG	Polyethylene glycol
PI	Propidium Iodide
PMA	*N*-(4-methoxyphenyl)-D-gluconamide
ppm	Parts per million
PVP	Polyvinyl pyrrolidone
q	Quartet;
QLL	Quasi-liquid layer
quint	Quintet
RBCs	Red blood cells
RI	Rock inhibitor
s	Singlet
SD	Standard deviation
SEM	Standard error of the mean
t	Triplet
TLC	Thin layer chromatography
UCB	Umbilical cord blood

Chapter 1: Cryopreservation and its limitations

1.1. Promise of cell therapies

Stem cell studies are increasing in demand exponentially due to their many uses, which include the following: use of disease modeling, regenerative medicine applications, the assessment of safety, and efficacy of new drugs. Stem cells are unspecialized cells that differentiate to become specialized cells and tissues. Understanding this process of differentiation is key to developing treatments for diseases.

Human-induced pluripotent stem cells (iPSCs) are utilized for disease modeling and regenerative medicine applications. Some of these applications include neurodegenerative and psychiatric disorders [1]. Furthermore, patients diagnosed with type 1 diabetes, heart disease, stroke, cancer, Parkinson's disease, Alzheimer's disease, amyotrophic lateral sclerosis, and osteoarthritis can benefit from stem cell therapies [2]. Stem cell products are injected or transplanted into patients to treat diseases [3]. The injection of stem cells produces a therapeutic effect in patients by promoting the release of cytokines, growth factors, or chemokines, all of which are targeted to activate self-healing mechanisms [3–5]. Also, transplanting iPSCs at the site of damage in the body targets the regeneration of damaged tissues. For example, a recent study by Ducan *et al*. discusses the effect of reversing the impairment of spatial memory by transplanting iPSC-derived cholinergic neuronal precursors into the intra-hippocampus of Alzheimer's disease mouse models [6, 7]. In addition, stem cell derived products, such as blood cells, brain cells, heart muscle cells, or bone cells, offer a great promise. For example, iPSCs have been shown to repair neurodegeneration from Alzheimer's disease by producing new neurons through the release of growth factors.

As the demand for new cellular therapies continues to increase, the need for a method to effectively store these cells and other cellular therapy products is essential. Long-term cryopreservation of stem cells has been previously carried out by storing cell products by slow-cooling to sub-zero temperatures. Cryopreservation has been essential to developing master stem cell banks as it allows access to cells or tissues for research and therapy purposes. Nonetheless, the cryopreservation of those cells and cell products remains suboptimal due to low yield in cell viability post-thaw.

1.2. Cryopreservation

To preserve biological specimens either for short-term or long-term storage, hypothermic storage, or cryopreservation can be utilized.

Hypothermic storage is beneficial for short term storage (days or weeks) of cellular products such as patient biopsies for shipment. Hypothermic storage preserves the cells and tissues at temperatures ranging between 4 ºC and 10 ºC. Similar to other methods, storing cells and tissues in hypothermic conditions lower the biological activity [8–10]. It is ideal to use short term storage materials as soon as possible due to the risk of bacterial growth and contamination [11, 12]. Overall, hypothermic storage limits the storage time-period and decreases the viability and functionality of the cells. Hence, to overcome the limiting shelf-life, cells and tissues can be stored in a frozen state.

Cryopreservation is beneficial for long-term storage where biological samples are preserved at sub-zero temperature conditions between -80 ºC and -196 ºC. At these temperature conditions, the biological activity is halted, and the risk of bacterial contamination is mitigated, allowing for samples to be stored for a more extended period (weeks, months, or years). When cells are cooled to -5 ºC, the cells extracellular and intracellular compartments remain supercooled [13–15]. As the temperature decreases to -10 ºC, ice will spontaneously nucleate in the extracellular environment. The nucleation of ice extracellularly increases osmolality and triggers osmotic stress. The osmotic gradient drives the water from cells outwards facilitating dehydration. Ice nucleation leads to uncontrolled ice growth and that negatively impacts post-thaw viability and functionality [16]. For example, the cells can experience cold-induced apoptosis, cell toxicity, cell death, or cell-

membrane instability. Therefore, the cooling-rate dependent fate of intracellular water from extracellular ice formation is illustrated in Figure 1.1 [17].

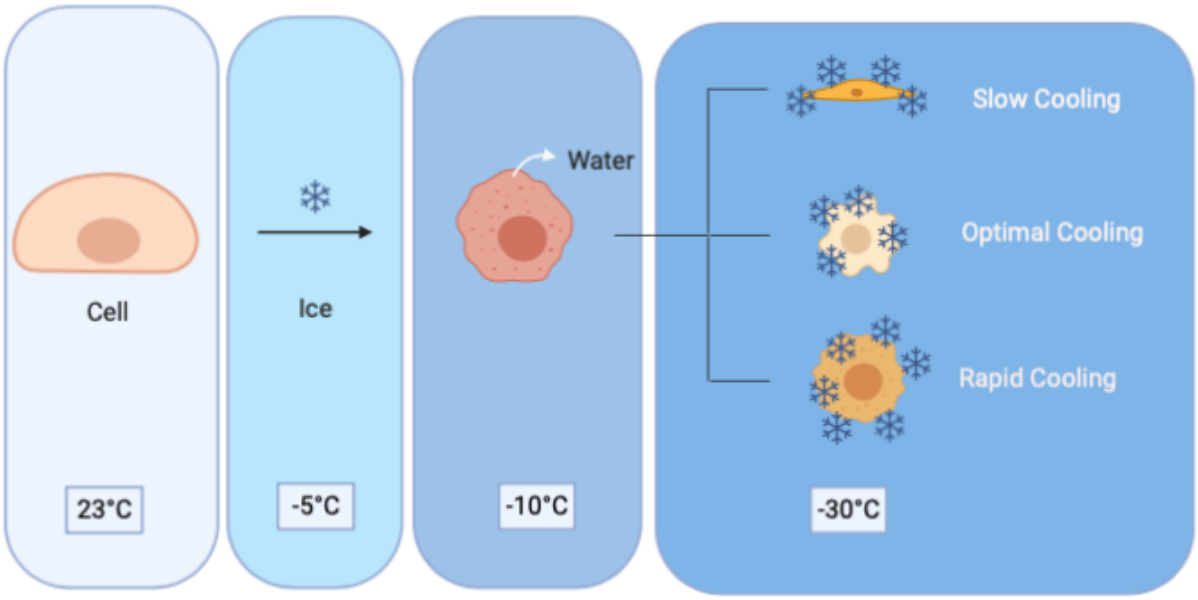

Figure 1.1. The illustration of the cooling-rate dependent fate of intracellular water from extracellular ice formation. As the temperature of the cells approaches freezing point, ice is formed in the extracellular medium. During slow cooling (4th panel, upper cell), dehydration occurs and increases the concentration of solutes inside the cell, leading to lethal solute effects. In rapid cooling conditions (4th panel, lower cell), the cells' extracellular environment spontaneously freezes and results in lethal intracellular ice formation. During optimal cooling (4th panel, middle cell), the cell experiences minimal intracellular ice formation and decreased solute effects depending upon the characteristics of each cell type. Figure adapted from Mazur, 1977 [17] with publication licensing and, created using free-license from BioRender.com.

During slow cooling, water supercools as the temperature decreases, and the formation of ice occurs (Figure 1.1). As ice grows, solutes are concentrated in the diminishing volume. The water extracellularly changes state to form ice, and the solutes are excluded causing an influx of solute concentration [18–20]. This increase in solute concentration can lead to cellular injury. The osmotic gradient acts as the driving force to efflux water to the extracellular medium (Figure 1.1). The efflux of water into the extracellular space (process of dehydration) is an essential mechanism for cells to reduce the chance of lethal intracellular ice formation (IIF) [21].

During rapid cooling, as the temperature decreases rapidly, the extracellular component freezes spontaneously, and intracellular components are immediately supercooled. The intracellular component freezes, and intracellular ice formation occurs, resulting in lethal intracellular ice formation (IIF) [22]. IIF has been suggested to occur through a number of different mechanisms; however, it is a propagation event where ice travels across the external cell membrane thereby rupturing the cell[23].

Mechanical damage also occurs when the recrystallization of intracellular ice occurs during thawing. However, intracellular ice can be devastating to the cells depending on the amount and location of the ice formation [24–29]. Cryoinjury during the thawing process occurs due to ice recrystallization. If the rate of thawing is too slow, the intracellular and extracellular ice crystals will increase in size dramatically through the process of ice recrystallization and cause the cell membrane to rupture. As a result, cells are thawed using rapid warming rates to minimize the effect of ice recrystallization [30]. It is not possible to eliminate the process of ice recrystallization, and cryoinjury arising from ice recrystallization has been reported to reduce post-thaw viability in different cell types [26, 29, 31, 32].

In contrast, rapid cooling rates trap the water inside the cell and promote lethal intracellular ice formation [33]. Thus, if fast cooling rates are utilized, it must be accompanied by dehydration mechanisms to the cell to mitigate cell death [34].

The combination of dehydration accompanied by increased concentration of solutes intracellularly is also deadly to cells [35]. This is known as the "solute effect" [14, 36–38]. These solute effects are documented to cause irreversible damage to the cell membrane [15, 35].

When the cell survival of different cell types was plotted as a function of cooling rate, a downward U-shaped curve was generated (Figure 1.2) [39]. The highest point of these curves represents the optimal cooling rate of each cell type, as illustrated in Figure 1.2. Each cell type holds different characteristics of cell permeability; hence, a precise cooling rate cannot be predicted and Mazur *et al.* have reported that different cell types have different optimal cooling rates [39].

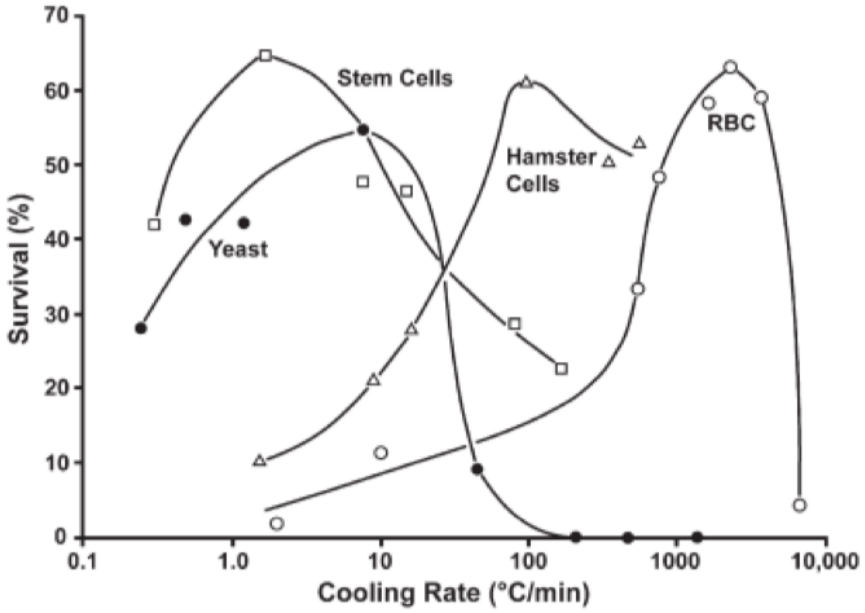

Figure 1.2. The percentage of cell survival as a function of cooling rate (ºC/min) is illustrated among the four cell types [35]. Depending on the increased water permeability of each cell, faster cooling rates can be applied without the result of cell death from intracellular ice formation. The exact optimal rate for each cell is also dependent on other factors such as warming rates and the use of cryoprotectants. The highest point on each curve is determined to be the sub-optimal cooling rate for each cell. This image has been derived from Mullen [35] with publishing licensing, and was originally adapted from Mazur [39]

Cryoprotectants help to mitigate cellular damage but do not prevent the damaging from occurring. There are two classes of cryoprotectants that are commonly utilized to reduce the formation of ice, penetrating and non-penetrating cryoprotectants. Penetrating cryoprotectants, penetrate through the cell membrane and reduce the concentration of the solute while maintaining larger cell volumes [40]. On the other hand, non-penetrating cryoprotectants are found to increase the osmolality of the extracellular medium and to facilitate dehydration. For example, DMSO mitigates damaging effects by facilitating the movement of water during the cellular dehydration.

Cryoprotectants result in increased cell survival during freezing. Without these compounds, studies have shown a decreased cell viability post-thaw [41–44]. For example,

cryoprotectants based upon sugars, alcohols, amides, diols, or polymers, have different mechanisms of action to increase cell survival during freezing [41, 45]. For example, many organisms living in climates where freezing temperatures are prominent have evolved to include the metabolic production of cryoprotectants as a strategy for survival [46, 47]. Therefore, many researchers have been extensively studying the metabolic production of different cryoprotectants in various animals at freezing temperatures [48, 49].

Under rapid-cooling conditions, non-penetrating cryoprotective agents (CPAs) are used to increase the osmolality and accelerate the dehydration of the cell [50–52]. A few examples from this class include the following: polyethylene glycol (PEG), hydroxyethyl starch (HES), and polyvinyl pyrrolidone (PVP), trehalose, sucrose, and dextran. The type of cryoprotectant to be utilized is dependent on the property of the cryoprotectant. For example, long-chain polymer-based cryoprotectants are not able to diffuse through the membrane and hence facilitate dehydration of the cell to avoid IIF. Non-penetrating CPA can decrease the formation of ice intracellularly, and increase the percent recovery of the cells [53].

Cell injury during cryopreservation is not limited to cryoinjury events. Cell exposure to a high concentration of cryoprotectant solutions before cooling can also be damaging due to toxic effects. Chemical toxicity is a significant concern when associated with a high concentration of cryoprotectants [43, 54]. The high concentrations of cryoprotectant particularly applies to the method of vitrification. In short, during vitrification, high concentrations of the cryoprotectants are required to achieve a vitreous state. The nature of chemical toxicity remains uncertain to a large degree and it is argued to be a result of cell death by cryopreservation. Overall, decreasing the amount of cryoprotectant toxicity is one of the critical steps to improve the cryopreservation of cellular products.

Most of the cell injury during cryopreservation occurs from the uncontrolled growth of ice (ice recrystallization). However, the CPA fails to control ice growth and ice recrystallization. Therefore, to minimize the ice recrystallization effects, the cells must be thawed using rapid thawing rates [30]. Since it is impossible to eliminate ice recrystallization even with the use of fast thawing conditions, cryoinjuries have been correlated to decrease the post-thaw viability [26, 29, 32, 51]. Current approaches have utilized ice recrystallization inhibitors to effectively cryopreserve hematopoietic stem and progenitor stem cells (HPSCs), mesenchymal stem cells (MSCs), and red blood cells (RBCs), with the addition of CPAs [55, 56].

1.3. Developing new cryoprotective agents

Ice recrystallization is a prosses by which ice crystals increase in size at the expense of smaller ice crystals, and these large crystals increase the effect of cell damage. As the temperature approaches below 0 ºC, ice will form. The growth of small ice crystals to large ones result in the reduction of free energy of the system [57]. The process of ice recrystallization occurs through the grain boundary migration [58, 59] or Ostwald ripening [60].

Grain boundary migration and Ostwald ripening study the growth of larger ice grains or crystals at a molecular level. For instance, in grain boundary migration, the focus is at the curvature of the large grains, as seen in figure 1.3. Grain boundary migration theory refers to ice crystals as ice grains.

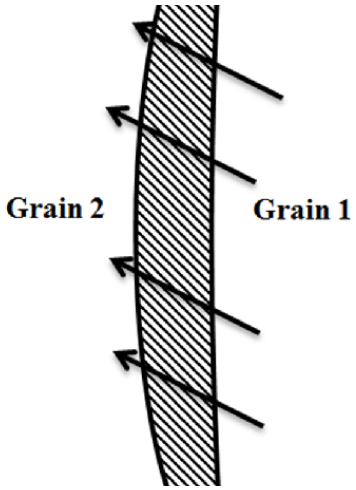

Figure 1.3. The process of grain boundary migration displayed between a liquid layer (shaded region) and two ice grains (grain 2 and grain 1- left to right). Large grains create concave boundaries (grain 2), while small grains contain convex boundaries (grain 1). Smaller grains decrease in size to reduce the overall degree of grain boundary curvature. Boundary migration is indicated by the direction of the arrow (small grain -grain 2 to large grain – grain 1) [61].

An ice crystal is shaped in a hexagonal arrangement (1_h) through the interactions of the water molecules. The location of the water molecules at the edge of the ice grain influences the orientation of the ice structure. Therefore, the grain boundary is defined as the difference between variety of oriented ice grains [58, 59]. Grain boundary migration occurs as the individual molecular transfers from a state of unfavorable ice orientation (convex shape) to a favorable ice orientation (concave shape). The boundaries of the ice grains are curved, and the degree of curvature results in the grain to be convex and thus increase in surface energy. Grain boundary migration functions to decrease the overall degree of curvature by moving towards the center of curvature. This migration results in ice grains with concave boundaries (larger grain) to grow larger and convex boundaries (smaller grains) to decrease in size, reducing the overall surface area [60]. Since smaller ice grains are of higher energy than the water molecules, these are found to be thermodynamically less stable. The enthalpic force drives the water molecules to migrate towards the large ice crystals from smaller ones, as shown by the arrows in Figure 1.3.

The Ostwald ripening theory of ice recrystallization implements the whole system of ice crystals and liquid water in the presence of a quasi-liquid layer (QLL) [57]. It is key to understand that in Ostwald ripening, the total volume of ice remains constant as the average ice crystals size increases [62]. Ostwald ripening is a process whereby large ice crystals are formed at the expense of smaller crystals leading to an overall decrease in energy and surface area of the ice crystal interface. In this mechanism, the presence of bulk-water is introduced. It is hypothesized that in ice, there are three layers, as seen in Figure 1.4 – ordered (ice crystals), semi-ordered (quasi-liquid layer), and non-ordered/randomized (bulk water).

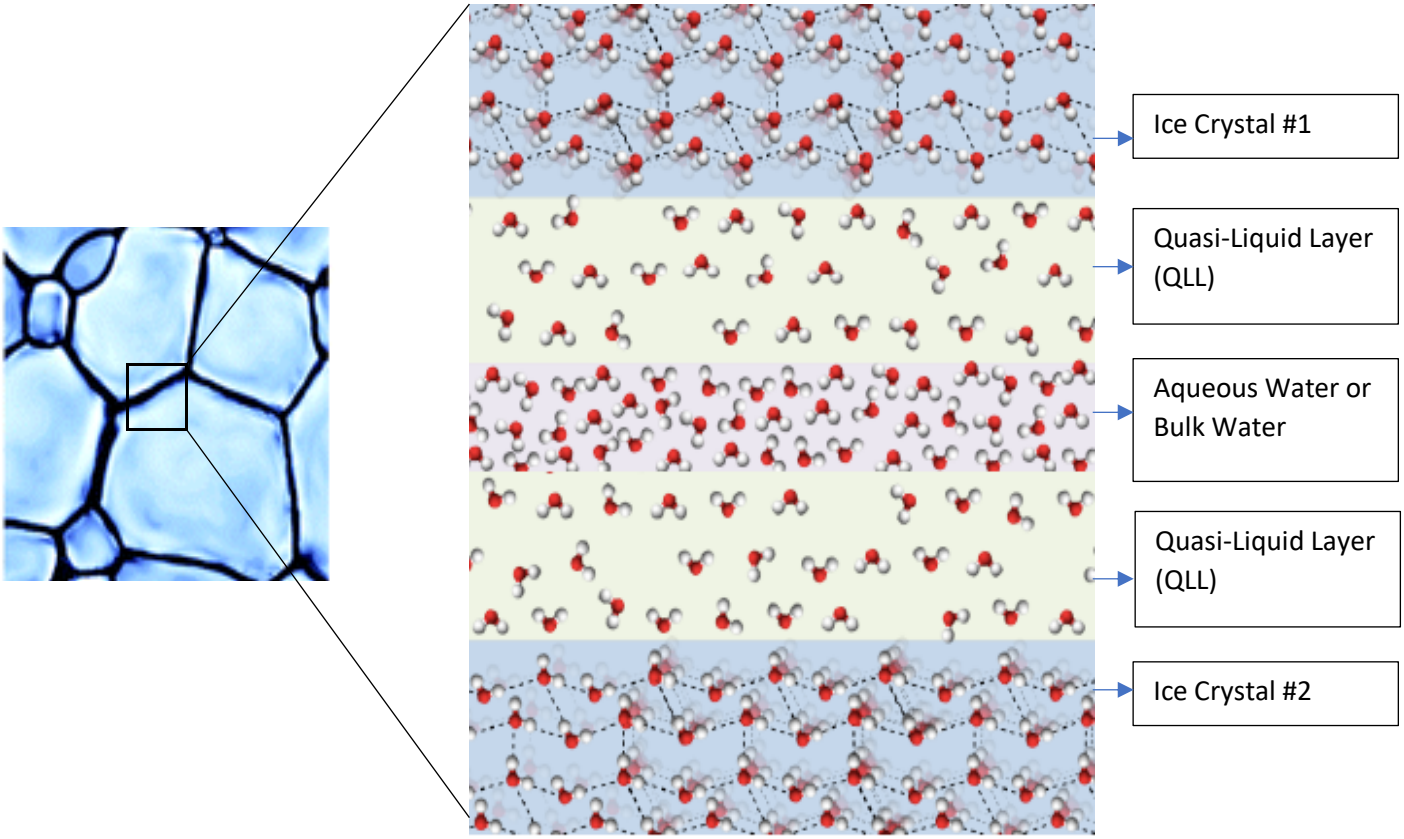

Figure 1.4. The schematic illustration of the quasi-liquid layer (QLL) present at the interface of two ice crystals [63]. Ice recrystallization phenomenon illustrated in the theory of Ostwald ripening, where large ice crystals are formed at the expense of smaller ice crystals. The net volume remains constant as the average crystal size increases. Ice crystals are seen to be present in an ordered crystallographic configuration (ice crystals #1 & #2). The QLL represents a semi-ordered configuration. The aqueous water or bulk water layer illustrates the non-ordered state. As the layers progress from an ordered to randomized state, the surface area to volume ratio decreases.

A greater number of smaller ice crystals result in a higher surface area to volume ratio, resulting in more elevated surface free energy since the water molecules (bulk water) near the surface are less stable than water molecules in ice [57, 64]. Conversely, a greater number of larger ice crystals have a smaller surface area to volume ratio and are more thermodynamically stable than smaller ice crystals. The water molecules move from small crystals to the bulk water to the larger crystals, as shown in figure 1.4. The net result is an increase in the size of the ice crystal and a decrease in the total number of ice crystals present at a constant total amount of ice. This process yields an overall reduction of the free energy of the system [62].

Overall, the effects of ice recrystallization are devastating to biological samples as the ice progresses to destruct the internal components of the cell, thus limiting its activity. Hence, a theory of Ostwald ripening states that ice recrystallization inhibitor (IRIs) prevent the process of ice recrystallization by residing as a solute at the QLL-bulk water interface (Figure 1.5) [65]. A disruption to the order of the water molecule configuration in the semi-ordered layer makes the transfer of the water molecules less favorable from the ordered ice crystals. The solutes' presence at the interface, therefore, results in smaller ice crystals, inhibiting the process of ice recrystallization.

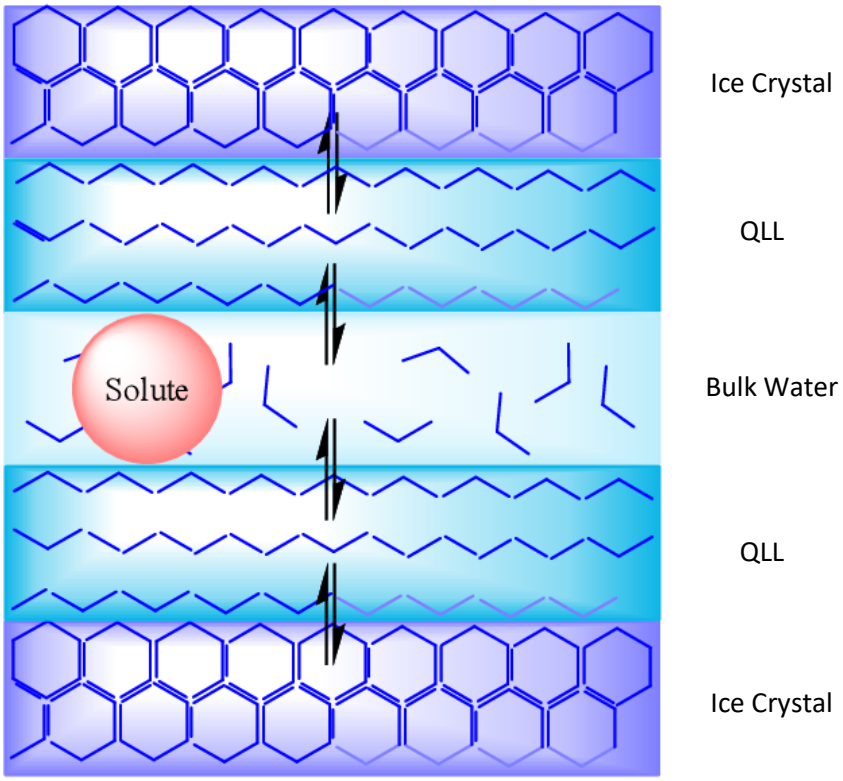

Figure 1.5. The illustration of the proposed mechanism by which the ice recrystallization inhibitor compounds inhibit ice recrystallization. The presence of the solute at the QLL-bulk water interface between the two ice crystals disrupts the semi-ordered layer, limiting the transfer of the water molecules to the ordered ice crystal layer. The illustration was obtained from Balcerzak et al., [65].

1.4. Ice recrystallization inhibitors and their development

One of the first compounds to be discovered is the antifreeze proteins (AFPs) and antifreeze glycoproteins (AFGPs). AFPs and AFGP compounds do not function as ideal cryoprotectants due to their ability to bind to ice and change the properties of the ice crystals [66]. Consequently, analogues of AFGPs were designed to "custom tailor" the antifreeze activity. Although these compounds were found to exhibit ice recrystallization inhibition (IRI) activity, the analogs did not bind to ice. Subsequently, mono- and disaccharides were designed, and these compounds also displayed IRI activity. This led to the discovery of many other small carbohydrate-based ice recrystallization inhibitors, which had a great potential to function as cryoprotectant additives.

1.4.1. Small carbohydrate-based ice recrystallization inhibitor applications

The large-scale chemical synthesis of AFGP analogs is challenging since large quantities are required for cell applications. Thus, current research efforts have focused on the design of small molecules that can inhibit ice recrystallization, one class of these small molecules are the *N*-aryl-D-aldonamides (Figure 1.6).

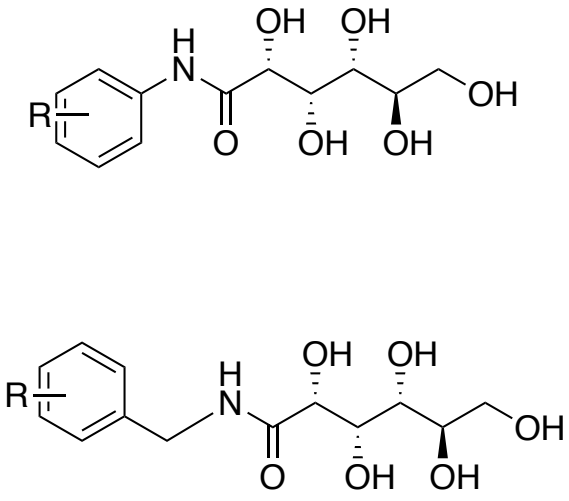

Figure 1.6. General structure of *N*-aryl-D-aldonamides.

These compounds have been found to improve the post-thaw functionality of hematopoietic stem and progenitor cells (HSPCs) [67]. In this study, four compounds from the class of *N*-aryl-D-aldonamides were assessed for their ability to enhance the post-thaw functionality of induced pluripotent stem cells (iPSCs). These compounds were previously found to be non-toxic and increased the potency of HSPCs in umbilical cord blood [67]. Each compound was assessed for its ability to inhibit ice recrystallization using a splat cooling assay. The compounds were dissolved in a phosphate-buffered saline (PBS) solution and evaluated at 11 mM concentration. The four compounds were characterized for their ability to inhibit ice recrystallization, identified by their respective IC_{50} values indicated on figure 1.7 ranging from 4 mM – 12 mM. These compounds are identified as potent inhibitors of ice recrystallization.

1.5. Goals and objectives of the thesis

Many researchers and clinicians face cell preservation challenges, even with the use of CPAs such as DMSO and glycerol. However, conventional CPAs on their own are not able to inhibit the growth of ice crystals during freezing/thawing processes. Hence, the development of a novel class of IRIs has been designed for their assessment in iPSCs by our lab. Four IRI compounds are of particular interest from the class of *N*-aryl-D-aldonamides, these include*;* *N*-(4-chlorophenyl)-D-gluconamide (4ClA); *N*-(2-fluorophenyl)-D-gluconamide (2FA); *N*-(4-methoxyphenyl)-D-gluconamide (PMA), and *N*-(2,6-difluorobenzyl)-D-gluconamide (2,6-DFB) (Figure 1.7).

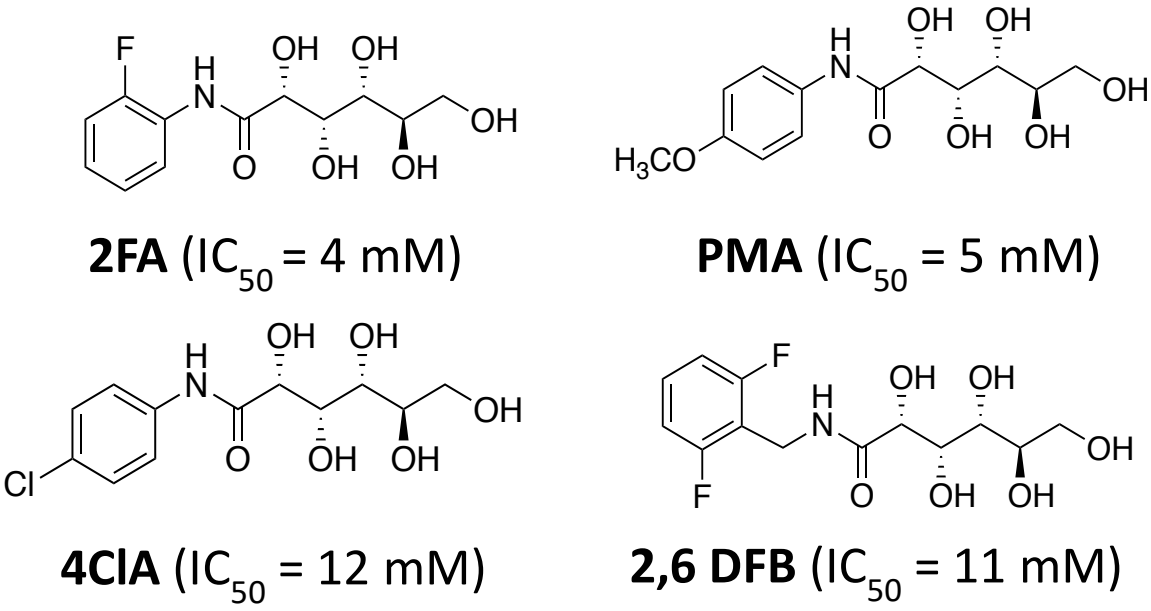

Figure 1.7. Ice recrystallization inhibitors from the class of *N*-aryl-D-aldonomides used in supplementing cryopreservation solutions to enhance post-thaw functionality of induced pluripotent stem cells (iPSCs).

The goal of this thesis is to increase the post-thaw viability and functionality of iPSCs. IRIs have been assessed previously in hematopoietic and progenitor stem cells (HPSCs), human liver cancer cell lines ($HEPG_2$) and cord blood cells [55, 68, 69]. Earlier studies from our lab identified a class of small molecule open chained carbohydrate IRI to display promising validity on the cryopreservation of HPSCs by enhancing functionality and potency [55, 66, 67]. The findings concluded that the addition of IRIs in cryopreservation media alternatively increased the engraftment of umbilical cord blood, which will lead to enhancing viability of the cells post-thaw.

Chapter 2: Determining the activity of *N*-aryl-gluconamide IRIs to cryopreserve in iPSCs

2.1 Ice Recrystallization Inhibition (IRI) Assay

IRI activity is quantified using the splat cooling assay method [70]. The analyte at concentration of 22 mM is dissolved in a phosphate buffered saline (PBS) solution. In some cases, when the analyte were found to be insoluble at higher concentration, a dose-response is required to determine the IC_{50}. a serial dilution to the following concentrations was sequentially tested at 11 mM, 5 mM or 0.5 mM. A 10 µL of the analyte solution was dropped from a height of 2 meters onto a pre-cooled (-80 ºC) block of polished aluminum. The drop instantly freezes and forms an ice wafer of 20 µm thick and 1 cm in diameter. The wafer is carefully dislodged from the aluminium plate and transferred to a cryostage held at -6.4 ºC covered with a glass coverslip. After 30 minutes of annealing, the wafer is then imaged using a microscope equipped with an LMPlanF1 20X, 0.40 objective. Three images in total are captured for each ice wafer and the solution is replicated three times.

The ice crystals which were formed during the flash freeze process are small and homogenous in size. The process of recrystallization occurs within the window of 30 minutes of annealing time and this results in an increase in ice crystal sizes. After the completion of the annealing process, the images are captured, and the area of each crystal is identified using ImageJ software which is extracted to an Excel file. The data of the domain areas of the ice crystals are plotted and analyzed using Microsoft Excel. The excel database allows for the calculation of the mean grain size (MGS) of the sample to be compared to the MGS of the PBS control which was tested independently at the beginning of each IRI activity assessment. The IRI activity is reported as the percentage of MGS (% MGS) relative to the PBS control. Hence, if the percentages are small, i.e. 10 %, this indicates that the IRI compound is highly active. The % MGS of each sample is plotted as a function of average velocity.

2.2. General Experiment

Thin layer chromatography (TLC) with 0.2 mm pre-coated silica gel aluminum plate 60 F254 were utilized to monitor the reaction progress or completion. Components of the reaction were visualized using a short-wavelength (254 nm) ultra-violet light and/or staining (ceric ammonium molybdate or orcinol/sulphuric acid stain solution) on the TLC plate.

The chemical shifts are reported as part per million (ppm) using the solvent residual peak as an internal standard. Splitting patterns are assigned as follows: s, singlet; d, doublet; t, triplet; q, quartet; quint, quintet; m, multiplet and br, broad. All NMR solvents for NMR analysis used deuterated DMSO (DMSO-*d6*). NMR characterization was recorded using Bruker Avance 400 with the selection of ^{1}H (300 MHz) and/or ^{13}C NMR (400 MHz). Low resolution mass spectrometry (LRMS) was performed on a Micromass Quatro-LC Electrospray spectrometer with a pump rate of 20 µL/min using electrospray ionization (ESI).

N-(2-fluorophenyl)-D-gluconamide

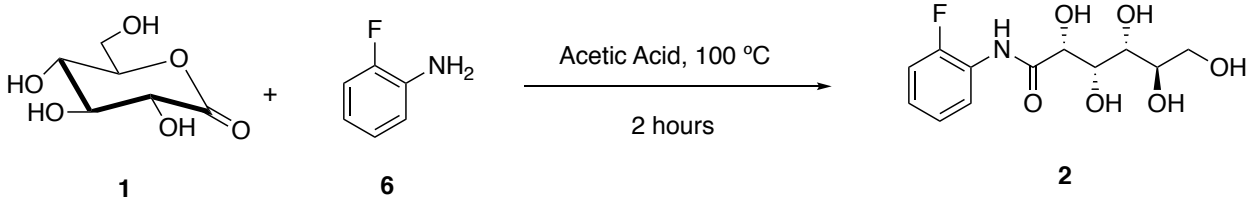

1 **6** **2**

Scheme 2.1. Synthesis of *N*-(2-fluorophenyl)-D-gluconamide (2).

To a solution of D-gluconic acid-*d*-lactone (1.00 g, 5.61 mmol) in acetic acid (10 mL) was added 2-fluoroaniline (1.63 mL, 16.84 mmol). The mixture was stirred for 2 hours at 100 ºC. The crude product was precipitated with hexane and filtered to obtain a dark brown sludge. The solid was recrystallized in ethanol to result in product as a white powder (37 %). Characterization data is consistent with previously published results [67]. ^{1}H NMR (400 MHz, DMSO-d_6): δ 9.19 (br. s, 1H), 8.09 (td, J= 15.86Hz, 8.0 Hz, 1H) , 7.30-7.24 (m, 1H), 7.19- 7.10 (m, 2H), 5.93 (d, J= 4.88 Hz, 1H), 4.64 (d, J= 7.28 Hz, 1H), 4.57 (t, J= 7.48 Hz,

5.44 Hz, 2H), 4.35 (t, J= 11.16 Hz, 5.56 Hz, 1H), 4.22 (t, J= 7.68 Hz, 3.68 Hz, 1H), 4.04-4.00 (m, 1H), 3.60 - 3.49 (m, 3H), 3.41-3.36 (m , 1H). ^{13}C NMR (400 MHz, DMSO- d_6): δ 172.0, 124.99 (d, J = 28.88 Hz), 122.49, 115.71 (d, J= 76.84 Hz), 74.41, 72.66 (d, J= 249.44 Hz), 70.71, 63.74. LRMS (ESI): m/z calc. for $C_{12}H_{16}FNaNO_6$ $[M+Na]^+$ 312.3; found 312.2.

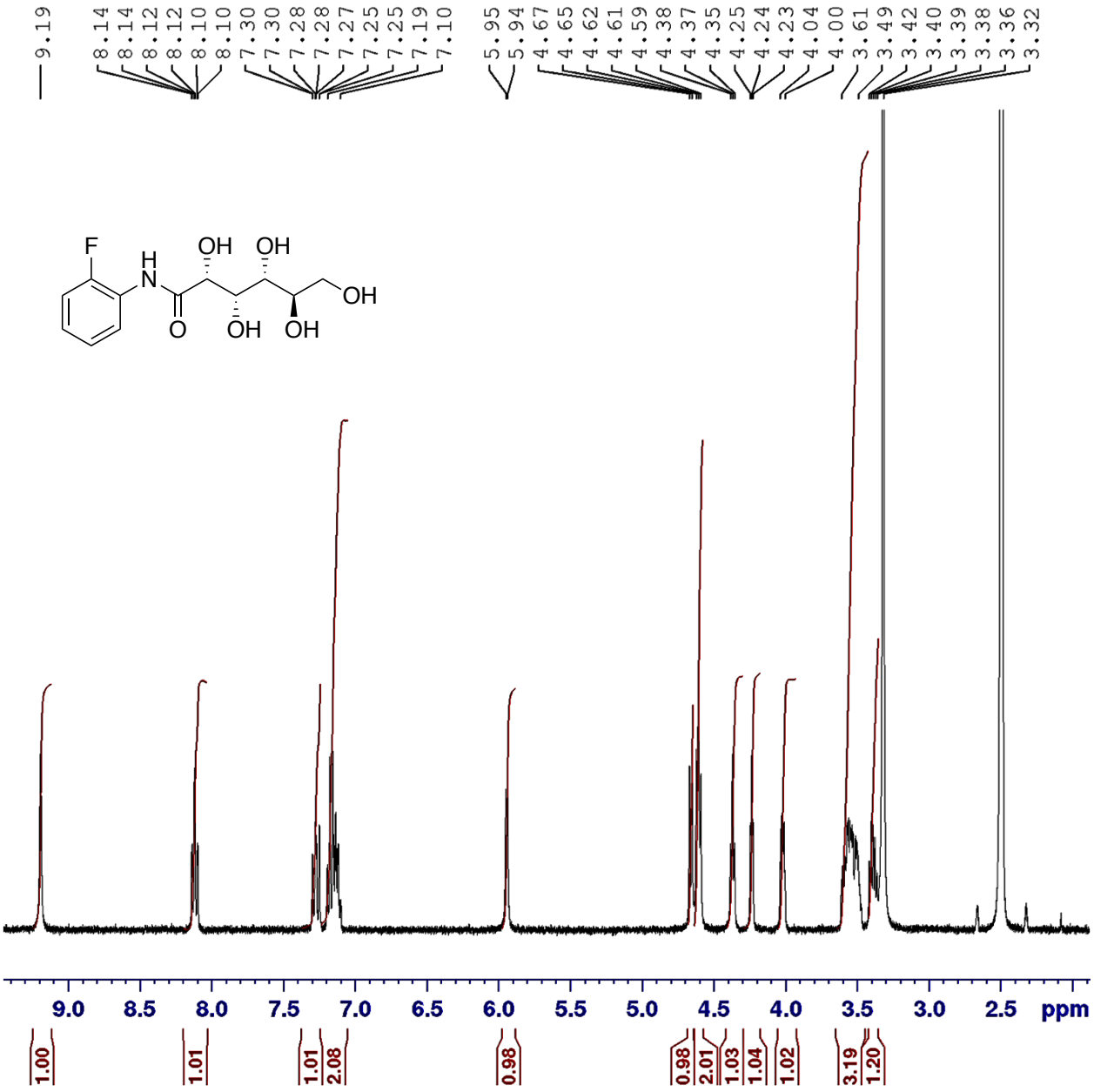

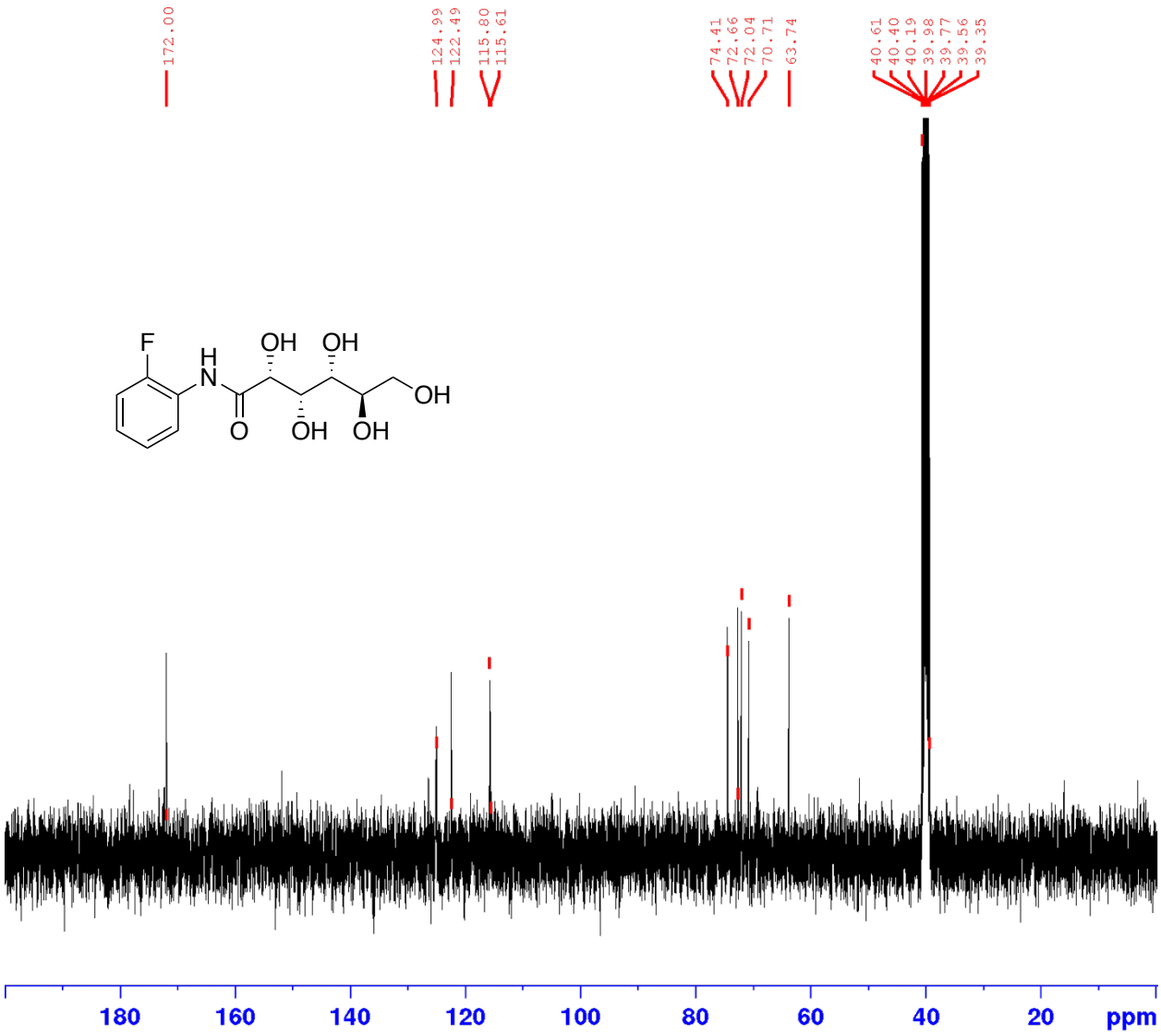
172.00
124.99
122.49
115.80
115.61
74.41
72.66
72.04
70.71
63.74
40.61
40.40
40.19
39.98
39.77
39.56
39.35
F
H
N
O
OH
OH
OH
OH
OH
180
160
140
120
100
80
60
40
20
ppm

N-(4-chlorophenyl)-D-gluconamide

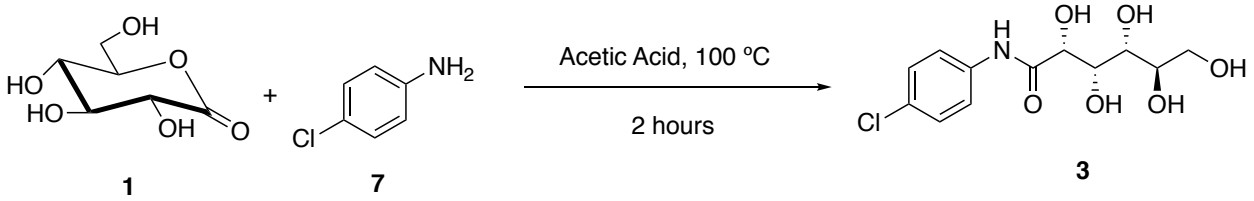

Scheme 2.2. Synthesis of *N*-(4-chlorophenyl)-D-gluconamide (3).

To a solution of D-gluconic acid-*d*-lactone (3.00 g, 16.84 mmol) in acetic acid (30 mL) was added 4-chloroaniline (2.15 g, 16.84 mmol). The mixture was stirred for 2 hours at 100 ºC. The crude product was precipitated with hexanes and filtered. The crude solid was recrystallized in ethanol to result in product as a white powder (24.5 %). Characterization data is consistent with previously published results [67]. ^{1}H NMR (400 MHz, DMSO-d_6): δ 9.72 (s, 1H), 7.75 (d, J= 8.88 Hz, 2H) , 7.35 (d, J= 8.84 Hz, 2H) 5.71 (d, J= 5.16 Hz, 1H), 4.59 (d, J= 4.80 Hz, 1H), 4.53 (d, J= 7.08, 2H), 4.35 (t, J= 11.28 Hz, 5.64 Hz, 1H), 4.17 (t, J= 8.72 Hz, 3.92 Hz, 1H), 4.00-3.99 (m, 1H), 3.61-3.57 (m, 1H), 3.47 (t. 2H), 3.42- 3.33 (m, 2H). ^{13}C NMR (400 MHz, DMSO- d_6): δ 171.99, 137.77, 128.61, 127.09, 121.36, 74.40, 72.38, 71.72, 70.51, 63.47. LRMS (ESI): m/z calc. for $C_{12}H_{16}ClNaNO_6$ $[M+Na]^+$ 328.7, found 328.0.

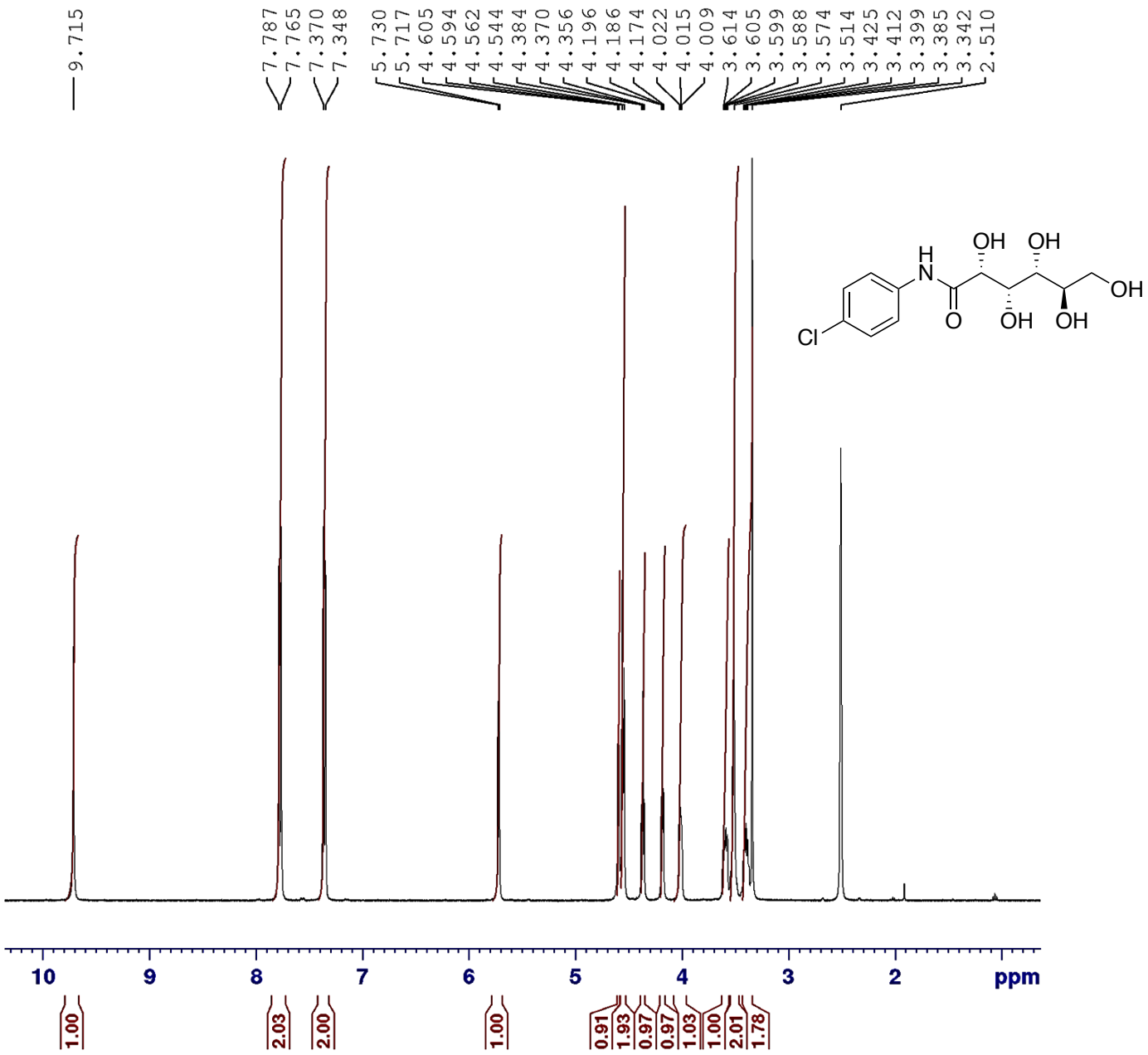
9.715
7.787
7.765
7.370
7.348
5.730
5.717
4.605
4.594
4.562
4.544
4.384
4.370
4.356
4.196
4.186
4.174
4.022
4.015
4.009
3.614
3.605
3.599
3.588
3.574
3.514
3.425
3.412
3.399
3.385
3.342
2.510
OH
OH
H
N
OH
O
OH
OH
Cl
10
9
8
7
6
5
4
3
2
ppm
1.00
2.03
2.00
1.00
0.91
1.93
0.97
0.97
1.03
1.00
2.01
1.78

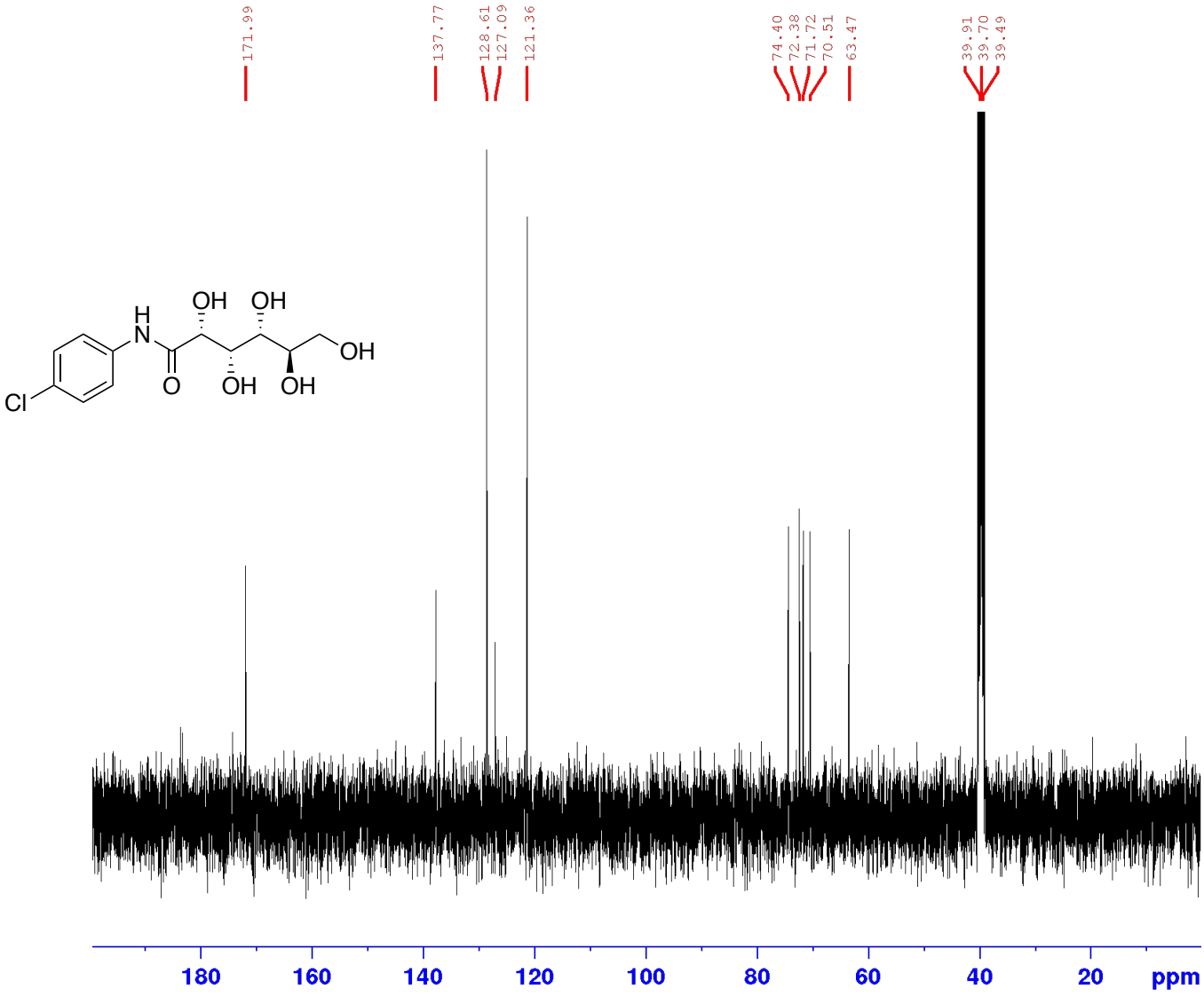
171.99
137.77
128.61
127.09
121.36
74.40
72.38
71.72
70.51
63.47
39.91
39.70
39.49
H
N
O
OH
OH
OH
OH
OH
Cl
180
160
140
120
100
80
60
40
20
ppm

N-(4-methoxyphenyl)-D-gluconamide

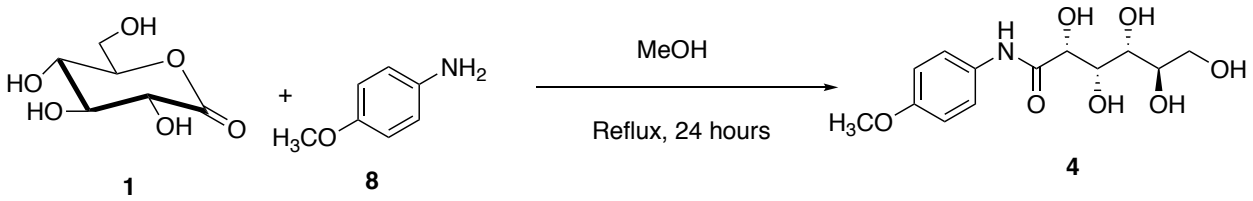

Scheme 2.3. Synthesis of *N*-(4-methoxyphenyl)- D- gluconamide (4).

_N_-(4-methoxyphenyl)- D- gluconamide

To a solution of D-gluconic acid-*d*-lactone (5.0 g, 28.07 mmol) in methanol (375 mL) was added p-anisidine (3.46 g, 28.07 mmol). The mixture was stirred for 24 hours at reflux. The solvent was evaporated, and the residue was recrystallized in ethanol to produce white crystals (73 %). Characterization data is consistent with that previously published [67, 71]. ^{1}H NMR (400 MHz, DMSO-*d6*): δ 9.38 (s, 1H), 7.59 (d, *J* = 9.28 Hz, 2H), 6.85 (d, *J* = 9.00 Hz, 2H), 5.62 (d, *J* = 5.32 Hz, 1H), 4.56 (d, *J* = 5.10 Hz, 1H), 4.52-4.50 (m, 2H), 4.33 (t, *J* = 5.85 Hz, 1H), 4.13 (dd, *J* = 4.10 Hz, 5.18 Hz, 1H), 3.99-3.96 (m, 1H), 3.71 (s, 3H), 3.60-3.54 (m, 1H), 3.51-3.49 (m, 2H), 3.39-3.35 (m, 1H).^{13}C NMR (400 MHz, DMSO-*d6*): δ 171.46, 155.74, 132.21, 121.52, 114.13, 74.59, 72.76, 71.99, 70.3, 63.78, 55.61. LRMS (ESI): *m/z* calc. for $C_{13}H_{18}NO_7$ $[M-H]^-$ 300.1, found 300.1.

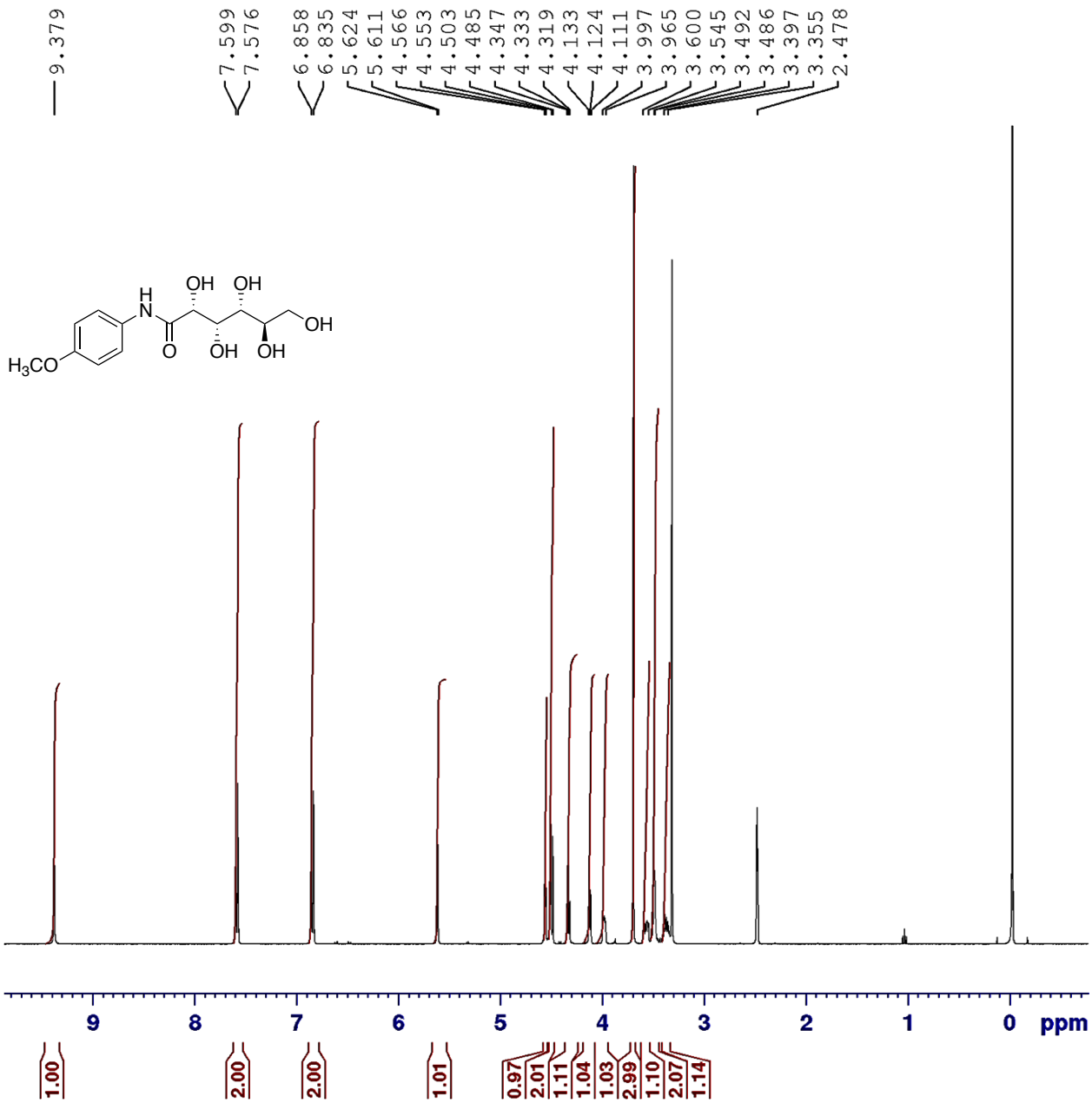
9.379
7.599
7.576
6.858
6.835
5.624
5.611
4.566
4.553
4.503
4.485
4.347
4.333
4.319
4.133
4.124
4.111
3.997
3.965
3.600
3.545
3.492
3.486
3.397
3.355
2.478
H
N
O
OH
OH
OH
OH
OH
H3CO
9
8
7
6
5
4
3
2
1
0
ppm
1.00
2.00
2.00
1.01
0.97
2.01
1.11
1.04
1.03
2.99
1.10
2.07
1.14

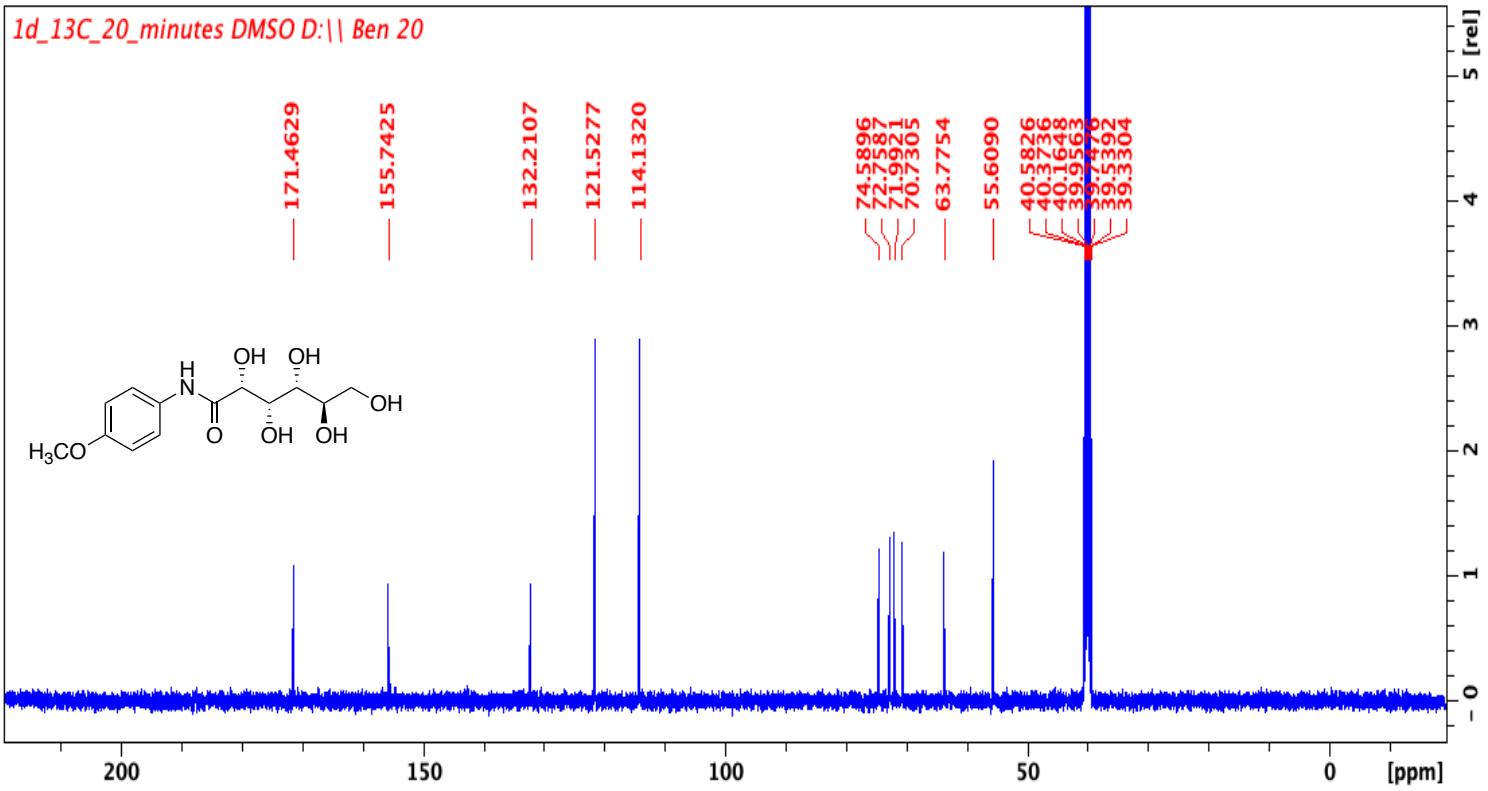
1d_13C_20_minutes DMSO D:\\ Ben 20
171.4629
155.7425
132.2107
121.5277
114.1320
74.5896
72.7587
71.9921
70.7305
63.7754
55.6090
40.5826
40.3736
40.1648
39.9563
39.7476
39.5392
39.3304
H
N
O
OH
OH
OH
OH
OH
H3CO
200
150
100
50
0
[ppm]
5 [rel]
4
3
2
1
0

N-(2,6-difluorobenzyl)-D-gluconamide

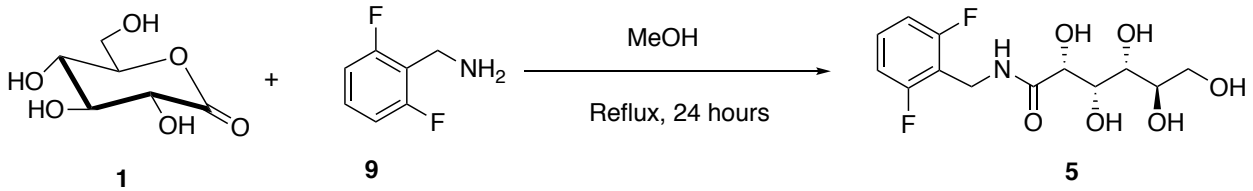

1 **9** **5**

Scheme 2.4. Synthesis of *N*-(2,6-difluorobenzyl)-D-gluconamide (5).

To a solution of D-gluconic acid-*d*-lactone (1.49 g, 8.36 mmol) in methanol (111.68 mL) was added 2,6-difluorobenzylamine (1.00 mL, 8.36 mmol). The mixture was stirred for 24 hours at reflux. The solvent was evaporated, and the residue was recrystallized in ethanol to produce white crystals (56 %). Characterization data is consistent with that of previously reported data [67]. ^{1}H NMR (300 MHz, DMSO-*d*6): δ 7.83 (t, *J* = 5.73 Hz, 1H), 7.33-7.41 (m, 1H), 7.08 (t, *J* = 8.09 Hz, 2H), 5.36 (d, *J* = 5.32 Hz, 1H), 4.53 (d, *J* = 5.00 Hz, 1H), 4.38-4.48 (m, 3H), 4.27-4.34 (m, 3H), 4.00 (dd, *J* = 5.18 Hz, 3.77 Hz, 1H), 3.87-3.90 (m, 1H), 3.53-3.59 (m, 1H), 3.44-3.45 (m, 2H). ^{13}C NMR (400 MHz, DMSO-*d*6): δ 172.64, 130.25, 111.95 (d, $J_{C,F}$ = 19.56 Hz), 112.0 (dd, $J_{C,F}$ = 18.85 Hz, 6.51 Hz), 74.00, 72.79, 71.96, 70.54, 63.81. ^{19}F NMR (300 MHz, DMSO-*d*6): δ -114.5. LRMS (ESI): *m/z* calc. for $C_{13}H_{17}F_2KNO_6$ $[M+K]^+$ 360.1, found 360.1.

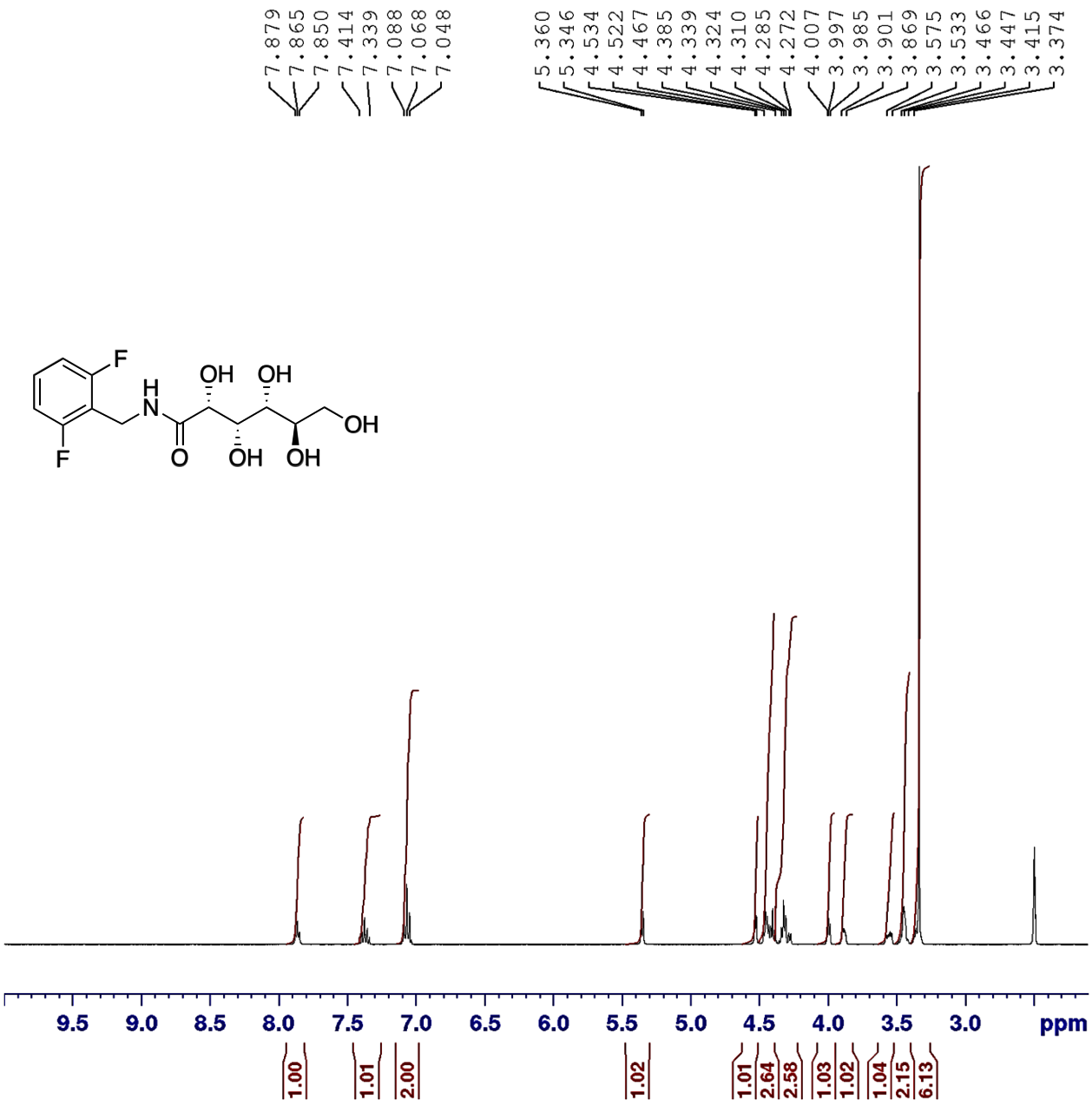
7.879
7.865
7.850
7.414
7.339
7.088
7.068
7.048
5.360
5.346
4.534
4.522
4.467
4.385
4.339
4.324
4.310
4.285
4.272
4.007
3.997
3.985
3.901
3.869
3.575
3.533
3.466
3.447
3.415
3.374
F
H
N
OH
OH
OH
O
OH
OH
F
9.5
9.0
8.5
8.0
7.5
7.0
6.5
6.0
5.5
5.0
4.5
4.0
3.5
3.0
ppm
1.00
1.01
2.00
1.02
1.01
2.64
2.58
1.03
1.02
1.04
2.15
6.13

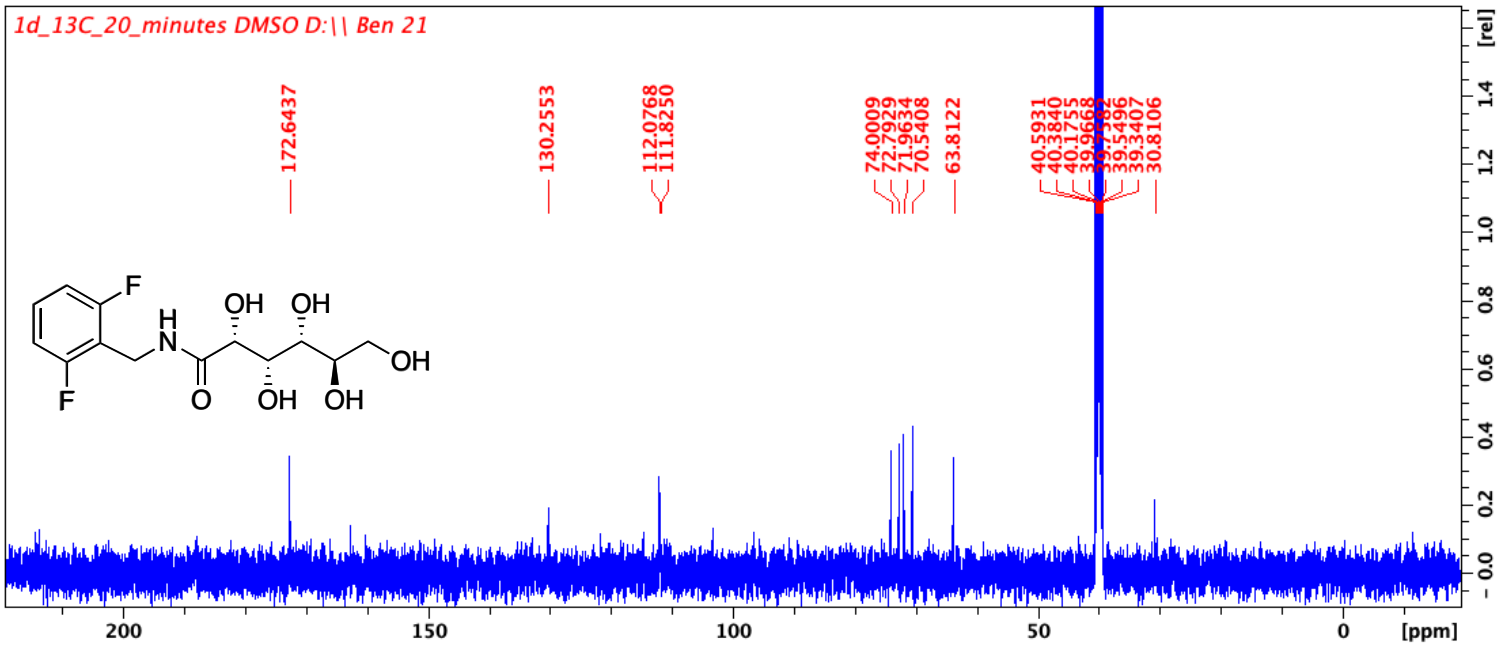
1d_13C_20_minutes DMSO D:\\ Ben 21
172.6437
130.2553
112.0768
111.8250
74.0009
72.7929
71.9634
70.5408
63.8122
40.5931
40.3840
40.1755
39.5496
39.3407
30.8106
F
H
N
OH
OH
OH
O
OH
OH
F
[rel]
1.4
1.2
1.0
0.8
0.6
0.4
0.2
0.0
200
150
100
50
0
[ppm]

2.3. Synthesis of N-aryl-gluconamides

As stated in Chapter 1, the four ice recrystallization inhibitors are synthesized and tested for the ability to cryopreserve human iPSCs. The process of ice recrystallization affects cellular damage to biological samples which incur the decrease of post-thaw viability, functionality, and recovery [72, 73]. Compounds such as IRIs have been developed to address ice recrystallization activity in frozen biological samples. Although there have been many methods of assessing the activity of ice recrystallization [70, 74–79], the modified splat cooling assay is used to quantify the activity in this report [70]. The quantification of ice recrystallization is measured by comparing the sizes of ice crystals formed, but the mechanism by which these IRIs functions is largely unknown. IRIs have been prominently designed by the Ben Lab for the past decade as antifreeze (glyco) proteins (AF(G)Ps) [80], synthetic polymers [58], c-linked AF(G)Ps [81], carbohydrate based surfactants and hydrogels [82], truncated c-linked glycopeptides [83], and small molecule carbohydrate-based inhibitors [84]. Among the numerous classes of IRIs previously investigated, the small molecule carbohydrate-based IRIs from the class of *N*-aryl-D-gluconamides will be assessed for their ability to enhance the cryopreservation efficacy of iPSCs. After the assessment of small molecule IRIs increasing the post-thaw functionality and potency of hematopoietic stem and progenitor cells (HSPCs) in umbilical cord blood (UCB) by previous Ben Lab members[67], these compounds are now being evaluated for thier functionality in iPSCs.

The synthesis of the four compounds are illustrated in reaction 2.1 & 2.2. The synthesis protocols have been previously published by our laboratory [67] and are summarized in the experimental section.

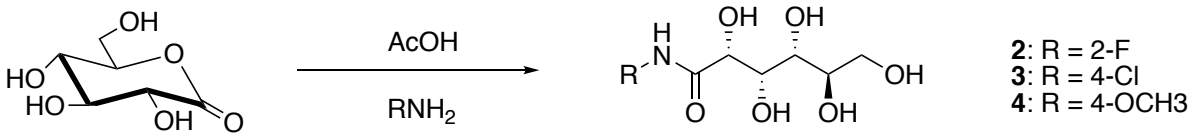

Reaction 2.1. Synthesis of a phenyl substituted *N*-aryl-D-aldonamide. **2**-**4** are *N*-(2-fluorophenyl)-D-gluconamide (2FA), *N*-(4-chlorophenyl)-D-gluconamide, (4ClA); *N*-(4-methoxyphenyl)-D-gluconamide, (PMA), respectively [67].

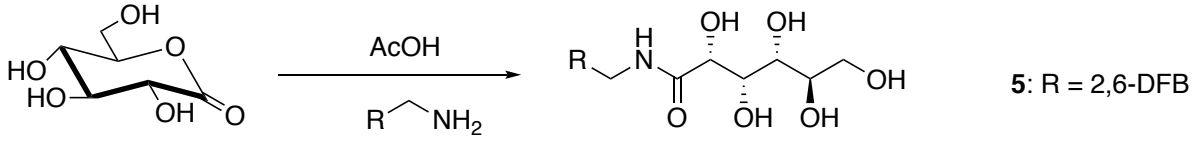

Reaction 2.2. Synthesis of a benzyl substituted *N*-aryl-D-aldonamide. **5** is (*N*-(2,6-difluorobenzyl)-D-gluconamide) [67].

The rate constants for the growth of ice crystals measured in splat cooling assay and it's IC_{50} calculations are generated for each of the IRIs displayed in Reaction 2.1 and 2.2. The splat cooling assay evaluates inhibition of ice recrystallization by measuring the growth of the ice crystals. In short, compound 2, 2FA, was dissolved in 11 mM PBS and all other compounds (**3-5**) were dissolved in a 22 mM PBS. Usually, the analytes can be assayed in a salt solution such as sodium chloride, calcium chloride, PBS, or a 30-45 % sucrose solution [58, 62, 85–87]. The solutes without analytes (i.e. PBS alone), are used as positive controls for the comparison of ice recrystallization activity to IRIs. Ten microliters of the preformulated solution (controls or samples) was dropped from a two meter height on to a precooled (-80 ºC) block of polished aluminum. Once the drop hits the aluminum surface it spontaneously forms a frozen ice wafer [85]. The ice wafer is then transferred to a Peltier unit with temperatures held at -6.4 ºC for 30 minutes and then imaged using a microscopic camera. The ice crystal sizes were calculated using ImageJ analysis software, where the ice crystals are quantified by measuring the mean ice grain area. The area of each crystal is measured by outlining the ice membrane in the Image J software. This software then calculates

the area of all outlined crystals and categorizes the different sizes of the crystals into various bins at increments of 0.001 mm^2 [88]. These areas are then transferred to an excel sheet which calculates the % mean grain size (% MGS) of each sample. The inhibitory activity of the compound is represented as % MGS relative to PBS positive control for ice recrystallization.

The compounds **2-5** result in 3 %, 35 %, 4 % and 13 % MGS, respectively. However, the determination of % MGS only measures the mean ice crystal size at an instantaneous time of 30 minutes. The IC_{50} of the IRI compound is determined using GraphPad software, where each sample concentration measured in triplicate sets was prepared and analyzed as discussed in the experimental section. Hence, the kinetic analysis of ice recrystallization determined for an extended period of time is documented to be a more reliable calculation of ice recrystallization activity [89]. To normalize the rate constant, an average is obtained by measuring the area of the samples with no inhibitory compound in PBS (0 mM IRI). The plot of the normalized rate constant (K_{norm}) as a function of inhibitory concentration ([I]) yields in a dose-response curve (data not shown). In summary, the IC_{50} results from the rate of ice recrystallization activity in each sample. The IC_{50} for the four IRIs (compounds **2-5**), which are assessed for enhancing cryopreservation in iPSCs, summarized in Table 1.0 [67].

Compound Structure	Compound Name	IC_{50}
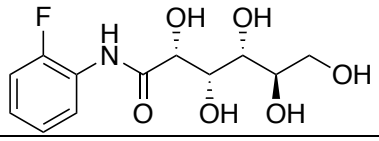	2FA	4.1 mM
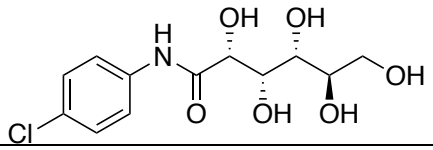	4ClA	12.0 mM
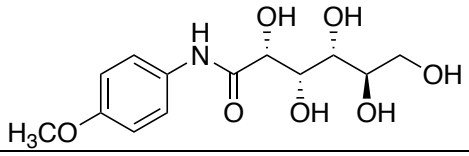	PMA	5.1 mM
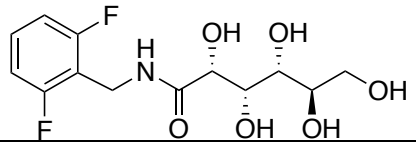	2,6-DFB	10.8 mM

Table 1.0. Summary of the IC_{50} of each IRI compound used for enhancing the cryopreservation of iPSCs. The table illustrates the chemical structure of IRIs, short-hand compound abbreviation, and the corresponding IC_{50}.

Chapter 3: Assessing the ability of IRIs to enhance the cryopreservation of iPSCs

3.1 Introduction

Human-induced pluripotent stem cells (iPSCs) are derived from fetal or adult somatic stem cells and the iPSCs are genetically reprogrammed to an embryonic stem cell (ESC) phenotype [90, 91]. ESCs are derived from human embryos and are characterized by two unique properties: pluripotency (unlimited self-renewal) and the ability to give rise to all the cell types of the human body. iPSCs are generated directly from a somatic cell by introducing reprogramming factors. The technology was pioneered by Yamanaka, who introduced four transcription factor genes (named SOX2, OCT3/4, Myc, and Klf4) that convert the somatic cells into pluripotent stem cells [92]. The Yamanaka factors can regulate the developmental signals necessary for stem cell pluripotency. SOX2 and OCT 3/4 are associated with the maintenance of pluripotency in stem cells [93]. Klf 4 and Myc are associated with the generation of the iPSCs [93].

Similar to ESCs, iPSCs are characterized by key pluripotent stem cell properties such as unlimited self-renewal, differentiation in all three germ layers, as well as increased telomere length and telomerase activity [94]. However, in contrast to ESC, iPSCs are not subjected to the ethical considerations related to ESCs. These are key hallmarks over adult stem cells that are limited in their self-renewal and restricted phenotypes. Given their broad differentiation capabilities, iPSCs are increasingly being used in applications such as drug discovery and disease modeling. They hold a great promise as cell replacement therapies in regenerative medicine and personalized medicines [95, 96, 105–114, 97, 115, 116, 98–104].

Despite their breadth of applications in both research and development (R&D) as well thier clinical potential, one key challenge in the culture of iPSC is cryopreservation. Genetic variations in iPSCs originate from heterogeneous genetic make-up of the cell populations. When low efficiency/decreased viability of iPSCs are derived, the iPSCs can select genetic variations from the initial starting cell source, even if the variation only occurs in a low frequency among the cell population [117]. Current cryopreservation techniques leverage CPAs such as dimethyl sulfoxide (DMSO) and glycerol in their cryopreservation

mediums to protect cells against cryoinjuries [118, 119]. These permeating cryoprotectants penetrate across the cell membrane to reduce cell dehydration and ice growth during freezing. However, the addition of CPA on its own does not suffice an optimal result since the iPSCs require customized freezing solutions to increase post-thaw viability, recovery, and functionality. Traditionally, fetal bovine serum (FBS) has been used as a universal growth supplement in cell culture medium with cryoprotectant in freezing media formulations [120]. The use of FBS in cell culture provides essential components to the cells, such as vitamins, hormones, cell attachment, and binding factors, and inhibits proteases [121–123]. However, FBS is not ideal for several reasons. Firstly, these undefined animal components (i.e., serums purified from blood, carrier proteins, hydrolysates, hormones, growth factors, and attachment factors) being introduced that can trigger spontaneous differentiation, limiting clinical applications [124]. Secondly, batch to batch variations of FBS occur. Lastly, the biosafety concerns involve contaminations with mycoplasma or endotoxins and the alteration of growth kinetics [120, 125]. Due to these limitations, recent studies have moved away from the use of FBS to more chemically defined cryopreservation strategies [126].

Routine cryopreservation strategies of iPSCs [127–132] use commercially available xeno-free and chemically defined mFreSR media (Stem Cell Technologies). mFreSR cryopreservation medium is routinely used in iPSC maintenance cultures with varying efficiencies of post-thaw recovery based on the iPSC lines used [127–132]. A significant advantage of mFreSR is its ability to pre-scan for its components to ensure batch to batch consistency [133]. Despite its wide use in R&D, mFreSR is not a GMP grade cryopreservation medium [45], and recent efforts in translational applications of iPSCs have shifted towards optimizing GMP-grade-cryopreservation media such as Cryostore 10 (CS10) [135–142]. Optimizing both mFreSR and CS10 formulations to increase post-thaw recovery of iPSCs holds tremendous value in supporting iPSC related research activities [126].

Efforts to optimize the post-thaw recovery of iPSC have been largely dependent on the addition of ROCK (Rho-associated, coiled-coil containing protein kinase) inhibitor (Y-27632) [143]. A major obstacle in human iPSCs and ESCs research is the reduced survival rate of cells after single-cell dissociation. The

Sasai group was the first to discover the ROCK inhibitor (Y-27632) [143]. The addition of ROCK inhibitor in cell culture medium results in decreased dissociation induced apoptosis in iPSCs and ESCs by inhibiting the activated Rho-associated kinase protein phosphorylation of the cytoskeletal myosin, initiating cell apoptosis (Figure 3.1) [144–147]. Similarly, ROCK inhibitor was also shown to inhibit post-thaw apoptosis of iPSC and increase iPSC recovery [148]. As a result, the ROCK inhibitor has been grandfathered into all conventional iPSC dissociation and post-thaw protocols due to its efficacy in post-thaw recovery after using mFreSR freezing medium [149]. However, the addition of ROCK inhibitor to iPSC culture induces a change in cell morphology from rounded to spindle-like structures and causes stress upon the cell [143]. Although post-thaw recovery of the cells is enhanced [143, 149, 150], the iPSC morphology change has unknown effects given its routine use in the maintenance of iPSC cultures. Optimally, increasing the post-thaw viability, recovery, and functionality of iPSCs without the requirement of ROCK inhibitor would eliminate any potential long-term adverse effects on the master clonal cell banks.

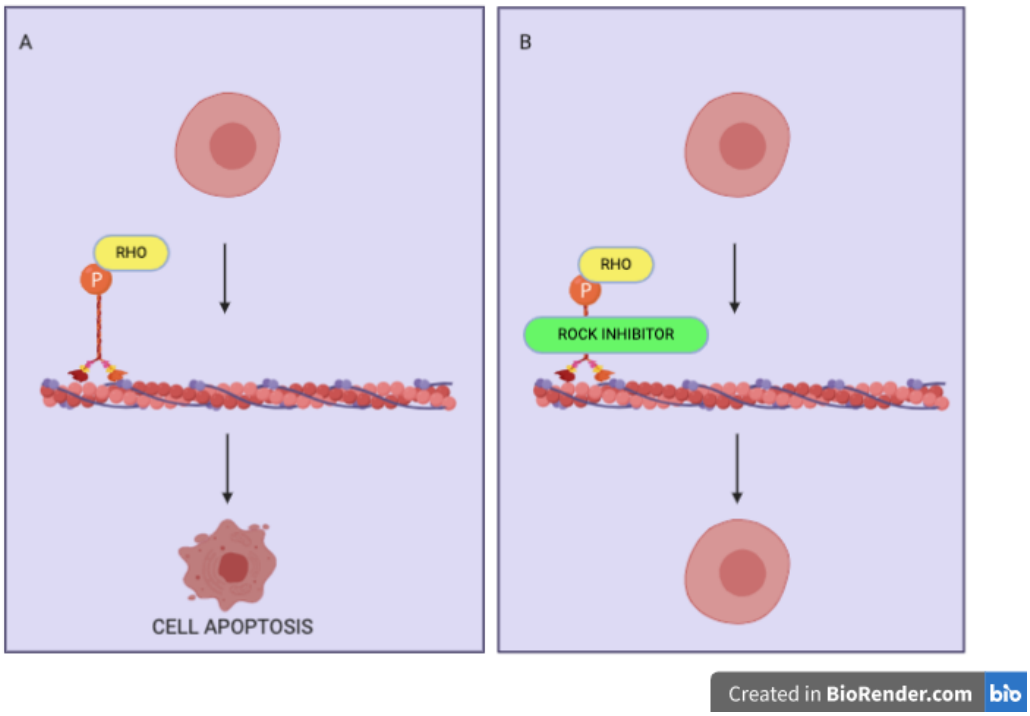

Figure 3.1. Schematic illustration of the ROCK inhibitor mechanism of action. **A)** Without the presence of a ROCK inhibitor, the ROCK phosphorylates the myosin cytoskeleton, inducing cell apoptosis. **B)** With the presence of a ROCK inhibitor, the ROCK is unable to phosphorylate the myosin cytoskeleton. The presence of ROCK inhibitor mitigates the risk of cell apoptosis. The image was created under free licensing with BioRender.com.

Due to the sub-optimal cryopreservation of iPSCs using mFreSR, our goal in this study was to improve the cryopreservation of iPSCs by developing a customized freezing solution by incorporating ice recrystallization inhibitors (IRIs) developed in our laboratory.

Given the promising results of IRIs in other stem cells such as hematopoietic stem cells (HSCs) [67] we hypothesize that supplementing commercially available cryopreservation mediums would increase post-thaw viability, recovery, and retention of pluripotency of the iPSCs. In addition, we sought to determine whether the addition of IRI would negate the need to use the ROCK inhibitor in post-thaw cultures, limiting unnecessary alterations to iPSCs.

3.2 Cryopreservation of HAF-iPSCs using a panel of *N*-aryl-aldonamide cryoprotectants

In this study, two different human iPSC lines were used to validate the effects of an ice recrystallization inhibitor (IRI) upon post-thaw cell recovery. The first iPSC line was reprogrammed from human amniotic fluid cells (HAFs) [151], and the second from a commercially sourced (Cell Systems) primary human brain microvascular endothelial cells (HBMEC) by researchers at the NRC. Both donor cells were reprogrammed using episomal reprogramming factors expressing Yamanaka factors (OCT4, SOX2, Nanog, and KLF4) [152]. A schematic illustration summarizing the derivation and reprogramming of each of the cell lines, HAF-iPSCs, and HBMEC-iPSCs is depicted in Figure 3.2.

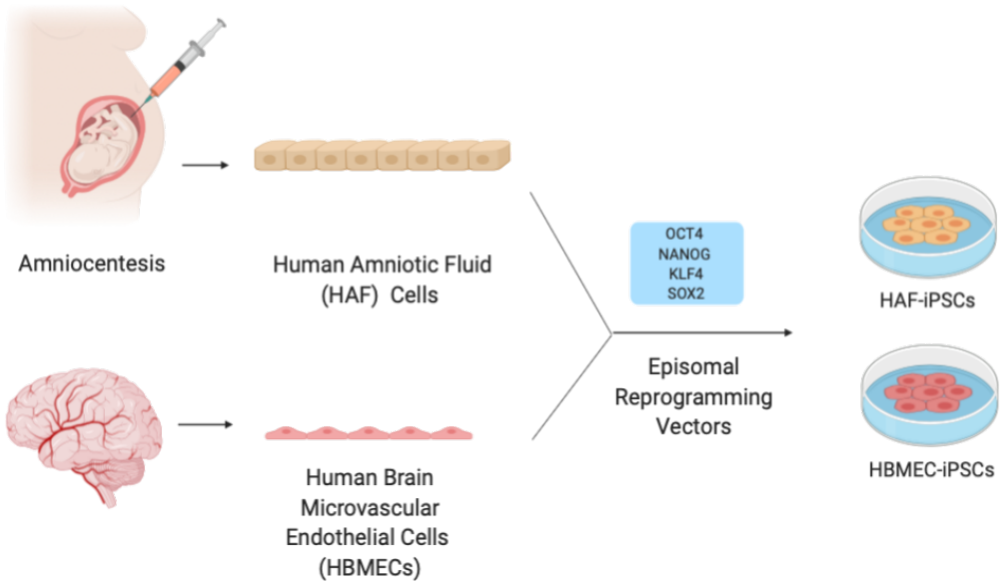

Figure 3.2. Illustration of the derivation of HAF-iPSCs and HBMEC-iPSCs. Human amniotic fluid (HAF) cells and human brain microvascular endothelial cells (HBMECs) were both reprogrammed using the episomal reprogramming factors, also known as Yamanaka factors (OCT4, Nanog, Klf4, and SOX2), to generate HAF-iPSC and HBMEC-iPSCs. Created using Free licensing from Biorender.com

For this study, the experiment was initiated by cryopreserving both types of iPSCs (HAF and BMEC) at passage 29 and passage 11, respectively, in a mFreSR cryopreservation medium containing 10%

DMSO. The mFreSR solution is a serum-free cryopreservation medium used for cryopreservation of human ESCs and iPSCs, in which the mFreSR contains DMSO that is pre-formulated in the medium.

HAF-iPSCs (hereafter referred to as iPSCs) were used for most of the studies. The iPSCs were cultured by thawing one vial of frozen stocks into mTeSR maintenance media until the desired confluency of 80% was achieved, and then the iPSCs were expanded into 6-well plates. When the confluency of the cells reached approximately 80% (roughly $2.0x10^6$ cells/well), the iPSCs were passaged or frozen with the addition of IRI containing mFreSR solution. Hence, the IRI is dissolved in mFreSR containing 10% DMSO and calculated for 1 mL per vial. This is known as the IRI formulation which is frozen for 24 hours before freezing iPSC lines.

The supplemented cryomedium (mFreSR + IRI) contains the following IRIs: 4CLA (mFreSR+4ClA), 2FA (mFreSR+2FA), PMA (mFreSR+PMA), or 2,6-DFB (mFreSR+2,6-DFB). A range of IRI concentrations from 0.5 mM to 25 mM was chosen explicitly due to prior literature studies reporting a toxicity concern at concentrations above 25 mM [67]. As mentioned before, IRIs in this concentration range have previously shown efficacy in other cell types [55, 153]. Hence, the first objective was to check for the toxicity of the compounds and then compare the different IRI compounds and concentrations that are required to enhance iPSCs viability post-thaw.

Toxicity can be observed from the identification of dead cells in cell culture. The iPSC colonies that were frozen in 2FA (Figure 3.3B) showed no apparent signs of toxicity-induced cell death and formed compact colonies with characteristic high nuclear to cytoplasmic ratios like mFreSR control colonies (Figure 3.3A). Although no toxicity was observed post-thaw for 10 mM 2FA, when the iPSCs were grown in maintenance media with 2FA in culture, toxicity was observed from light micrographs only. Based on the images obtained, it highlights the importance of proper cell washing to remove residual IRI and DMSO components. The viability and toxicity results can be applied to subsequent studies to conform to the use of 10 mM 2FA and mFreSR controls. Further studies can determine the portion of cells which are apoptotic with the use of Caspase 3/7 assay.

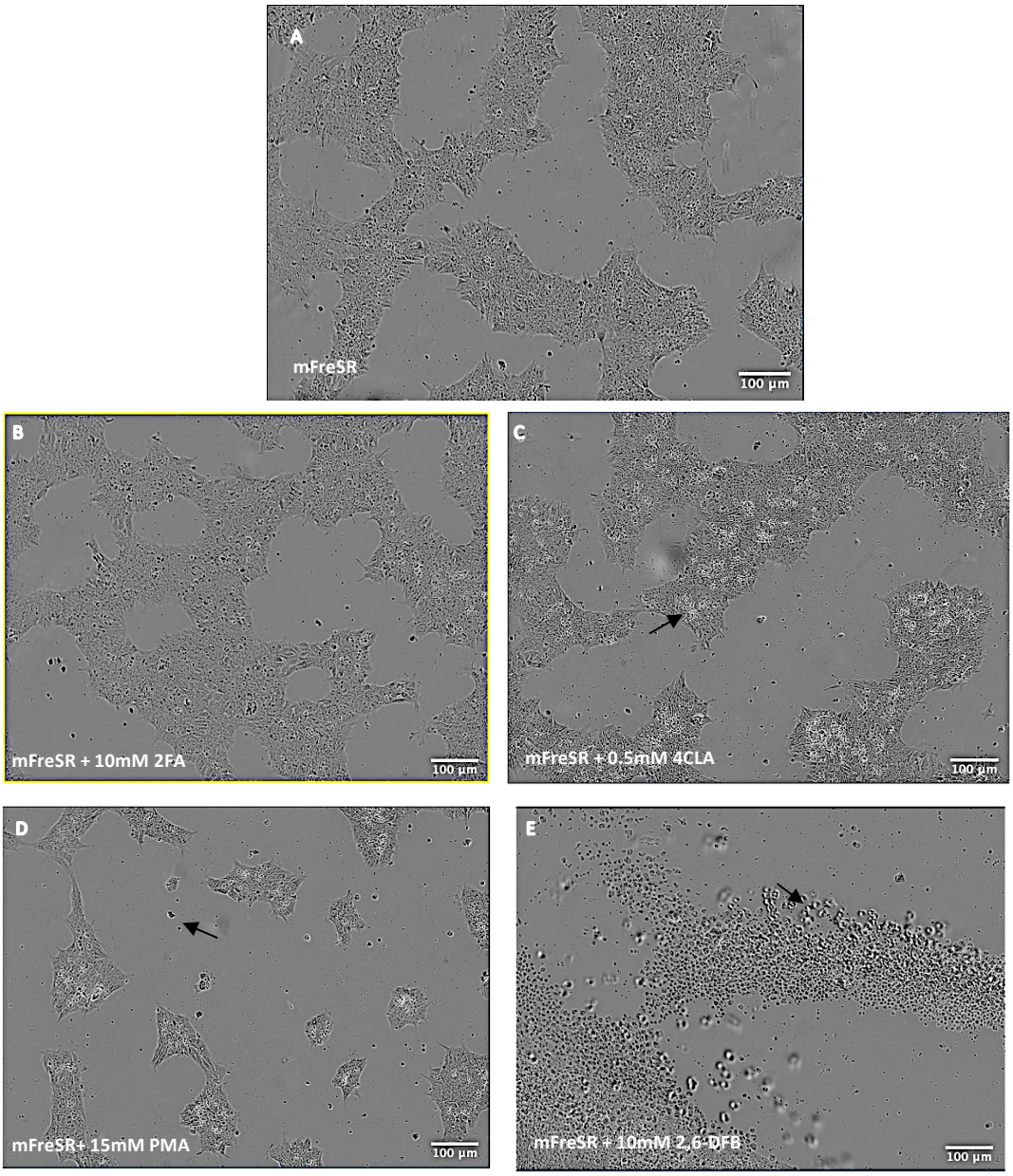

Figure 3.3. Micrograph of iPSCs cultured for 48 hours after thawing with four IRIs. The control – mFreSR containing 10% DMSO (**A**), 10mM 2FA supplemented mFreSR containing 10% DMSO (**B**), 0.5mM 4ClA supplemented mFreSR containing 10% DMSO (**C**), 15mM PMA supplemented mFreSR containing 10% DMSO (**D**), and 10mM 2,6-DFB supplemented mFreSR containing 10% DMSO (**E**). The most toxic IRI compound, observed from dead cells spread across in 10 mM 2,6DFB (**E)**, and the most potent IRI, based on post-thaw viability and recovery observed in 10 mM 2FA (**B)**. Figures **A-E** present the phase-contrast images showing the iPSC cell morphology, colony size, and apoptosis 48 hours post-

seeding. Images captured using BioRad ZOE™ fluorescent cell imaging system. Arrows: indicate apoptotic cells.

Cytotoxicity is scored based on altered cell morphology, decreased cell proliferation, smaller colony sizes, and evidence of apoptotic cell death (Figure 3.4). These IRIs may cause toxicities if cell membranes are breached or damaged, if the mitochondrial function is reduced, or if DNA, protein or other macromolecules are damaged. The most toxic IRI compound, based on cell death, was 10 mM 2,6-DFB. The most potent IRI, based on post-thaw viability and recovery, was 10 mM 2FA.

Figure 3.4 shows the percent post-thaw viability of iPSCs frozen in different conditions. The results of Figure 3.4 tested four IRI compounds in different concentrations to identify their effects of toxicity. The effect of toxicity was identified as a decrease in post-thaw viability in comparison to mFreSR. The formulation of the IRIs, freezing process and thawing of the cells are explained in more detail in the methods section. Briefly, based on the two-factor hypothesis [14], slow cooling rates, in conjunction with rapid warming rates, are key to maintaining high cell viability and recovery post-thaw, especially in iPSCs. In cryopreservation experiments, it is essential to keep the parameters of cooling and warming rates consistent to determine the functionality of the IRI compounds accurately.

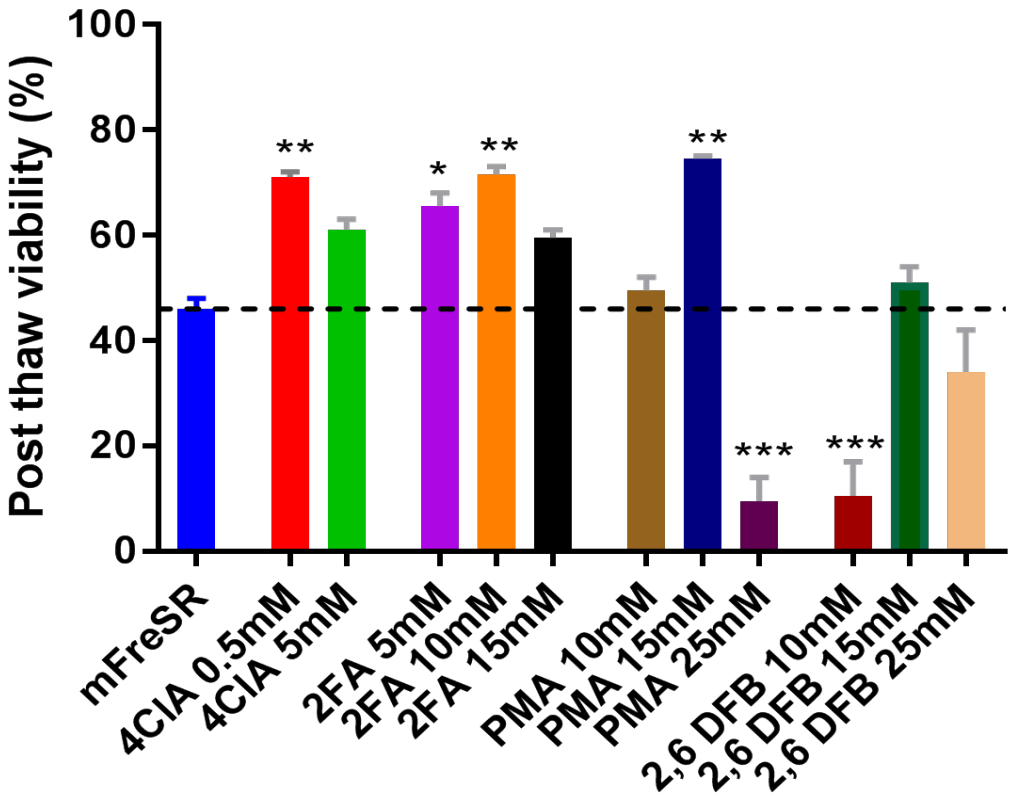

Figure 3.4. Assessment of post-thaw viability in HAF-iPSCs using IRIs supplemented in mFreSR containing 10% DMSO. The percentage of post-thaw viability of human iPSCs is shown on the y-axis with the formulation mediums (mFreSR, mFreSR containing 10% DMSO supplemented with 4ClA, 2FA, PMA, and 2,6-DFB) and concentrations on the x-axis. Before thawing, all cells were frozen at a rate of 1 ºC/min to -80 ºC before being transferred to -196 ºC. After 24 hours, the iPSCs were thawed in a 37 ºC water bath for 2 minutes. The viability data was assessed using the Trypan blue exclusion assay immediately post-thaw, in the presence of 10µm Rock Inhibitor (RI). Percent viability is expressed as the mean and standard error of the mean (SEM). Statistical significance marked by asterisks assessed by one-way analysis of variance (ANOVA) for comparison to control (mFreSR), where ns=P>0.05, *= P≤0.05, **= P≤0.01, and ***= P≤0.001 (n=2).

The highest percentage of post-thaw viability was 4ClA, 2FA, and PMA, where 71 % ± 0.01 was observed for 0.5 mM 4ClA, 71.5 ± 0.01 for 10 mM 2FA, and 74.5 % ± 0.01 for 15 mM PMA (Figure 3.4). The IRI treated formulations resulted in a 20 % increase in post-thaw viability compared to mFreSR containing 10% DMSO (46 % ± 0.05). A technical replicate of n=2 for each IRI dose-dependent compound can be seen in Figure S1. In the IRI supplemented cryomedium, the DMSO in the mFreSR acts as a cryoprotective agent (CPA), and the IRI compound inhibits ice recrystallization. Additively, this results in an increase of post-thaw viability of approximately 20 % in comparison to the control, mFreSR (Figure 3.4).

iPSCs are the initial cell lines used to derive various specialized cells such as neurons or stem cell progenitor products. The quality of the iPSCs is a key factor while moving forward to therapeutic applications. Hence, it is important to maintain high-quality stock with increased cell survival. Quality of the cells is achieved by mitigating cryopreservation injuries from freezing or thawing events or with the reduction in toxicities of the cells with an additive response from IRIs supplemented in cryopreservation medium containing DMSO. Given that the IRIs increased the post-thaw viability by 20 % compared to the mFreSR controls, our next approach was to assess the post-thaw recovery of the iPSCs over 42 hours.

3. 3 Increased HAF-iPSC recovery and proliferation post-thaw in the presence of 2FA.

After the conclusion of viability and toxicity assessments, our approach was to evaluate the post-thaw recovery and subsequent proliferation of the iPSCs using 10 mM 2FA as a supplement in mFreSR. Since the ROCK inhibitor has been shown to mitigate iPSC apoptosis and increase survival, the next step was to assess the post-thaw recovery of the iPSC in the presence and absence of 10 µm ROCK inhibitor (RI). Figure 3.5 details the experimental workflow, where the cells were plated on a 6-well plate immediately post-thaw.

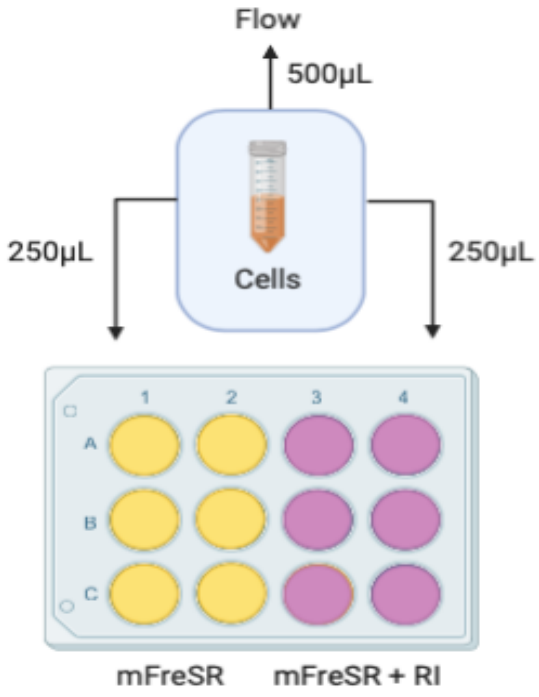

Figure 3.5. The summarized workflow of the cells immediately after thawing, removing CPAs and IRIs, and resuspending with maintenance medium, mTeSR. iPSCs of $2.5x10^5$ cells were plated on 6-well Matrigel-coated plates with or without ROCK inhibitor. The remaining $5.0x10^5$ cells were used for measuring percent post-thaw viability. The figure was created using Biorender.com

The ROCK inhibitor functions to increase the viability and attachment of the iPSCs post-thaw, which allows for increased proliferation capability [154]. The ROCK inhibitor activates RHO, which consequently activates Rho-associated protein kinase (ROCK). ROCK phosphorylates the cytoskeletal myosin to cause contractions within the cell leading to apoptosis via membrane bedding [144–147]. Therefore, ROCK inhibitors function by reducing dissociation induced apoptosis, which leads to an increase in survival and recovery of the iPSCs post-thaw [148]. Addition of ROCK inhibitor will allow more iPSC colonies to adhere to the matrix thereby increase the percentage of recovery. We want to test the condition with an absence of ROCK inhibitor to examine the effects of iPSCs without the drawbacks of ROCK inhibitor such as spindle like morphology. The thawed cells are washed out from freezing medium containing DMSO and IRIs; hence we are investigating the effects of recovery without ROCK inhibitor with prior protection of IRI compounds during the freezing events.

In this study, recovery of the iPSCs frozen with 2FA +/- ROCK Inhibitor supplemented cryomedia (mFreSR, mFreSR+RI, 2FA, 2FA+RI) was assessed and analyzed using IncuCyte live-cell imaging software (Sartorius). IncuCyte can set specific parameters to capture images of confluence. iPSC confluency was acquired by an average of nine images per each well in a 12 well plate every 30 minutes for up to 42 hours. Figure 3.6 shows iPSC proliferation as a function of confluency over time.

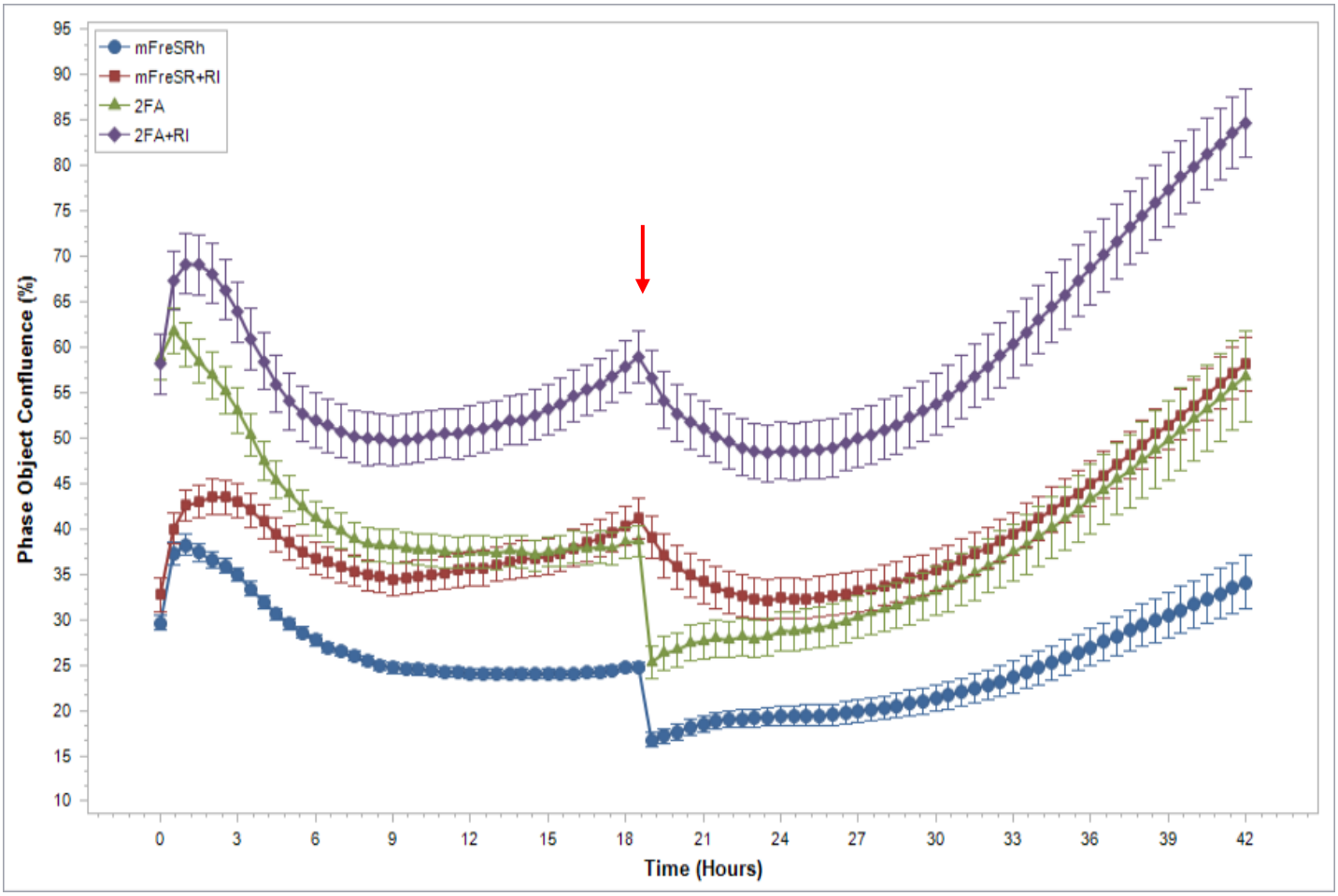

Figure 3.6. Increased survival and proliferation of iPSC frozen with mFreSR+10mM 2FA+RI observed using IncuCyte® Live-cell Imaging. Graphical analysis of confluence as a function of time is depicted above, where blue correlates to mFreSR with no RI, green correlates to 2FA with no ROCK Inhibitor treatment, red correlates to mFreSR with ROCK Inhibitor treatment, and purple correlates to 2FA with ROCK Inhibitor treatment in HAF-iPSCs P33. The graphical data was obtained by averaging the confluency of nine images captured for each well of the triplicate condition at 48 hours. The red arrow indicates the media change at 20 hours.

iPSC confluency immediately post-thaw is shown at time 0 hrs for each treatment condition (Figure 3.4). The first set of samples, 2FA + ROCK inhibitor (RI), and 2FA, report post-thaw confluency of 55%. The second set of samples, mFreSR + ROCK Inhibitor (RI), and mFreSR alone, report confluency of 29%. The confluence data is in accordance with the post-thaw viability data measured using flow cytometry and representative of the images captured at 42 hours using IncuCyte (Figure 3.6). Post-thaw recovery was assessed, based on confluency measurements, as a measure of iPSC proliferation over time. Initially, within 0-3-hours, the iPSC colonies attached and flatten as indicated by the increased confluency. From 3– 20 hours, the iPSCs enter a recovery phase characterized by a second wave of apoptosis coupled with clustering and compaction of adherent and viable iPSC colonies, indicated by a decrease in confluence. Similar apoptotic trend is seen by the primary apoptosis immediately post-thaw. After a 20-to-24-hour period, the media is removed and replenished with fresh mTeSR media (indicated by the red arrow in Figure 3.6) wherein the ROCK inhibitor is also washed out. Following this media change, the cells are observed to decrease in confluence a second time. This is due to the cells recovering from ROCK inhibitor-induced spindle-like morphology to more conventional rounded and more compacted colonies. Figure 3.7 illustrates the difference in RI functionality between mFreSR and mFreSR with RI (Figure 3.7). There is an increased confluency of cells treated with RI than cells without RI. The samples which were not in the presence of ROCK inhibitor result in minimal post-thaw recovery, and therefore, the media change at 20-24 hour, discards all dead cells. The software recalculates the confluence of viable cells, which is explained by the negative slope at the 20-hour mark of green (2FA) and blue (mFreSR) samples (Figure 3.6).

From 24 to 42 hours, the iPSC cells enter an active proliferative phase, and colony size increases. Based on this analysis, comparing equivalent treatments, 2FA (green), and mFreSR (blue), there is a 20 % difference between the two conditions. This indicates the enhanced effect of IRIs upon iPSC recovery. The 2FA (green) has no significant recovery post-thaw, and mFreSR (blue) has a 5 % increase post-thaw recovery when calculated based on input confluency over endpoint confluency. Endpoint confluency is defined as the calculated difference between the plating confluency at 0 hours and final confluency at 42

hours. The second set of treatments, 2FA + RI (purple) and mFreSR +RI (red), have a 30 % difference between the two conditions at the endpoint confluence. The 2FA + RI (purple) has a 28 % increase in confluence for post-thaw recovery of the cells, and mFreSR + RI (red) results in a 21 % increased confluency for post-thaw recovery when calculated based on input confluency over endpoint confluency.

Comparing the conditions of mFreSR + RI, the ROCK inhibitor enhances the post-thaw recovery of by 20 % in output confluency. Whereas the conditions of 2FA + RI, the ROCK inhibitor enhances the recovery by 30 % in the output confluency, indicating an additive effect between IRI and ROCK inhibitor (RI) (Figure 3.7). The recovery of the mFreSR+RI and 2FA treatments results in similar recovery rates. This suggests that 10 mM 2FA can potentially be used as a substitution to RI without causing obvious changes to iPSC's morphology.

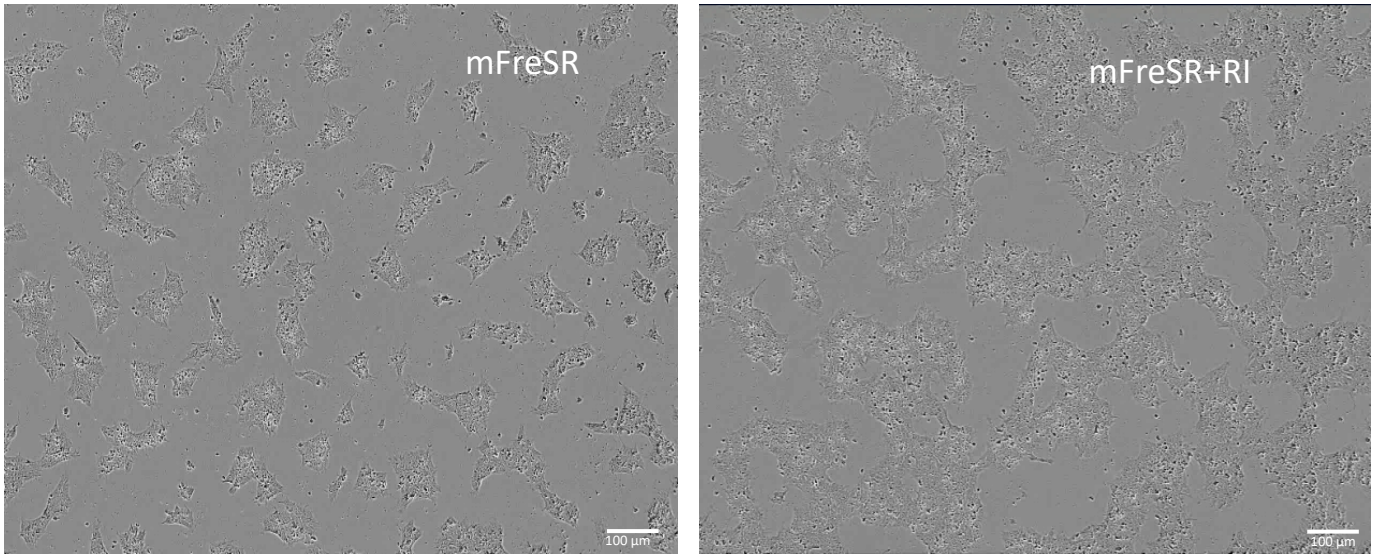

Figure 3.7. Highlighting the morphological features of RI treated cell populations at 40X magnification. Comparison of cell morphology differences between RI treated and non- ROCK Inhibitor treated iPSCs after 48 hours post-thaw. ROCK Inhibitor is washed out after 24 hours of seeding the iPSCs at $2.5x10^5$ cells.

Representative images captured by IncuCyte during the post-thaw recovery phase are shown in Figure 3.8 at 42 hours. Four images represent the two different treatment conditions that were graphically analyzed in Figure 3.8. Figure 3.8A and B represents mFreSR and mFreSR +RI, respectively. Whereas Figure 3.8 C and D represent 2FA and 2FA +RI. Comparing the four images from Figure 3.8 shows that the highest confluence of the iPSCs was observed in 2FA+ RI conditions, and these cells proliferate in higher quality and quantity. This observation can conclude an additive effect of 2FA and ROCK inhibitor.

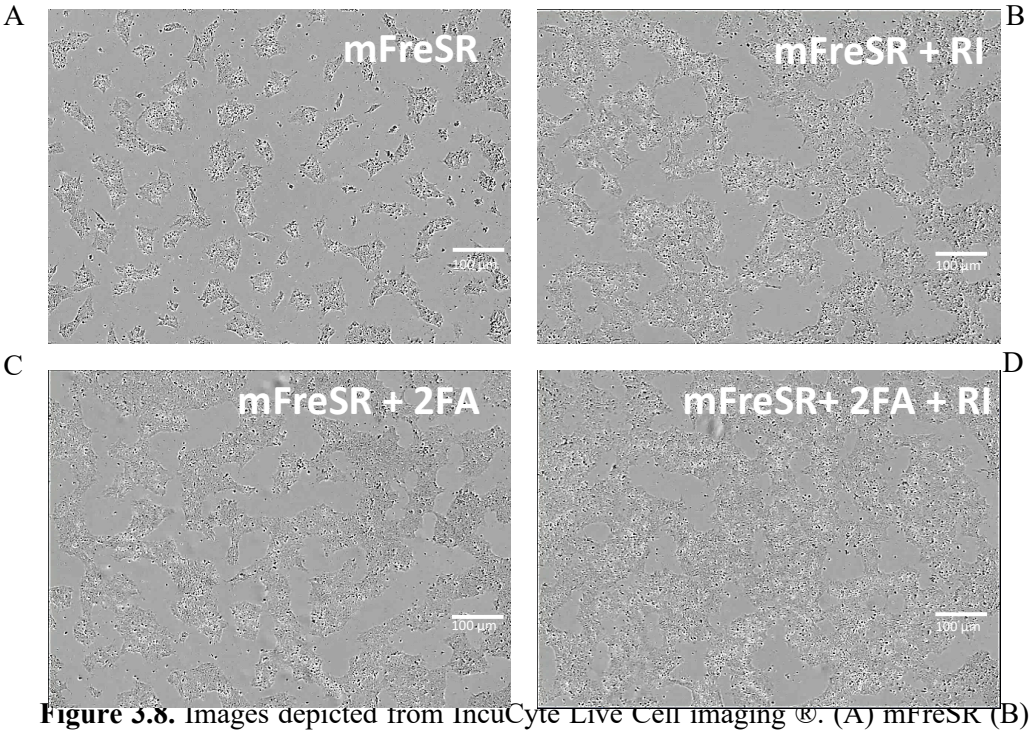

Figure 3.8. Images depicted from IncuCyte Live Cell Imaging ®. (A) mFreSR (B) mFreSR +RI (C) mFreSR + 2FA (D) mFreSR+2FA+RI. Cells are imaged at a magnification of 10X at the 42-hour time point. The image from each condition was selected to represent the confluence of one of the nine images captured for each well of the triplicate condition at 42 hours.

3.3.1. Assessment of Post-thaw viability in HBMEC-iPSCs

Interestingly, the mFreSR+RI (Figure 3.8 B) and 2FA (Figure 3.8 C) treatments result in similar post-thaw viability rates observed in Figure 3.6. This is a promising finding as it suggests that optimizing IRI cryoformulations to use 2FA as supplements may replace the use of ROCK inhibitor in the future. Since RI causes morphological stress to the cells and prolongs the handling of the cells in culture, it is ideal to replace the use of RI. To examine the reproducibility of the results for HAF-iPSC, we test the same treatments using a second iPSC line (HBMEC-iPSC). Given known variabilities between iPSC lines derived from different donors [155], we wanted to validate the findings in second where iPSCs were derived from HBMEC. Similar trends in post thaw viability was observed but some notable changes were observed in the overall recovery for HBMEC- iPSCs (Figure 3.9). The following results demonstrate the enhancement of post-thaw viability and recovery upon the IRI supplemented cryopreservation technique in HBMEC-iPSCs (Figure 3.9).

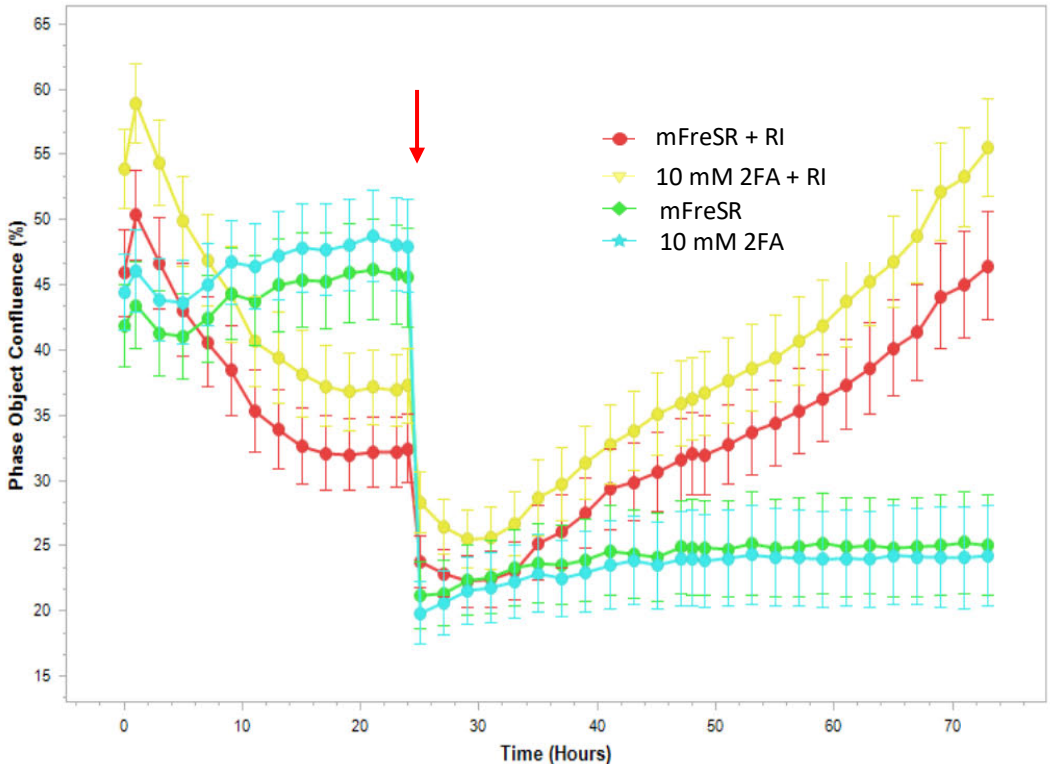

Figure 3.9. Assessment of post-thaw recovery in HBMEC – iPSCs. Graphical analysis of the additive effect between 2FA and ROCK inhibitor observed in HBMEC-iPSCs P13 frozen in mFreSR cryopreservation medium derived from IncuCyte live-cell imaging. Red represents mFreSR + RI, yellow represents 10 mM 2FA + RI, green represents mFreSR and blue represents 10 mM 2FA. The graphical data was obtained by averaging the confluency of nine images captured for each well of the triplicate condition at 72 hours. Each data point on the graph represents the average confluency calculated every 2 hours for 72 hours. The statistics of the output confluency of each IRI are as follows, 10 mM 2FA (43%), mFreSR (24%), 10 mM 2FA + RI (56%), and mFreSR + RI (44%). The red arrow indicates the media change at 24 hours.

The comparison of mFreSR (green) and 10 mM 2FA (blue) results in a difference in value of 24% post-thaw viability. On the contrary, equivalent conditions of ROCK inhibitor treatment upon mFreSR (red)

and 10mM 2FA (yellow) frozen cells, the post-thaw recovery after 70 hours results in 44% and 56%, respectively. This graph has been assessed for a longer period than HAF-iPSCs due to the slower growth kinetics, which are characteristics of the HBMEC-iPSCs.

If the 42-hour time point were to be analyzed, the post-thaw recovery confluence would vary significantly for HBMEC-iPSCs. Additionally, similar to Figure 3.6, the media change to the samples are observed by the vertical slope at 20 – 24-hour time period. In Figure 3.9, the conditions with no ROCK inhibitor treatment increase in confluence and drastically decrease 20% when the media is changed (indicated by the red arrow). The accumulation of dead cells can explain this drastic decrease in confluence; the replacement of the media washes the dead cells, and the software recalculates the confluence of the viable cell population based on cell attachment. The ROCK inhibitor-treated conditions of HBMEC-iPSCs are similar in trend with the HAF-iPSCs, where dissociation induced cell apoptosis is improved by treatment with the ROCK inhibitor. After the change in media, from 20 – 70 hours (Figure 3.9), the cells start to proliferate and recover from the removal of ROCK inhibitors. Both HAF-iPSCs (Figure 3.6) and HBMEC-iPSCs (Figure 3.9) show the same trends towards an additive response with 2FA and ROCK inhibitor. After the confirmation of 2FA's cryopreservation in HAF iPSCs and HBMEC iPSC lines, it is concluded that there is a difference between mFreSR and 2FA conditions, and the ROCK inhibitor studies show no statistically significant difference in comparison to the control groups (mediums without ROCK Inhibitor). Therefore, there is an urgent need for the optimization of cryopreservation strategies per cell line.

iPSC lines exhibit variability influenced largely by their epigenetic signatures based on donor cells resulting in a great deal of variability and reproducibility between iPSC lines. It is essential to formulate customized cryopreservation formulations to accommodate for these variabilities in different cell types. However, one possible combination of supplemented cryopreservation medium may not be optimal for all cell types to achieve therapeutically appropriate viability post-thaw. However, a combination of IRI and ROCK inhibitors may aid in formulating universal cryopreservation solutions. Furthermore, the future

directions can also investigate the additive effect of other IRI compounds in other commercially available cryopreservation media, such as GMP-grade Cryostore 10 (CS10).

3.4 Assessing post-thaw apoptosis of HAF-iPSCs

To investigate the effects of enhanced cryopreservation in HAF-iPSCs, we were interested in evaluating its reduction of apoptosis, maintenance of pluripotency & tri-lineage differentiation capability, and long-term cryopreservation effects of IRIs upon HAF-iPSCs post-thaw viability and recovery. The apoptotic behavior of iPSCs arises due to cryoinjury related cell death. Based upon the observation that 2FA functions similarly to ROCK inhibitor, we wanted to assess if the apoptotic potential of the iPSCs were also impacted.

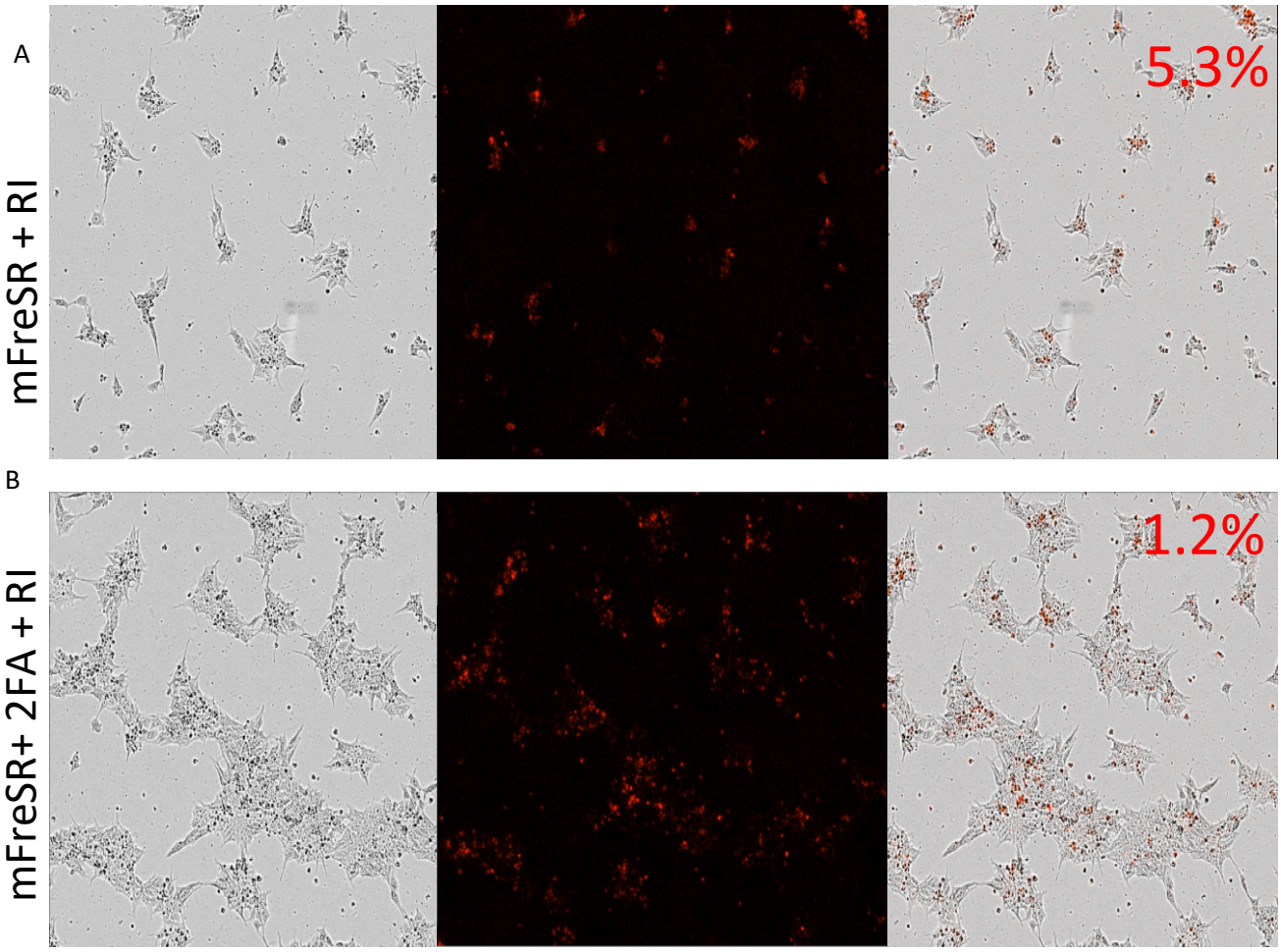

Caspase3/7 was normalized to phase (red area/phase area)

Figure 3.10. The effect of IRI and RI is displayed by the addition of ROCK Inhibitor 24 hours post-thaw. Increased recovery and colony size of iPSCs frozen in mFreSR + 2FA is dependent on RI. Caspase 3/7 reagent is used to measure the percentage of apoptotic characteristics and results in 5.3 % in

mFreSR+ RI and 1.2 % in mFreSR +2FA+ RI for confluency.

To assess the degree of apoptosis post-thaw of HAF-iPSCs, we performed a live Cell Event Caspase 3/7 assay to quantify apoptotic cell death post-thaw. The Caspase-3/7 reagent is intrinsically non-fluorescent as the DEVD peptide inhibits the ability of the dye to bind to DNA [156–158]. However, after activation of Caspase 3/7 in apoptotic cells, the DEVD peptide is cleaved to enable the dye to bind to DNA and produce a bright red fluorogenic response. The fluorescent emission of the dye can be quantified and normalized to phase confluence (red area/phase area). This is evident in Figure 3.10, where the red fluorescence represents dead cells within the underlying adherent colonies in culture. Based on confluency, more apoptotic cells were observed in the mFreSR (Figure 3.9 A) condition compared to 2FA (Figure 3.9 B). Percentage of Caspase 3/7 positive cells, assessed by the ratio of red fluorescence over confluency, reported a confluency data of 5.3 % of the iPSC frozen with mFreSR compared to only 1.2 % in 2FA HAF-iPSCs. The confluency data was acquired by calculating for the difference between the red area to the phase area. Although some apoptosis is also occurring in the 2FA frozen HAF-iPSCs, the quantity and size of the HAF-iPSCs colonies are larger, contributing to the increased cell recovery and proliferation observed in Figure 3.10. Overall, the use of Caspase 3/7 assay confirms that 2FA reduces the apoptotic events in iPSCs, and therefore, 2FA has an additive effect with ROCK inhibitor. The future directions of this project can evaluate the mechanism of apoptotic inhibition. Additionally, 2FA's mechanism of action will require further investigation, but it appears that it may affect decreased secondary cell death and better quality of recovered cells post-thaw.

3.5 Confirmation of pluripotency of HAF-iPSCs post-thaw.

To ensure that IRI in cryomedia does not negatively affect iPSC pluripotency, we assessed TRA-1-81 expression of the iPSC post-thaw. TRA-1-81 is an antibody that recognizes the expression of proteins in an undifferentiated cell. The TRA-1-81 antibody reacts with a carbohydrate epitope on TRA-1-81 glycoprotein that is expressed on iPSCs. If the iPSCs are differentiated, then the TRA-1-81 antibody is unable to detect the epitope on the cells since the TRA-1-81 epitope is only present in distinguished cell lines such as human embryonical carcinoma (EC), embryonic germ (EG), ESCs, iPSCs, and rhesus monkey and rat ES cell lines. Therefore, using TRA-1-81 can be an excellent measure to detect undifferentiated characteristics of stem cells. The detection is performed by using flow cytometry to detect the signal of TRA-1-81 labeled Fluorescein isothiocyanate (FITC).

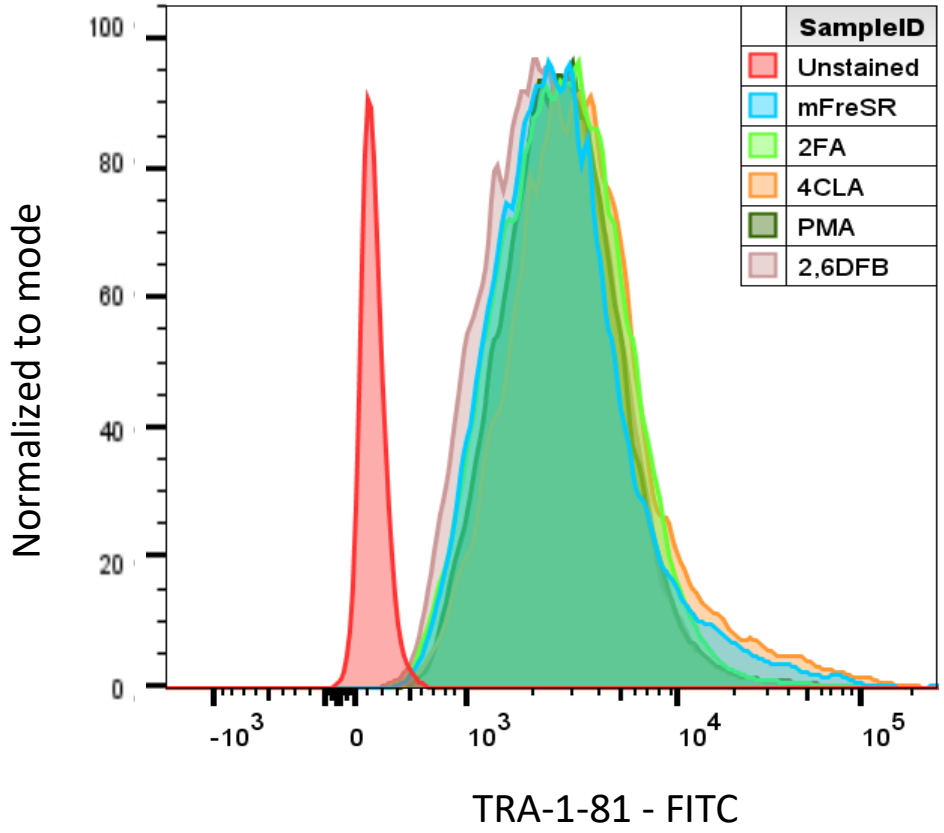

Figure 3.11. Assessment of pluripotency marker TRA 1-81 expression post-thaw Flow cytometry histogram comparing TRA-1-81 expression for all iPSCs post-thaw in the presence of IRI compounds and mFeSR control (blue; mFreSR, light green, 10 mM 2FA, orange; 0.5 mM 4ClA, dark green; 15 mM PMA, pink; 10 mM 2,6-DFB). Unstained cells (controls) are shown in red.

This flow cytometry generates a histogram consisting of unstained and stained samples (Figure 3.11). The unstained sample (red) represents cells that have no treatment of TRA-1-81 stain, controlling for any autofluorescence that is used for gating relative to fluorescently stained iPSCs. The samples (blue, light green, orange, dark green, and pink), indicated by the sample ID in Figure 3.11, show similar TRA-1-81 expression compared to mFreSR controls. The raw data of all flow cytometry figures are seen in figure S2-S5. TRA-1-81 expression is unaltered in all treatments suggesting that no adverse effects on pluripotency are observed. Since IRI compounds are a relatively new approach to enhancing cryopreservation, it is

important to perform quality control experiments to ensure pluripotency is maintained post-thaw and that no spontaneous differentiation can be detected. Although fidelity of TRA-1-81 expression was retained post two weeks cryopreservation, we also set out to determine if long term cryopreservation would affect iPSC confluency.

To ensure no adverse effects of 2FA are present following long-term cryopreservation, we assessed HAF-iPSC quality and pluripotency after six months of storage at -196 ºC. Post thaw, the HAF-iPSCs retain their characteristic cell morphology (Figure 3.12 A) and expression of pluripotency markers OCT4 and SOX2 (Figure 3.12 A) and TRA-1-81 (Figure 3.11 B) confirm retention of pluripotency markers following long term storage in 2FA supplemented cryomedia.

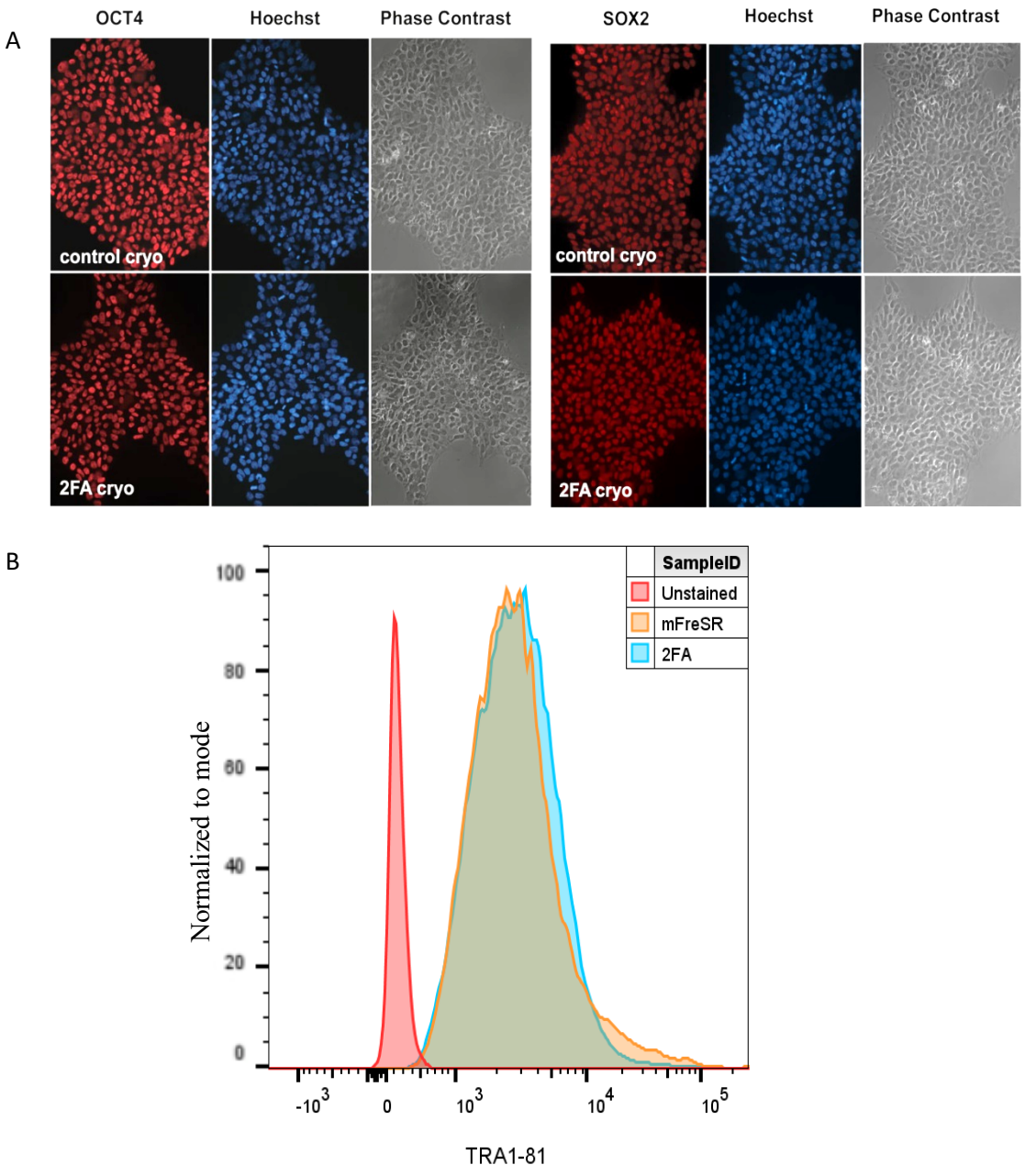

Figure 3.12. Confirmation of pluripotency post-long-term cryopreservation. A) Immunocytochemistry confirming expression of pluripotency markers (Red: SOX2, OCT4) in 2FA (2FA cryo) and mFreSr cryopreservation media (mFreSr cryo). The blue stains for Hoechst (a DNA nuclei marker). B) Confirmation of TRA 1-81 expression by flow cytometry (Red: unstained control, orange: mFreSR and blue: 2FA).

The immediate post-thaw viability of the iPSCs resulted in 84 % for 10 mM 2FA and 64% for mFReSR control (Figure 3.13). Figure 3.12 A, red immunofluorescence confirms the expression of pluripotency related transcription factors OCT4 and SOX2, respectively, left and right. The phase-contrast represents the image of the unstained or non-fluorescent state of the cells captured 24 hours after plating. Both the conditions of mFreSR (control cryo) and 2FA (2FA cryo) retain OCT4 and SOX2 pluripotency markers. This concludes that the long-term preservation of HAF-iPSCs with 2FA does not alter the pluripotency markers.

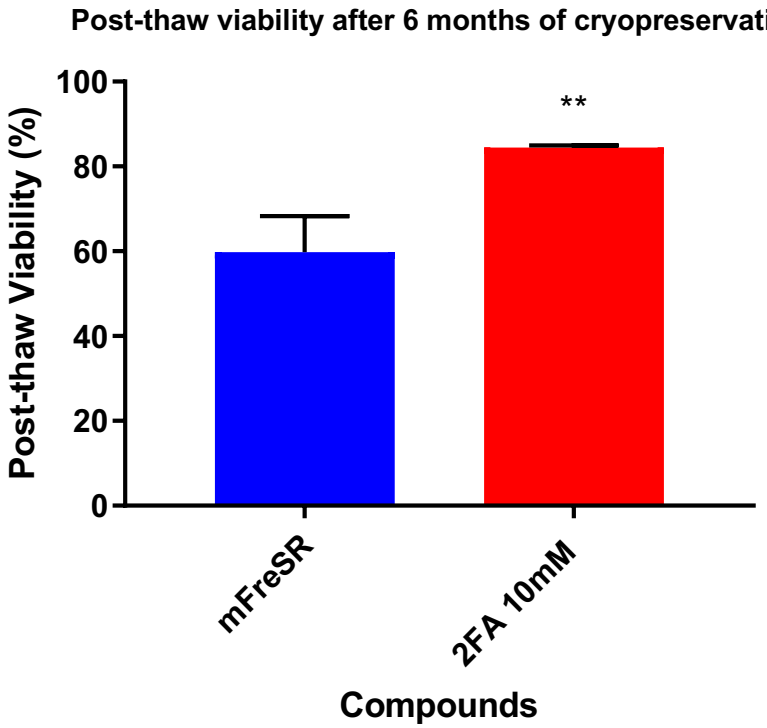

Figure 3.13. Post-thaw viability measurement for HAF-iPSCs with 10 mM 2FA and mFreSR. Immediate post-thaw viability for long-term cryopreservation of HAF-iPSCs with 2FA 10 mM (red) and control, mFreSR (Blue), where the samples are shown as an average of triplicates. Viability was assessed by Trypan blue exclusion assay immediately post-thaw. Percent viability is expressed as the mean and standard error of the mean (SEM). Statistical significance marked by asterisks assessed by student t-test, where ns=P>0.05, *= P≤0.05, **= P≤0.01, and ***= P≤0.001 (n=3).

3.6. Teratoma formation of cryopreserved HAF-iPSCs

To confirm that 2FA treatment did not alter the ability of the HAF-iPSC to differentiate into all three germ layers, we performed a teratoma assay to assess tri-lineage differentiation potential. The teratoma formation *in vivo* is an established pluripotent assay because of its reliable and comprehensive confirmation to validate the quality and pluripotency of iPSCs. Teratomas are characterized as benign tumors that grow rapidly to form a mixture of tissues and semi-semblances such as organs, teeth, hair, muscle, cartilage, and bone [159]. These are considered the critical characteristics of robust pluripotent cell lines. Therefore, the formation of teratomas is used widely in stem cell-based research as a "gold standard" for its assessment of pluripotency. For our study, we tested the formation of malignant teratomas using the "gold standard" assay. The comparative analysis for the size of teratomas between the control and the IRI will justify the functionality of the iPSCs.

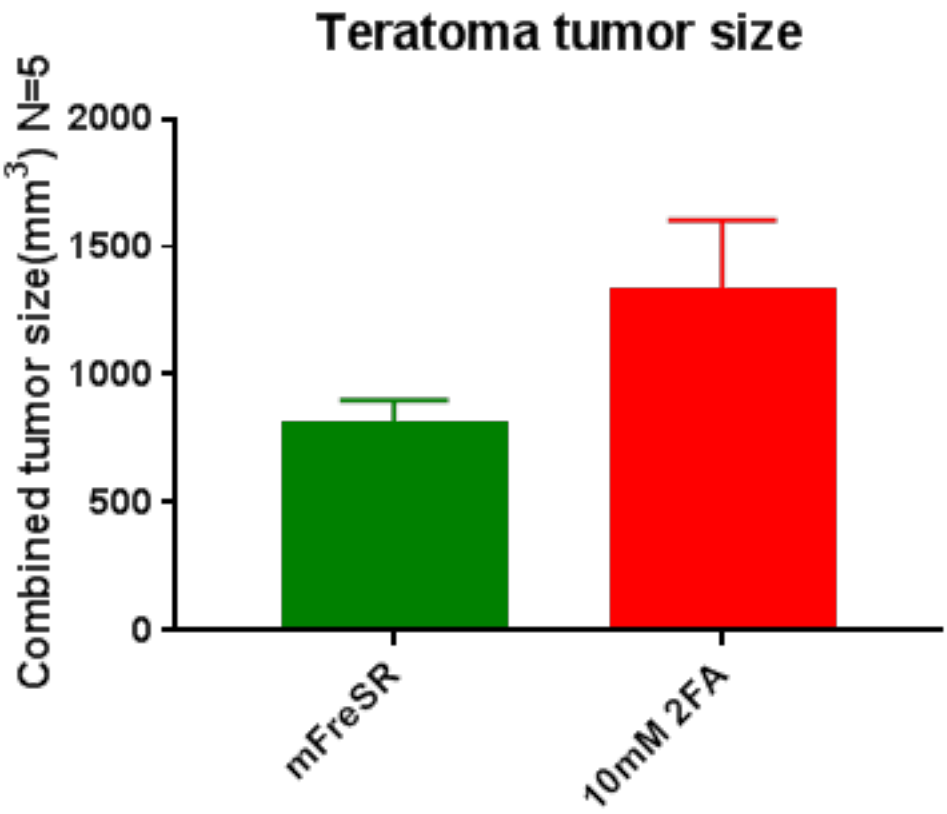

Figure 3.14. Size of the teratoma tumors for mFreSR and 10 mM 2FA. The size of the tumor is measured in mm^3 for the mean of five replicates of each condition, a statistical analysis of $p > 0.05$ was performed using student t-test for unpaired sets with a two-tailed gaussian distribution. Combined tumor size (mm^3) is expressed as the mean and standard error of the mean (SEM). Statistical significance marked by asterisks assessed by one-way analysis of variance (ANOVA) for comparison to control (mFreSR), where ns=P>0.05.

The *in vivo* teratoma assay was performed by injecting 2FA and mFreSR frozen HAF-iPSCs into the anterior tibialis muscle of an immunocompromised SCID mouse. Following eight weeks post-injection, the 2FA and mFreSR cryopreserved HAF-iPSCs gave rise to teratomas. The size analysis of teratomas from mFreSR or 10 mM 2FA is illustrated in a bar graph in Figure 3.14. The teratoma for the mFreSR (control) is approximately 800 mm^3. The teratoma for 2FA condition is 1250 mm^3 with the statistical analysis of $p > 0.05$, where the p-values were calculated using the student t-test. Given the difference in teratoma size, it is observed that 2FA frozen iPSCs retain higher viability post-injection into the mice and hence give rise to larger tumors due to more proliferating cells. Immunohistochemistry staining confirmed all three germ layers present in teratomas: endoderm, mesoderm, and ectoderm (Figure 3.15). The histology slides may not display the different tissue lineages on a single section of the slide. Therefore, images from different sections of the same teratomas are illustrated. Representative tissues from all three embryonic germ layers can be visualized in the teratoma sections.

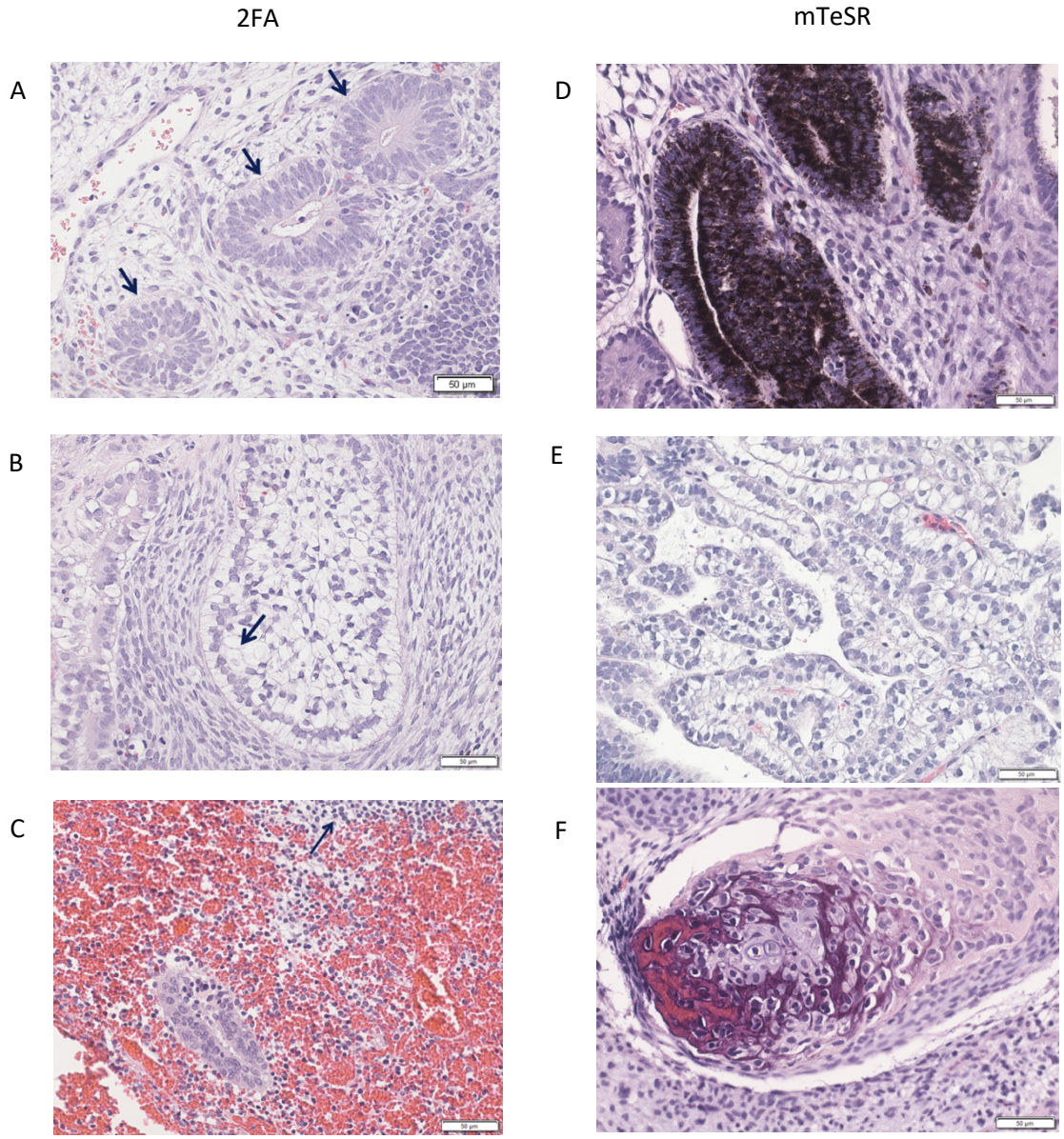

Figure 3.15. Histopathologic characterization of human iPSC derived teratomas xenografted into immunodeficient SCID mice. 2FA post-thaw and mFreSR post-thaw iPSCs generated teratomas that contained all three germ layers, ectoderm, endoderm, and mesoderm. A) Ectoderm was imaged at 50 µm, which included immature neural tissues with a black arrow pointing to the neuroepithelial rosettes. B) endoderm was imaged at 50 µm, displaying squamous epithelial cells, and the black arrow indicates the glycogen. C) Mesoderm was imaged at 50 µm, illustrating the extramedullary hematopoiesis, and the black arrow points to the bone marrow cell formation. D) Ectoderm was imaged at 50 µm, which contained

pigmented epithelial cells. E) The endoderm was imaged at 50 μm displaying epithelial cells. F) Mesoderm was imaged at 50 μm, showing bone formation with peripheral calcification.

More specifically, the endodermal layer can be visualized by the presence of pancreatic tissues, gastrointestinal cells, mucinous glandular epithelium, thyroid tissue, squamous epithelium, and respiratory epithelium [159]. The mesodermal layer can be visualized by the presence of lymphatic tissue, skeletal muscle, cartilage bone, smooth muscle, and adipose tissue [159]. Ectodermal tissue can be visualized by the presence of neuroectodermal tissue, epidermis, and sebaceous glands [159]. Figure 3.15 displays a panel of images, A-C, with 2FA post-thaw iPSCs, which generated teratomas that contained all three germ layers. The immature neural rosettes are often observed in the neural tissues and can be classified as part of the ectoderm, as seen in Figure 3.15A. Figure 3.15B depicts the endoderm layer, which illustrates the squamous epithelial cells, and the black arrow points to the glycogen storages inside the endoderm layer. The mesoderm layer shown in Figure 3.15C contains extramedullary hematopoiesis, where the black arrow indicates the location of the bone cells. Based on these germ layer images, it can be concluded that the 2FA treatment does not compromise iPSCs differentiation capabilities *in vivo*. The 2FA treated iPSCs can be compared to the control (no 2FA) to have similar germ layers depicted in Figure 3.15 D-F. Figure 3.15 D displays the ectoderm layer containing pigmented epithelial cells. Figure 3.15E shows the endoderm layer containing epithelial cells, and Figure 3.15 F displays the mesoderm layer with the presence of bone marrow formation with peripheral calcification. These results indicate that pluripotency is retained, and the differentiation capabilities of the HAF-iPSCs remained unaltered. In addition, when the size of the teratomas was compared graphically, there was no statistical significant difference in cell sizes between the two conditions (Figure 3.14).

The discovery of iPSCs has dramatically accelerated in the development of disease-specific and normal pathological mechanisms, which required a need for long-term storage of tissues, cells, and organs [160–168]. Current approaches have targeted the use of CPAs to manifest suboptimal cryopreservation techniques. Our goal of this study is to evaluate the application of IRI as an improved cryopreservation

strategy for iPSCs to facilitate in the development of master cell banks while maintaining quality control attributes of the cells over time. The development of master cell banks can aid as a first step in generating iPSCs derived specific tissue for clinical applications and disease modeling.

3.7. Conclusion and Future directions

As discussed throughout this thesis, the discovery of iPSCs has strengthened the research in stem cell-based therapies due to their unique capabilities to differentiate into numerous cell types for application towards regenerative medicine and tissue engineering. Traditionally, the derivation of specialized cells was performed using ESCs; however, given its ethical controversies, iPSCs have been used as a new alternative approach. As the demand for iPSCs is increasing, the development of the master iPSC cell bank is required. This remains a challenge due to the sensitive nature of iPSCs. Currently, the cryopreservation of stem cells has resulted in low post-thaw viability (40 -60%) using serum-free commercially available cryopreservation media [169]. The use of ice recrystallization inhibitors as supplementations in the serum-free cryopreservation represents an exciting new technology to enhance post-thaw viability and recovery of iPSCs. Given the dexterity of the applications of iPSCs, it is ideal for moving forward with GMP grade cryopreservation medium, such as Cryostore 10 (CS10), supplemented with IRIs.

Furthermore, given the success of IRIs, these compounds could be tested further for their efficacy in cryopreservation strategies towards iPSCs-derived cell products such as iBECs (iPSC derived brain endothelial cells), neurons, and immunotherapies such as iPSC-derived CAR-T. Despite the research focused on the improvement of cell preservation, cryopreservation is not equally assessed for all mammalian cell types. Mazur has stated that the problems of cryopreservation today comes from the misconception that application of biophysics is the only means to solve the challenges of cryobiology [170]. As the application of cryopreservation is applied to non-terminally differentiated mammalian cells, many of these cell types are refractory to the process of cryopreservation under traditional approaches. Even when the cells are successfully preserved, significant death of 30 – 70% is observed within 24-48 hours post-thaw [171]. Cryopreservation offers structural protection to the cells, but presents a critical issue of mitigation of preservation-induced stress response due to biomolecular based cell death after several hours of post-thaw [10]. Research in cryopreservation have provided effective strategies for the preservation of different cell types but, only until recently, they have determined the lack of molecular tools which are necessary to understand and mitigate the severe post-thaw damages. There are several stress factors which are associated

with the molecular based apoptotic cell death in cryopreservation. Some of these factors include hypothermia, energy deprivation, freezing, cell volume excursions, hyperosmolality, cytoskeletal disassembly or protease activations [10]. IRIs can potentially offer a solution mainly to preserve the functionality, viability, and recovery of the cells. Human iPSC based clinical approaches are yet to reach their true effective potential [172]. Future advancements in stem cell research could address implementing -omics methodology approaches, next-generation sequencing, cryopreservation techniques to optimize unique requirements of cell lines, biobanking, automated high throughput drug discovery, and the use of artificial intelligence [173] will significantly advance the use of iPSC-based cell therapies. In summary, IRIs are great candidates for their ability to improve cryopreservation of iPSCs for cell biobanking, quality of post-thaw recovered cells, and increasing the cryopreservation of therapeutic products. These advancements in cryopreservation techniques will implement towards clinical applications of iPSCs.

3.8 Experimental

Equipment

The following types of equipment were used for all experiments: Biosafety cabinet (BSC) Level 2; Cell Culture incubator, 37ºC – 5 % CO_2- 95 % humidity; Water Bath; Inverted Microscope; Nalgene™ Cryo Freezing container (achieves a 1ºC/min rate of cooling); Incubator with a rotary platform, slow speed (20 rpm); Centrifuge with swing bucket for conical tubes; Hemacytometer; Pipette Aid; Serological Pipettes (2,5,10, and 25mL); Pipettors, single-channel variable volume (10,100, and 1000µL); Sterile filter pipette tips (10, 100, and 1000µL); Repeater pipettor and combi-tips; Cell culture plates, 6 well (Falcon 353046), 12 well (Falcon 352070); Cell strainers, sterile 40µm mesh (Falcon 3523043); Stericup filter unit, 500 mL (Millipore SCGPU05RE); Microcentrifuge tubes, low retentive, 1.5 mL (Fisher 02-681-320) and Microcentrifuge tubes, low retentive, 2.0 mL (Fisher 02-681-321). Liquid nitrogen tank, IncuCyte live image system, Fluorescence Assisted Cell-sorting (FAC) tubes, BD Accur™ C6 Plus flow cytometer, and equipment used for teratoma (needles and syringes). Equipment used for immunocytochemistry (slides, coverslips, and fluorescence microscope).

Methods

Induced Pluripotent Stem cells - Cell culture

Amniotic fluid (AF) cells at 26 weeks of gestation were obtained for the Ottawa Hospital (Ottawa, Ontario, Canada) after routine amniocentesis. Informed consent was obtained with appropriate guidelines and regulations as approved by the Ottawa Hospital Research Ethics Boards, and the National Research Council approved all experimental protocols using AF cells of Canada by amending to their guidelines. The iPSCs were generated from amniotic fluid-derived cells and differentiated to induced pluripotent stem cells, as described in Ribecco and colleagues [151]. The iPSCs cell stock was frozen on June 19, 2016, and these stocks were expanded to P30 and frozen on January 29, 2019, to be used for all experiments. The cell stock was thawed and plated on 6 well cell culture plates pre-coated with Matrigel hESC qualified (Corning). The Matrigel coating was performed one hour before starting the experiment by the addition of Matrigel in DMEM/F12 with Glutamax (Life technologies). The iPSCs were cultured in medium mTeSR (mTeSR-Stem Cell Technologies) supplemented with 10µM Y27632 (ROCK Inhibitor, dissolved in DMSO as a 10

mM stock according to manufacturer's instructions, Stem Cell Technologies). After 24 hours, the medium was switched to mTesR (Stem Cell Technologies) and replaced daily. Once the iPSC colonies were developed, the cells were passaged at 80 % confluency at a 1:12 ratio, approximately every 5 days, using ReLeSR (Stemcell Technologies) onto Matrigel-coated plates. The pluripotency and the reprogramming efficiency of iPSCs colonies were confirmed with Alkaline phosphatase staining (AP, Invitrogen) and StainAlive Dylight 488 Mouse anti-human TRA-1-81 Antibody (Stemgent), according to the manufacturer's manual. All experiments were carried out between passage numbers 29-34.

Freezing iPSCs

The iPSCs were harvested using ReLeSR (Stem cell technologies) for 7 minutes, and cells were collected using mTeSR. An aliquot of $1x10^6$ cells was placed in 15mL Falcon tubes and centrifuged for 5 minutes at 300xg. The iPSC cell pellet of 1 $x10^6$ cell was resuspended in the cryopreservation medium of mFreSR (Stem Cell Technologies) or mFreSR supplemented with Ice recrystallization inhibitor (IRI) (see Table 2.0 for details). The cryovials were frozen at -80ºC for 24 hours using Mr.Frosty™ Freezing container (Thermo Scientific™) and transferred to -196ºC liquid nitrogen tank (Thermo Scientific™- Locator 8 Plus).

Name of Medium	Ingredients
Media A (mFreSR)	mFreSR (Stem Cell Technologies)
Media B (2FA)	mFreSR (Stem Cell Technologies) + 2FA compound
Media C (4ClA)	mFreSR (Stem Cell Technologies) + 4ClA compound
Media D (PMA)	mFreSR (Stem Cell Technologies) + PMA compound
Media E (2,6-DFB)	mFreSR (Stem Cell Technologies) + 2,6-DFB compound

Table 2.0. List of all cryopreservation mediums and formulations.

Thawing IRI supplemented cryopreserved iPSCs

After a minimum of one week of samples being cryopreserved at -196ºC, the samples were thawed to 37ºC in a water bath. The cryopreserved medium and supplemented IRI solution was removed from the cells by centrifuge techniques. The cell pellets were resuspended with mTeSR (Stem cell technologies). Half of the cell solution was added to 12 well cell culture plates pre-coated and supplemented with mTeSR and 10µM Y27632 (ROCK Inhibitor, dissolved in DMSO as a 10 mM stock according to manufacturer's instructions, Stem Cell Technologies). Another half of the cell solution was added to 12 well cell culture plated pre-coated and supplemented with mTeSR (no presence of Y27632 ROCK Inhibitor (RI)). After 24 hours, both culture conditions were switched to mTeSR plus (Stem Cell Technologies), and live-cell imaging was recorded for 48 hours using IncuCyte (Sartorius).

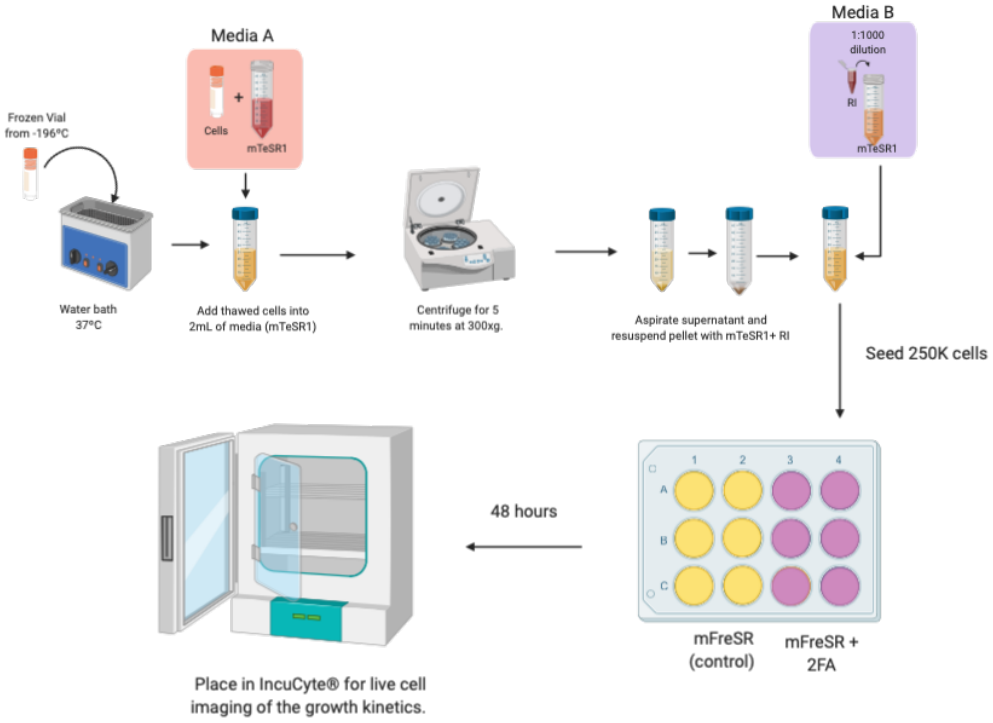

Figure 3.16. Schematic illustration of thawing iPSCs and plating the cells for growth rate analysis using IncuCyte®. The illustration was created using BioRender software.

Live Cell Staining using Anti- TRA-1-81-VIO® 488

The Anti-TRA-1-81-VIO® Live stain was diluted at 1:100 in mTeSR (stem cell technologies). The diluted antibody cell culture medium was added to the cells and incubated for 30 minutes at 37 ºC at 5 % CO_2. After removing the antibody, the cells were washed twice with mTeSR and replaced with mTeSR to examine the staining using a fluorescence microscope (data not shown).

Flow Cytometry

The thawed iPSCs were resuspended with mTeSR (Stemcell Technologies). The iPSCs of $3.0x10^5$ cells were added to Fluorescence Assisted Cell-sorting (FAC) tubes. A 10µL of propidium iodide (PI) was added to cells and incubated at room temperature for 10 minutes. Using the BD Accur™ C6 Plus on a 24 tube rack plate, the FAC tubes were selected for the auto collection of the cells. Run limit of 50,000 events with medium flow fluidics rate were set as the parameters, and the cells were gated on their population via forward/sideward scatter at P1 events. For each experiment, at least $3.0x10^5$ to $5.0x10^5$ cells were sorted. The PI stain was used to assess the viability of iPSCs post-thaw. The viability was collected within a time frame of 30 minutes upon thaw. For pluripotency, cells were blocked with 3% BSA in PBS for 30 min at room temperature and incubated with Human Anti-TRA-1-81-VIO® Live stain conjugated Antibody (Stem Cell Technologies) at a dilution of 1:100 in 100 µl of 1% BSA in PBS and 2 mM EDTA for 30 mins at room temperature. Cells were washed three times with 1% BSA in PBS and resuspended in 500 µl 1% BSA in PBS. The BD Accur™ C6 Pl was used to analyze samples, and the FAC tubes were selected for the auto collection of the cells. Run limit of 50,000 events with medium flow fluidics rate were set as the parameters, and the cells were gated on their population via forward/sideward scatter at P1 events. For each experiment, at least $3.0x10^5$ to $5.0x10^5$ cells were sorted.

Immunohistochemistry

Cells grown in 12-well plates with 15 mm round coverslips were coated with Matrigel in the growth medium. The cells were fixed using Genofix (DNA Genotex) with 4% PFA (Sigma). The cells were then permeable with 0.2% Triton X-100 (Sigma) in PBS (without Ca^{2+}/ Mg^{2+}) for 20 minutes, washed and blocked using DAKO protein block serum-free (Agilent) for 20 minutes at room temperature. After preparing the primary antibody of 1:100 dilution for OCT4 (SantaCruz, SC-5279, mouse monoclonal with the secondary antibody of rhodamine-conjugated rabbit anti-mouse IgG) and 1:5000 dilution for SOX2 (in house, rabbit polyclonal with rhodamine-conjugated goat antirabbit IgG). The coverslips were incubated for 1 hour at room temperature in a humidifying chamber. After three washes of PBS to coverslips for 5 minutes, these were incubated with secondary antibody (1:500) in antibody diluent at room temperature for 1 hour with no exposure to light. Coverslips were washed three times for 5 minutes with PBS and mounted with DAKO fluorescent mounting medium (Agilent) spiked with 5µg/mL of Hoechst 33258 (Sigma) to counterstain the nuclei. Images were captured using the Axiovert 200M microscope (ZEISS). Imaged cells using 20 X/ 0.4LD Archroplan Korr (DICII) objective. Protocol obtained from Ribecco et al., [151].

Statistical Analysis

All experiments were performed in three technical experiments with three replicates. Results are given as a mean $\pm$ standard deviation (SD) or standard error of the mean (SEM). The statistical tests are indicated in figure captions, and the level of significance was set at $p \leq 0.05$, indicated with an asterisk (*). The grading of significance is indicated as: $*p \leq 0.05$, $**p \leq 0.01$, $***p \leq 0.001$.

Teratoma assay

Preparing mice and workstation

The teratoma assay experiment was performed by Junzhuo Huang, Ewa Baumann, Risini Weeratna, Scott McComb, Shawn Makinen, Melissa Hewitt, and Jagdeep Sandhu from the NRC. The mice were prepared according to the protocol indicated in literature with the initiation of injecting insulin syringes and keeping the injected mice on ice. The mice are provided with an anesthetic using isoflurane vaporized in oxygen at 2 % to 3 % to induce anesthesia and reduce to 1 % - 2 % to maintain it once the mouse is

unconscious. Once anesthesia is confirmed, the next step was to shave the fur at the site of injection using hair removal cream for 1 min and wipe off the remaining hair.

Preparing the pluripotent stem cells for injection

An iPSC line was obtained from culture or frozen stock. If the cells were in culture, pluripotency expression markers were verified using immunohistochemistry. If the cells were derived from frozen stock, the cells were re-plated and passaged at least once before harvesting.

Preparation of the injection mixture

For injection into mice, iPSCs were pretreated with Y27632 ROCK Inhibitor for one hour. iPSCs were dissociated to single cells using Accutase (Stem Cell Technologies). Cell numbers were adjusted to $1x10^6$ iPSCs per injection. Harvested iPSCs were centrifuged at 300 g for 5 min and gently resuspended in hESC qualified Matrigel on ice.

Injection of iPSCs

The anesthetized mice were placed on the surgical station, and the nose of each mouse was connected to the anesthetic airflow. Then, 50µl cell suspension was injected into the anterior tibialis muscles, and the mice were kept under anesthesia for 10 to 15 minutes to make sure the cell mixture remains localized to the injection site.

Monitoring the mice post-injection

The mice were monitored for six to eight weeks post-injection to confirm that they were healthy and that the mass is growing at the injection sites. Precautions were taken to prevent the immunodeficient mice from getting sick by providing appropriate housing conditions with the addition of antibiotics to drinking water. Next, the mice were euthanized and the teratomas, when they are no larger than 1 cm^3, were explanted; this was also done earlier if any mouse showed visible signs of distress, pain, or illness.

Preparing the teratomas for histological analysis

The mouse was euthanized in accordance with the regulations of the institution. Muscle fascia and other connective tissues directly attached to the tumor of the skin were cut away. The teratoma was

transferred to the 50 mL tubes 10 times the tissue volume of 4 % PFA. The fixed teratoma was transferred to the following increasing concentrations of ethanol at room temperature: 70 % for 1 hour; 90 % for 1 hour; 95 % for 1 hour; and 100 % for 1 to 2 hours. Afterward, the teratomas were removed from the ethanol, and excess ethanol was removed by gently tapping the teratoma over a paper towel. The teratomas were transferred to xylene and kept at room temperature for 1 hour. This was repeated in fresh xylene for another hour. The teratomas were placed in labeled immunohistochemistry cassettes and heat paraffin to 60ºC to form a liquid and were then added to the cassettes containing the specimens. One hour was allocated for the samples to cool at room temperature to cut serial sections, 4 to 6 µm thick, using a microtome. The sections were mounted on to the microscope slides and heat to 60ºC for 1 hour to melt it onto the slides.

Staining and analyzing the sections

The teratomas sections were submitted to a facility for H&E staining. At the facility, the trained personnel would transfer the fixed teratomas into 50 mL falcon tube with 5 mL of 30 % sucrose solution. The cryomolds are then filled with cooled isopropanol on dry ice, and the sample takes approximately 5 minutes to freeze. The samples would then be cut into 10 to 50 µm thick serial section using a cryostat, and two sections per slide on three to four superfrost slides would be applied. Next, 80 µL of the primary antibody was added to dilute in blocking solution to each slide and incubated overnight at 4 ºC in the humidified staining box. The slides were washed in the solution three times for 10 minutes each, all at room temperature. The slides were then returned to the staining box and incubated with the secondary antibody diluted in the blocking solution for 1 hour at room temperature. Lastly, 100µL of mounting medium was added to the slide in a line on one side of the sample.

Preparing solutions

To prepare a wash solution, 0.1 % (v/v) Tween 20 was added to PBS and prepared fresh before use and was stored at room temperature. To prepare permeabilizing solution, 0.5 % (v/v) TritonC-100 was added to PBS and prepared fresh before use. To prepare a block solution, 0.1 % (v/v) Tween 20 was added to 5 % (v/v) animal serum and prepared fresh prior to use.

3.9 Supplemental Figures

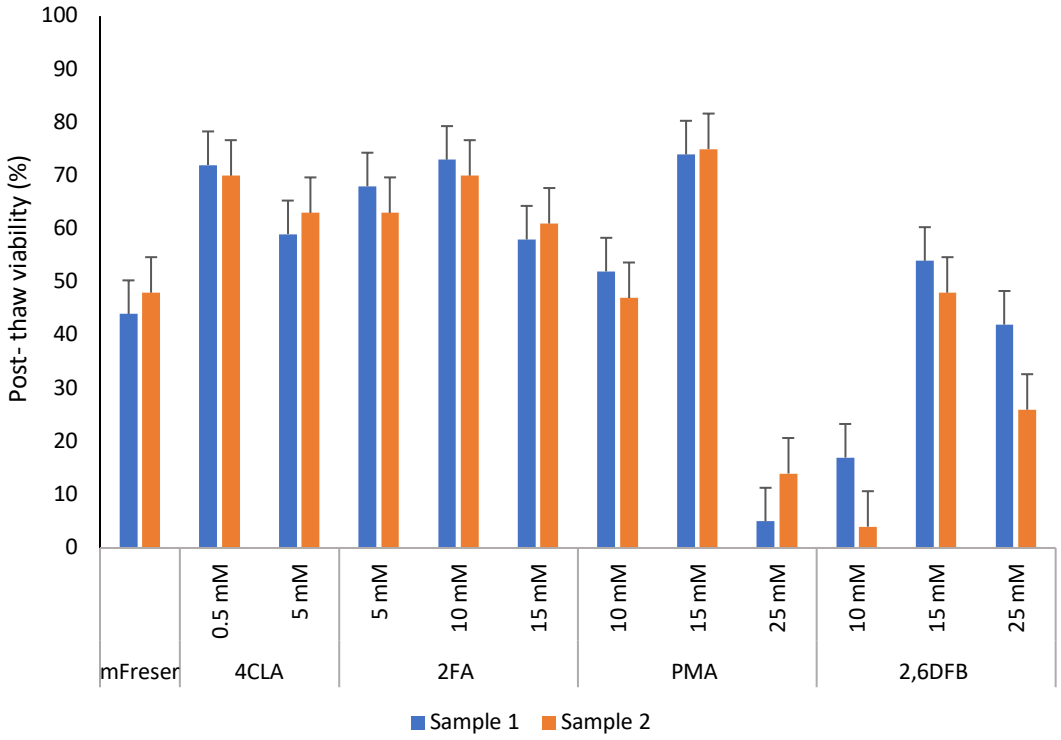

Figure S1. Assessment of post-thaw viability in HAF-iPSCs using IRIs supplemented in mFreSR. Post-thaw viability percentage of human iPSCs cryopreserved with 2FA, 4ClA, PMA, and 2,6-DFB supplemented in control, mFreSR. Cells were frozen at a rate of 1ºC/min to -80ºC before being transferred to -196ºC. Samples were thawed rapidly in a 37ºC water bath. Viability was assessed by Trypan blue exclusion assay immediately post-thaw in the presence of 10µm Rock Inhibitor (RI). Percent viability is expressed as the mean and standard error of the mean (SEM). Statistical significance marked by asterisks assessed by one-way analysis of variance (ANOVA) for comparison to control (mFreSR), where ns=P>0.05, *= P≤0.05, **= P≤0.01, and ***= P≤0.001 (n=2).

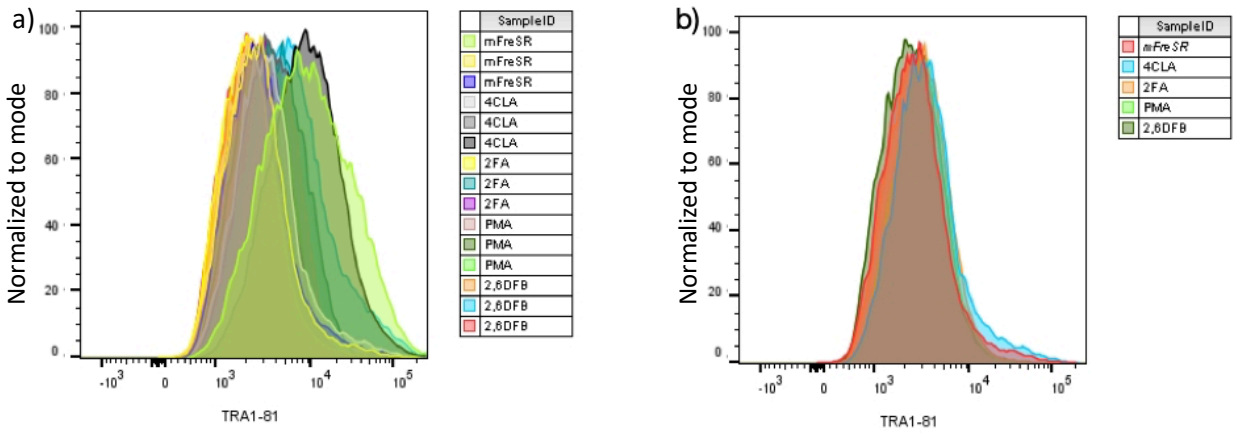

Figure S2. Results of FACs studies using TRA-1-81 after 48 hours of cell colony formation A) The histogram plot of all cell conditions after 48 hours of post-thaw. B) represents the overall response of all the conditions tested.

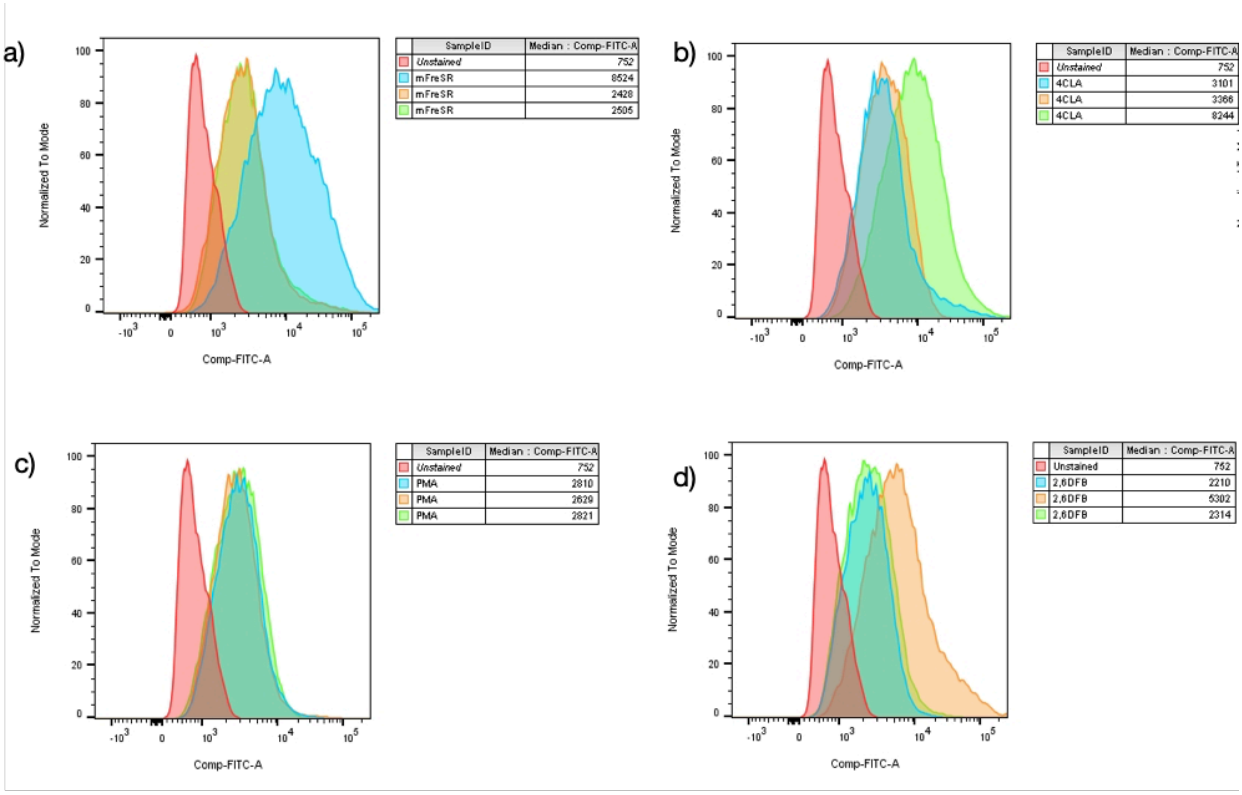

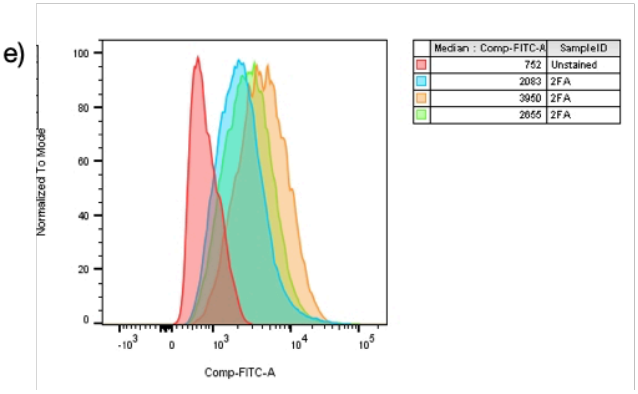

Figure S3. Results of FACs studies using TRA-1-81 after 48 hours of cell colony formation. Triplicate response of each condition compared to unstained (red). a. mFreser, b. 4ClA at 0.5 mM, c. PMA at 15 mM, d. 2,6DFB at 15mM, e. 2FA at 10 mM.

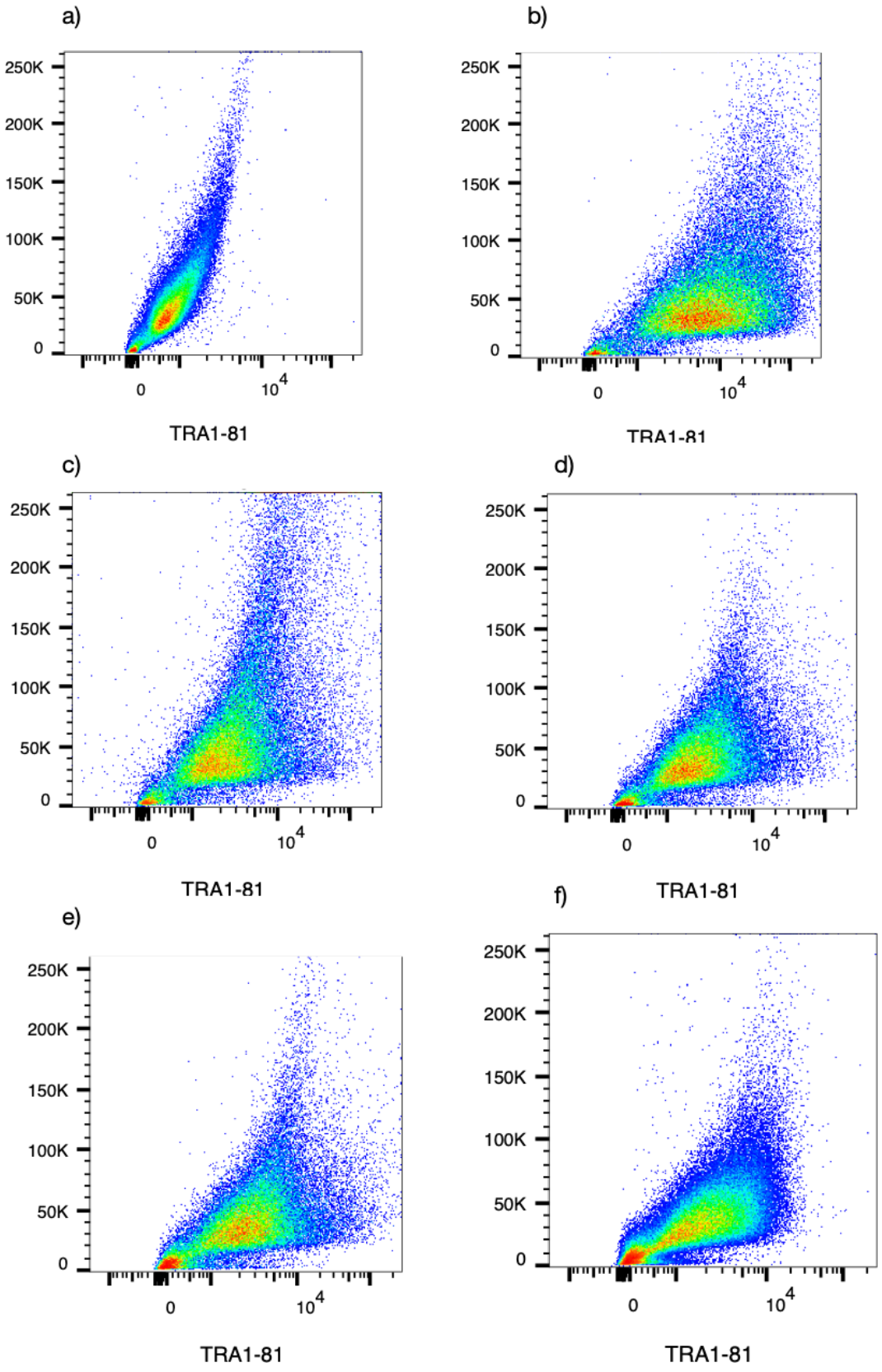
a)
b)
c)
d)
e)
f)
250K
200K
150K
100K
50K
0
0
10^4
TRA1-81

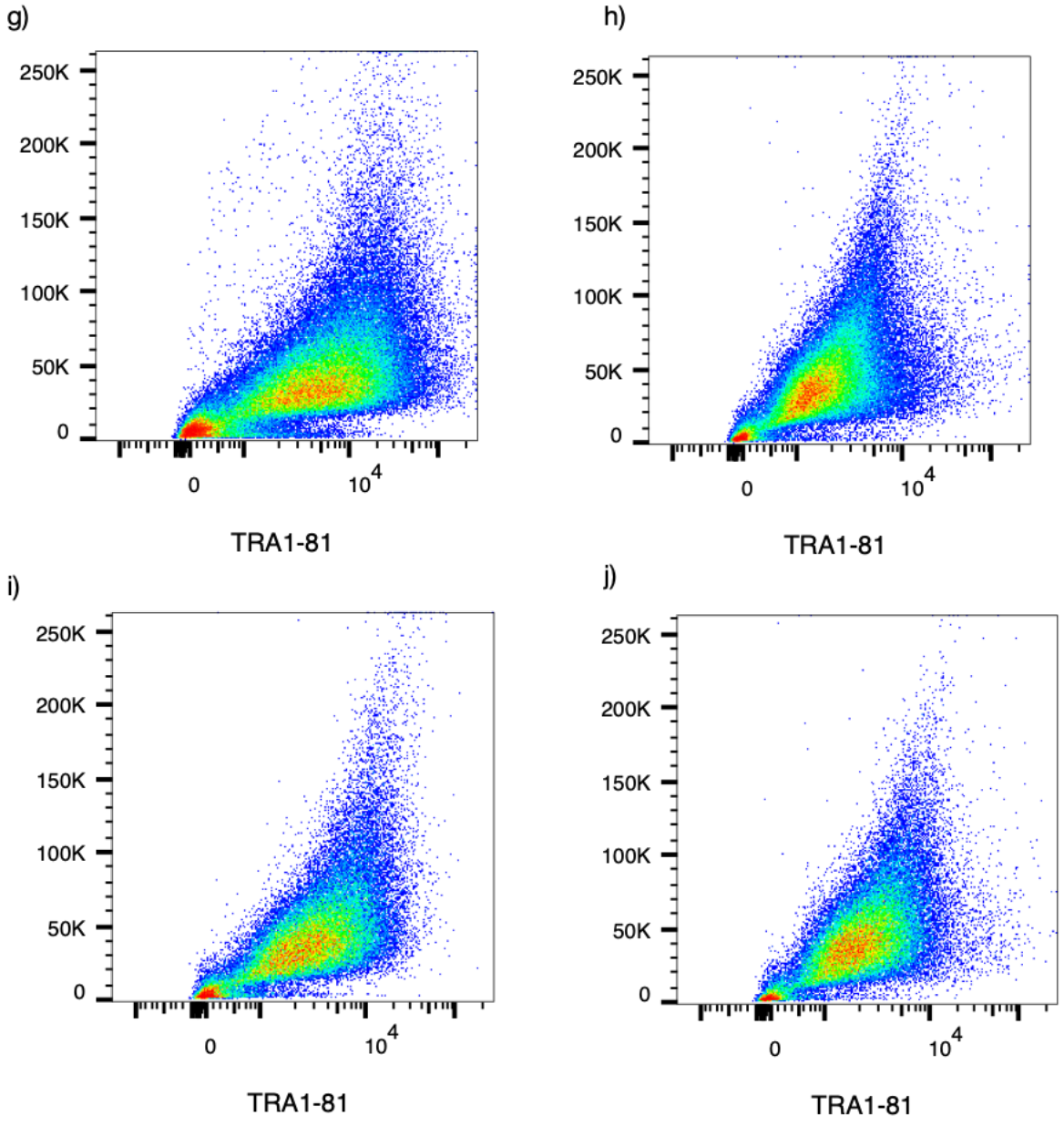
g)
250K
200K
150K
100K
50K
0
0
10^4
TRA1-81
h)
250K
200K
150K
100K
50K
0
0
10^4
TRA1-81
i)
250K
200K
150K
100K
50K
0
0
10^4
TRA1-81
j)
250K
200K
150K
100K
50K
0
0
10^4
TRA1-81

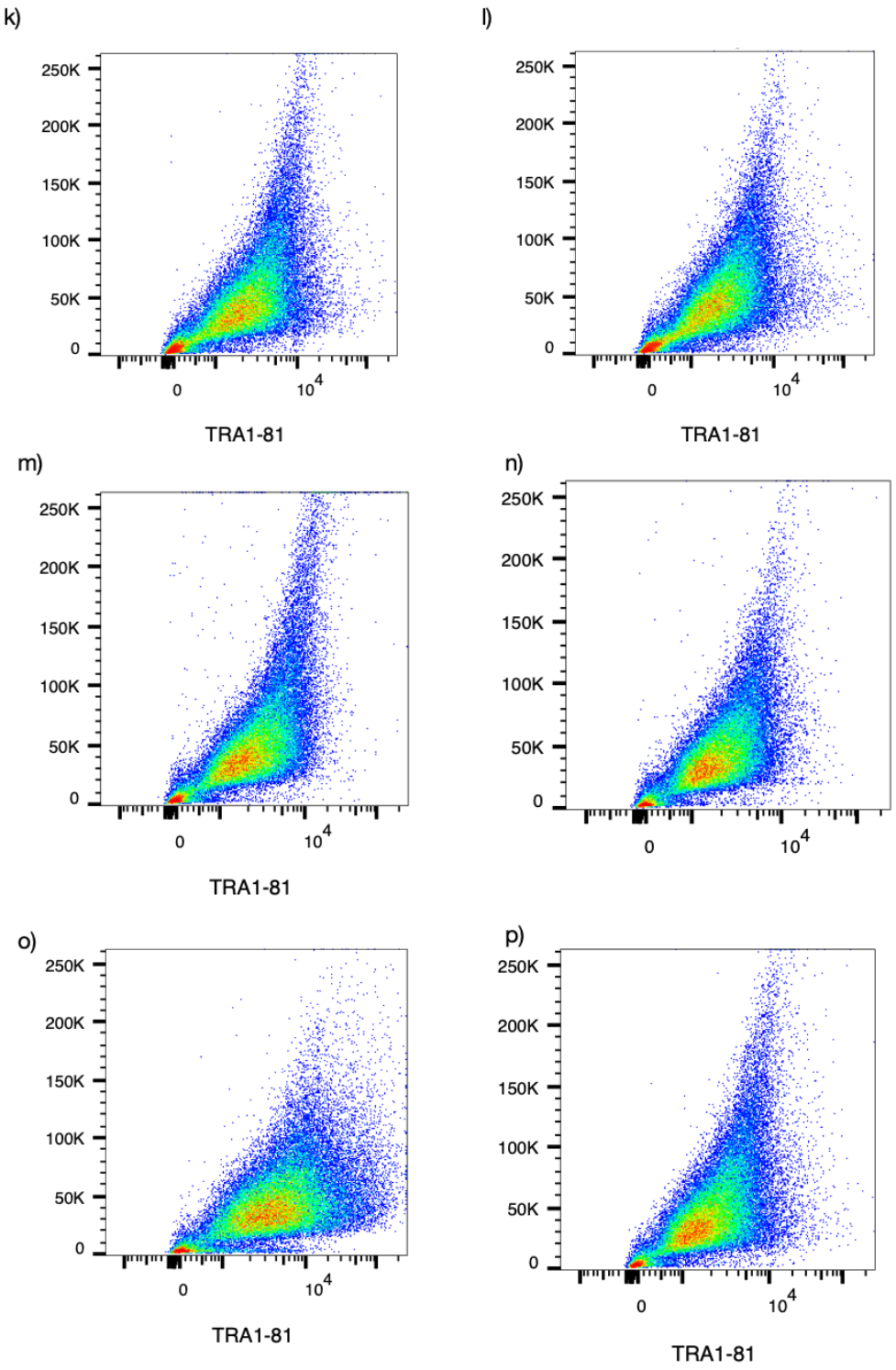

Figure S4. Graphical analysis of flow cytometry with TRA-1-81 stain to measure pluripotency and proliferation response of cells compared to the unstained control. A) unstained control, b—d) control-mFreSR, e—g) 4ClA 0.5 mM, h—j) 2FA 10mM, k—m) PMA 15mM, n—p) 2,6DFB 15mM.

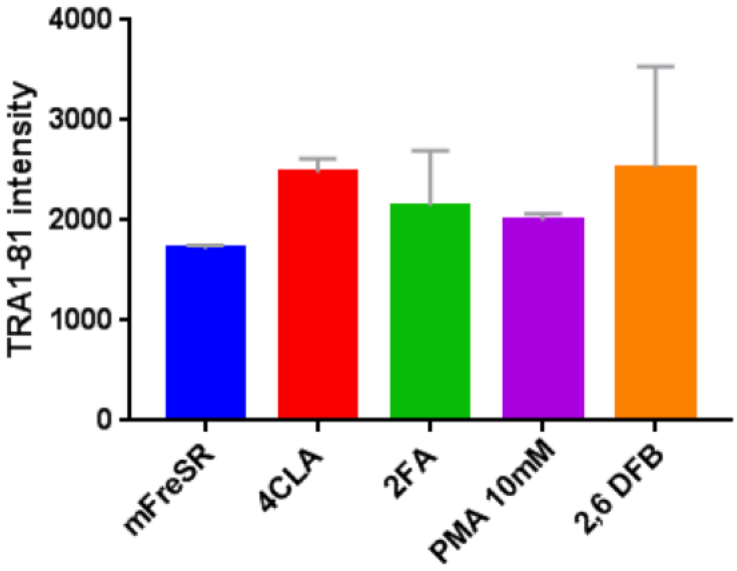

Figure S5. The graphical measure of response attained from flow cytometry data. No alteration in pluripotency was observed following the thaw of iPSC cryopreserved in the presence of each IRI. TRA-1-81 intensity was used as a surrogate measure of pluripotency.

References

1. LaMarca, E. A., Powell, S. K., Akbarian, S., & Brennand, K. J. (2018). Modeling Neuropsychiatric and Neurodegenerative Diseases With Induced Pluripotent Stem Cells. *Frontiers in pediatrics*, *6*, 82. doi:10.3389/fped.2018.00082
2. Hunt, C. J. (2011). Cryopreservation of Human Stem Cells for Clinical Application: A Review. *Transfusion Medicine and Hemotherapy*, *38*(2), 107–123. doi:10.1159/000326623
3. Starzl, T. E. (2000). History of clinical transplantation. *World journal of surgery*, *24*(7), 759–782. doi:10.1007/s002680010124
4. Deuse, T., Peter, C., Fedak, P. W. M., Doyle, T., Reichenspurner, H., Zimmermann, W. H., … Schrepfer, S. (2009). Hepatocyte growth factor or vascular endothelial growth factor gene transfer maximizes mesenchymal stem cell-based myocardial salvage after acute myocardial infarction. *Circulation*, *120*(SUPPL. 1), 247–254. doi:10.1161/CIRCULATIONAHA.108.843680
5. Kelly, M. L., Wang, M., Crisostomo, P. R., Abarbanell, A. M., Herrmann, J. L., Weil, B. R., & Meldrum, D. R. (2010). TNF receptor 2, not TNF receptor 1, enhances mesenchymal stem cell-mediated cardiac protection following acute ischemia. *Shock (Augusta, Ga.)*, *33*(6), 602–607. doi:10.1097/SHK.0b013e3181cc0913
6. Fujiwara, N., Shimizu, J., Takai, K., Arimitsu, N., Saito, A., Kono, T., … Suzuki, N. (2013). Restoration of spatial memory dysfunction of human APP transgenic mice by transplantation of neuronal precursors derived from human iPS cells. *Neuroscience Letters*, *557*, 129–134. doi:https://doi.org/10.1016/j.neulet.2013.10.043
7. Duncan, T., & Valenzuela, M. (2017). Alzheimer's disease, dementia, and stem cell therapy. *Stem Cell Research & Therapy*, *8*(1), 111. doi:10.1186/s13287-017-0567-5
8. Scott, K. L., Lecak, J., & Acker, J. P. (2005). Biopreservation of red blood cells: past, present, and future. *Transfusion medicine reviews*, *19*(2), 127–142.
9. Holovati, J. L., Gyongyossy-Issa, M. I. C., & Acker, J. P. (2009). Effects of trehalose-loaded liposomes on red blood cell response to freezing and post-thaw membrane quality. *Cryobiology*, *58*(1), 75–83. doi:10.1016/j.cryobiol.2008.11.002
10. Baust, J. G., Gao, D., & Baust, J. M. (2009). Cryopreservation: An emerging paradigm change. *Organogenesis*, *5*(3), 90–96. doi:10.4161/org.5.3.10021

11. Jackson, K. A., Majka, S. M., Wang, H., Pocius, J., Hartley, C. J., Majesky, M. W., … Goodell, M. A. (2001). Regeneration of ischemic cardiac muscle and vascular endothelium by adult stem cells. *The Journal of clinical investigation*, *107*(11), 1395–1402. doi:10.1172/JCI12150
12. Baust, J. G., Gage, A. A., Klossner, D., Clarke, D., Miller, R., Cohen, J., … Baust, J. M. (2007). Issues critical to the successful application of cryosurgical ablation of the prostate. *Technology in Cancer Research and Treatment*, *6*(2), 97–109. doi:10.1177/153303460700600206
13. Gao D, C. J. (2000). Mechanisms of cryoinjury in living cells.ILAR J 2000;41:187–96), *4*(4), 187–96.
14. Mazur, P., Leibo, S. P., & Chu, E. H. Y. (1972). A two-factor hypothesis of freezing injury. Evidence from Chinese hamster tissue-culture cells. *Experimental Cell Research*, *71*(2), 345–355. doi:10.1016/0014-4827(72)90303-5
15. Mazur, P. (1970). Cryobiology: the freezing of biological systems. *Science (New York, N.Y.)*, *168*(3934), 939–949. doi:10.1126/science.168.3934.939
16. Gao, D., & Critser, J. K. (2000). Mechanisms of Cryoinjury in Living Cells. *ILAR Journal*, *41*(4), 187–196. doi:10.1093/ilar.41.4.187
17. Mazur, P. (1977). The role of intracellular freezing in the death of cells cooled at supraoptimal rates. *Cryobiology*, *14*(3), 251–272. doi:10.1016/0011-2240(77)90175-4
18. Lovelock, J. E. (1953). The haemolysis of human red blood-cells by freezing and thawing. *Biochimica et biophysica acta*, *10*(3), 414–426. doi:10.1016/0006-3002(53)90273-x
19. Lovelock, J. E. (1953). The mechanism of the protective action of glycerol against haemolysis by freezing and thawing. *Biochimica et biophysica acta*, *11*(1), 28–36. doi:10.1016/0006-3002(53)90005-5
20. Meryman, H. T., Williams, R. J., & Douglas, M. S. J. (1977). Freezing injury from "solution effects" and its prevention by natural or artificial cryoprotection. *Cryobiology*, *14*(3), 287–302. doi:https://doi.org/10.1016/0011-2240(77)90177-8
21. Meryman, H. T. (1971). Osmotic stress as a mechanism of freezing injury. *Cryobiology*, *8*(5), 489–500. doi:10.1016/0011-2240(71)90040-x
22. Mazur, P. (1963). Kinetics of Water Loss from Cells at Subzero Temperatures and the Likelihood of Intracellular Freezing. *The Journal of General Physiology*, *47*(2), 347 LP –

369. doi:10.1085/jgp.47.2.347

23. Muldrew, K., & McGann, L. E. (1994). The osmotic rupture hypothesis of intracellular freezing injury. *Biophysical Journal*, *66*(2), 532–541. doi:10.1016/S0006-3495(94)80806-9
24. Acker, J. (2015). 23. Innocuous intracellular ice formation: Ice growth in complex systems. *Cryobiology*, *71*(1), 171. doi:https://doi.org/10.1016/j.cryobiol.2015.05.029
25. Acker, J. P., & McGann, L. E. (2002). Innocuous intracellular ice improves survival of frozen cells. *Cell transplantation*, *11*(6), 563–571.
26. Farrant, J., Walter, C. A., Lee, H., & McGann, L. E. (1977). Use of two-step cooling procedures to examine factors influencing cell survival following freezing and thawing. *Cryobiology*, *14*(3), 273–286. doi:10.1016/0011-2240(77)90176-6
27. Bischof, J. C., & Rubinsky, B. (1993). Large ice crystals in the nucleus of rapidly frozen liver cells. *Cryobiology*, *30*(6), 597–603. doi:10.1006/cryo.1993.1062
28. Hunt, C. J. (1984). Studies on cellular structure and ice location in frozen organs and tissues: The use of freeze-substitution and related techniques. *Cryobiology*, *21*(4), 385–402. doi:https://doi.org/10.1016/0011-2240(84)90077-4
29. Shimada, K., & Asahina, E. (1975). Visualization of intracellular ice crystals formed in very rapidly frozen cells at −27 °C. *Cryobiology*, *12*(3), 209–218. doi:https://doi.org/10.1016/0011-2240(75)90019-X
30. Day, J. G., & Stacey, G. (2007). Cryopreservation and freeze-drying protocols. Totowa, N.J.: Humana Press. Retrieved from http://site.ebrary.com/id/10197339
31. Mazur, P. (1984). Freezing of living cells: mechanisms and implications. *Am. J. Physiol. Cell. Physiol.*, *247*(3), C125-142. Retrieved from http://ajpcell.physiology.org/content/247/3/C125
32. Sakai, A., & Otsuka, K. (1967). Survival of plant tissue at super-low temperatures v. An electron microscope study of ice in cortical cells cooled rapidly. *Plant physiology*, *42*(12), 1680–1694. doi:10.1104/pp.42.12.1680
33. Karlsson, J. O., Cravalho, E. G., Borel Rinkes, I. H., Tompkins, R. G., Yarmush, M. L., & Toner, M. (1993). Nucleation and growth of ice crystals inside cultured hepatocytes during freezing in the presence of dimethyl sulfoxide. *Biophysical journal*, *65*(6), 2524–2536. doi:10.1016/S0006-3495(93)81319-5

34. Mazur, P. (1990). Equilibrium, quasi-equilibrium, and nonequilibrium freezing of mammalian embryos. *Cell biophysics*, *17*(1), 53–92. doi:10.1007/bf02989804
35. Mullen, S. F., & Critser, J. K. (2007). The Science of Cryobiology BT - Oncofertility Fertility Preservation for Cancer Survivors. In T. K. Woodruff & K. A. Snyder (Eds.), (pp. 83–109). Boston, MA: Springer US. doi:10.1007/978-0-387-72293-1_7
36. Lovelock, J. E., & Bishop, M. W. H. (1959). Prevention of Freezing Damage to Living Cells by Dimethyl Sulphoxide. *Nature*, *183*(4672), 1394–1395. doi:10.1038/1831394a0
37. Meryman, H. T. (2003). Freezing Injury and its Prevention in Living Cells. *Annual Review of Biophysics and Bioengineering*, *3*(1), 341–363. doi:10.1146/annurev.bb.03.060174.002013
38. Meryman, H. T. (1974). Freezing Injury and its Prevention in Living Cells. *Annual Review of Biophysics and Bioengineering*, *3*(1), 341–363. doi:10.1146/annurev.bb.03.060174.002013
39. Mazur, P., Leibo, S. P., Farrant, J., Chu, E. H. Y., Hanna, M. G., & Smith, L. H. (1970, January 1). Interactions of Cooling Rate, Warming Rate and Protective Additive on the Survival of Frozen Mammalian Cells. *Ciba Foundation Symposium - The Frozen Cell*. doi:10.1002/9780470719732.ch5
40. Capicciotti, C. J., Malay, D., & Ben, R. N. (2013). Ice Recrystallization Inhibitors: From Biological Antifreeze to Small Molecules. *Recent Developments in the Study of Recrystallization*, 177–224. doi:http://dx.doi.org/10.5772/54992
41. Fuller, B. J. (2004). Cryoprotectants: the essential antifreezes to protect life in the frozen state. *Cryo letters*, *25*(6), 375–388.
42. Ashwood-Smith, M. J. (1987). Mechanisms of cryoprotectant action. *Symposia of the Society for Experimental Biology*, *41*, 395–406.
43. Fahy, G. M. (1986). The relevance of cryoprotectant "toxicity" to cryobiology. *Cryobiology*, *23*(1), 1–13. doi:10.1016/0011-2240(86)90013-1
44. Karow, A. M. (1969). Cryoprotectants—a new class of drugs. *Journal of Pharmacy and Pharmacology*, *21*(4), 209–223. doi:10.1111/j.2042-7158.1969.tb08235.x
45. Acker, J. P. (2006). The Use of Intracellular Protectants in Cell Biopreservation. *Advances in biopreservation*, 299–320.
46. Diller, K. R. (1997). Pioneers in cryobiology: Nikolay aleksandorvich Maximov

(Maksimov)(1880-1952). *Cryo-letters*, *18*(2), 81–92.

47. Benson, E. E. (2004). Cryoconserving algal and plant diversity: historical perspectives and future challenges. In *Life in the frozen state* (pp. 325–354). CRC Press.
48. Barrett, J. (2001). Thermal hysteresis proteins. *The international journal of biochemistry & cell biology*, *33*(2), 105–117.
49. Knight, C. A., DeVries, A. L., & Oolman, L. D. (1984). Fish antifreeze protein and the freezing and recrystallization of ice. *Nature*, *308*(5956), 295–296. doi:10.1038/308295a0
50. Muldrew, K., & McGann, L. E. (1990). Mechanisms of intracellular ice formation. *Biophysical journal*, *57*(3), 525–532. doi:10.1016/S0006-3495(90)82568-6
51. Mazur, P. (1984). Freezing of living cells: mechanisms and implications. *American Journal of Physiology-Cell Physiology*, *247*(3), C125–C142. doi:10.1152/ajpcell.1984.247.3.C125
52. Meryman, H. T. (1971). Cryoprotective agents. *Cryobiology*, *8*(2), 173–183. doi:https://doi.org/10.1016/0011-2240(71)90024-1
53. Best, B. P. (2015). Cryoprotectant Toxicity: Facts, Issues, and Questions. *Rejuvenation research*, *18*(5), 422–436. doi:10.1089/rej.2014.1656
54. Baxter, S. J., & Lathe, G. H. (1971). Biochemical effects on kidney of exposure to high concentrations of dimethyl sulphoxide. *Biochemical pharmacology*, *20*(6), 1079–1091.
55. Jahan, S., K. Adam, M., Manesia, J., Charlton, T., Ben, R., & Pineault, N. (2018). The Ice Recrystalization Inhibitor 2FA Increases the Engraftment Activities of Cord Blood Stem and Progenitor Cells. *Experimental Hematology*, *64*, S74. doi:10.1016/j.exphem.2018.06.254
56. Briard, J. G., Poisson, J. S., Turner, T. R., Capicciotti, C. J., Acker, J. P., & Ben, R. N. (2016). Small molecule ice recrystallization inhibitors mitigate red blood cell lysis during freezing, transient warming and thawing. *Scientific Reports*, *6*, 23619. Retrieved from http://dx.doi.org/10.1038/srep23619
57. Hagiwara, T., Hartel, R., & Matsukawa, S. (2006). Relationship between Recrystallization Rate of Ice Crystals in Sugar Solutions and Water Mobility in Freeze-Concentrated Matrix. *Food Biophysics*, *1*, 74–82. doi:10.1007/s11483-006-9009-0
58. Knight, C. A., Wen, D., & Laursen, R. A. (1995). Nonequilibrium Antifreeze Peptides and the Recrystallization of Ice. *Cryobiology*, *32*(1), 23–34.

doi:https://doi.org/10.1006/cryo.1995.1002

59. Knight, C. A. (1966). Grain Boundary Migration and Other Processes in the Formation of Ice Sheets on Water. *Journal of Applied Physics*, *37*(2), 568–574. doi:10.1063/1.1708217
60. Alley, R. B., Perepezko, J. H., & Bentley, C. R. (1986). Grain growth in polar ice: I. Theory. *Journal of Glaciology*, *32*, 415–424. doi:10.1017/S0022143000012120
61. Capicciotti, C. J., Doshi, M., & Ben, R. N. (2013). Ice Recrystallization Inhibitors: From Biological Antifreezes to Small Molecules. In P. Wilson (Ed.), *Recent Developments in the Study of Recrystallization*. Rijeka: IntechOpen. doi:10.5772/54992
62. Budke, C., Heggemann, C., Koch, M., Sewald, N., & Koop, T. (2009). Ice Recrystallization Kinetics in the Presence of Synthetic Antifreeze Glycoprotein Analogues Using the Framework of LSW Theory. *The Journal of Physical Chemistry B*, *113*(9), 2865–2873. doi:10.1021/jp805726e
63. Balcerzak, A. K., Capicciotti, C. J., Briard, J. G., & Ben, R. N. (2014). Designing ice recrystallization inhibitors: from antifreeze (glyco)proteins to small molecules. *RSC Adv.*, *4*(80), 42682–42696. doi:10.1039/C4RA06893A
64. Sutton, R. L., Lips, A., Piccirolli, G., & Sztehlo, A. (1996). Kinetics of Ice Recrystallization in Aqueous Fructose Solutions. *Journal of Food Science*, *61*(4), 741–745. doi:10.1111/j.1365-2621.1996.tb12194.x
65. Balcerzak, A. K., Capicciotti, C. J., Briard, J. G., & Ben, R. N. (2014). Designing ice recrystallization inhibitors: From antifreeze (glyco)proteins to small molecules. *RSC Advances*, *4*(80), 42682–42696. doi:10.1039/c4ra06893a
66. Ampaw, A., A. Charlton, T., Briard, J., & Ben, R. (2018). Designing the next generation of cryoprotectants – From proteins to small molecules. *Peptide Science*, *111*. doi:10.1002/pep2.24086
67. Briard, J. G., Jahan, S., Chandran, P., Allan, D., Pineault, N., & Ben, R. N. (2016). Small-Molecule Ice Recrystallization Inhibitors Improve the Post-Thaw Function of Hematopoietic Stem and Progenitor Cells. *ACS Omega*, *1*(5), 1010–1018. doi:10.1021/acsomega.6b00178
68. S. Poisson, J., Turner, T., Acker, J., & Ben, R. (2018). Cryopreservation of red blood cells using ice recrystallization inhibitors as novel cryoprotectants. *Cryobiology*, *85*, 131–132. doi:10.1016/j.cryobiol.2018.10.058

69. S. Poisson, J., Acker, J., Briard, J., Meyer, J., & Ben, R. (2018). Modulating Intracellular Ice Growth with Cell Permeating Small Molecule Ice Recrystallization Inhibitors. *Langmuir*, *35*. doi:10.1021/acs.langmuir.8b02126

70. Knight, C. A., Hallett, J., & DeVries, A. L. (1988). Solute effects on ice recrystallization: An assessment technique. *Cryobiology*, *25*(1), 55–60. doi:10.1016/0011-2240(88)90020-X

71. Arévalo, M. J., Avalos, M., Babiano, R., Cabanillas, A., Cintas, P., Jiménez, J. L., & Palacios, J. C. (2000). Optically active sugar thioamides from δ-gluconolactone. *Tetrahedron: Asymmetry*, *11*(9), 1985–1995. doi:https://doi.org/10.1016/S0957-4166(00)00140-3

72. Baust, J. M., Van Buskirk, R., & Baust, J. G. (2000). Cell viability improves following inhibition of cryopreservation-induced apoptosis. *In Vitro Cellular & Developmental Biology-Animal*, *36*(4), 262–270.

73. Baust, J. M. (2002). Molecular mechanisms of cellular demise associated with cryopreservation failure. *Cell Preservation Technology*, *1*(1), 17–31.

74. Tomczak, M. M., Marshall, C. B., Gilbert, J. A., & Davies, P. L. (2003). A facile method for determining ice recrystallization inhibition by antifreeze proteins. *Biochemical and Biophysical Research Communications*, *311*(4), 1041–1046. doi:10.1016/j.bbrc.2003.10.106

75. Yu, S. O., Brown, A., Middleton, A. J., Tomczak, M. M., Walker, V. K., & Davies, P. L. (2010). Ice restructuring inhibition activities in antifreeze proteins with distinct differences in thermal hysteresis. *Cryobiology*, *61*(3), 327–334. doi:10.1016/j.cryobiol.2010.10.158

76. Yagci, Y. E., Antonietti, M., & Börner, H. G. (2006). Synthesis of poly(tartar amides) as bio-inspired antifreeze additives. *Macromolecular Rapid Communications*, *27*(19), 1660–1664. doi:10.1002/marc.200600451

77. Baruch, E., & Mastai, Y. (2007). Antifreeze properties of polyglycidol block copolymers. *Macromolecular Rapid Communications*, *28*(23), 2256–2261. doi:10.1002/marc.200700501

78. Mastai, Y., Rudloff, J., Cölfen, H., & Antonietti, M. (2002). Control over the structure of ice and water by block copolymer additives. *ChemPhysChem*, *3*(1), 119–123.

doi:10.1002/1439-7641(20020118)3:1<119::AID-CPHC119>3.0.CO;2-R

79. Wharton, D. A., Wilson, P. W., Mutch, J. S., Marshall, C. J., & Lim, M. (2007). Recrystallization inhibition assessed by splat cooling and optical recrystallometry. *Cryo letters*, *28*(1), 61–68.

80. Shah, S. H. H., Kar, R. K., Asmawi, A. A., Rahman, M. B. A., Murad, A. M. A., Mahadi, N. M., … Bhunia, A. (2012). Solution structures, dynamics, and ice growth inhibitory activity of peptide fragments derived from an antarctic yeast protein. *PloS one*, *7*(11), e49788. doi:10.1371/journal.pone.0049788

81. Eniade, A., Purushotham, M., Ben, R. N., Wang, J. B., & Horwath, K. (2003). A serendipitous discovery of antifreeze protein-specific activity in C-linked antifreeze glycoprotein analogs. *Cell Biochemistry and Biophysics*, *38*(2), 115–124. doi:10.1385/CBB:38:2:115

82. Capicciotti, C. J., Leclère, M., Perras, F. A., Bryce, D. L., Paulin, H., Harden, J., … Ben, R. N. (2012). Potent inhibition of ice recrystallization by low molecular weight carbohydrate-based surfactants and hydrogelators. *Chemical Science*, *3*(5), 1408–1416. doi:10.1039/C2SC00885H

83. Trant, J. F., Biggs, R. A., Capicciotti, C. J., & Ben, R. N. (2013). Developing highly active small molecule ice recrystallization inhibitors based upon C-linked antifreeze glycoprotein analogues. *RSC Advances*, *3*(48), 26005–26009. doi:10.1039/C3RA43835J

84. Czechura, P., Tam, R. Y., Dimitrijevic, E., Murphy, A. V, & Ben, R. N. (2008). The Importance of Hydration for Inhibiting Ice Recrystallization with C-Linked Antifreeze Glycoproteins. *Journal of the American Chemical Society*, *130*(10), 2928–2929. doi:10.1021/ja7103262

85. Knight, C. A., Hallett, J., & DeVries, A. L. (1988). Solute effects on ice recrystallization: An assessment technique. *Cryobiology*, *25*(1), 55–60. doi:https://doi.org/10.1016/0011-2240(88)90020-X

86. Gibson, M. I., Barker, C. A., Spain, S. G., Albertin, L., & Cameron, N. R. (2009). Inhibition of Ice Crystal Growth by Synthetic Glycopolymers: Implications for the Rational Design of Antifreeze Glycoprotein Mimics. *Biomacromolecules*, *10*(2), 328–333. doi:10.1021/bm801069x

87. Inada, T., & Lu, S. S. (2003). Inhibition of recrystallization of ice grains by adsorption of

poly(vinyl alcohol) onto ice surfaces. *Crystal Growth and Design*, *3*(5), 747–752. doi:10.1021/cg0340300

88. Abraham, S., Keillor, K., Capicciotti, C. J., Perley-Robertson, G. E., Keillor, J. W., & Ben, R. N. (2015). Quantitative Analysis of the Efficacy and Potency of Novel Small Molecule Ice Recrystallization Inhibitors. *Crystal Growth & Design*, *15*(10), 5034–5039. doi:10.1021/acs.cgd.5b00995
89. Budke, C., Dreyer, A., Jaeger, J., Gimpel, K., Berkemeier, T., Bonin, A. S., … Koop, T. (2014). Quantitative Efficacy Classification of Ice Recrystallization Inhibition Agents. *Crystal Growth & Design*, *14*(9), 4285–4294. doi:10.1021/cg5003308
90. Robinton, D. A., & Daley, G. Q. (2012). The promise of induced pluripotent stem cells in research and therapy. *Nature*, *481*(7381), 295–305. doi:10.1038/nature10761
91. Yu, J., & Thomson, J. A. (2014). Chapter 30 - Induced Pluripotent Stem Cells. In R. Lanza, R. Langer, & J. B. T.-P. of T. E. (Fourth E. Vacanti (Eds.), (pp. 581–594). Boston: Academic Press. doi:https://doi.org/10.1016/B978-0-12-398358-9.00030-6
92. Takahashi, K., & Yamanaka, S. (2006). Induction of Pluripotent Stem Cells from Mouse Embryonic and Adult Fibroblast Cultures by Defined Factors. *Cell*, *126*(4), 663–676. doi:10.1016/j.cell.2006.07.024
93. Liu, X., Huang, J., Chen, T., Wang, Y., Xin, S., Li, J., … Kang, J. (2008). Yamanaka factors critically regulate the developmental signaling network in mouse embryonic stem cells. *Cell research*, *18*(12), 1177–1189. doi:10.1038/cr.2008.309
94. Seymour, T., Twigger, A.-J., & Kakulas, F. (2015). Pluripotency Genes and Their Functions in the Normal and Aberrant Breast and Brain. *International journal of molecular sciences*, *16*(11), 27288–27301. doi:10.3390/ijms161126024
95. Csete, M. (2013). Chapter 84 - Regenerative Medicine. In B. H. Shaz, C. D. Hillyer, M. Roshal, & C. S. B. T.-T. M. and H. (Second E. Abrams (Eds.), (pp. 559–563). San Diego: Elsevier. doi:https://doi.org/10.1016/B978-0-12-397164-7.00084-7
96. Scudellari, M. (2016, June). How iPS cells changed the world. *Nature*. England. doi:10.1038/534310a
97. Ebert, A. D., Yu, J., Rose, F. F. J., Mattis, V. B., Lorson, C. L., Thomson, J. A., & Svendsen, C. N. (2009). Induced pluripotent stem cells from a spinal muscular atrophy patient. *Nature*, *457*(7227), 277–280. doi:10.1038/nature07677

98. Agarwal, S., Loh, Y.-H., McLoughlin, E. M., Huang, J., Park, I.-H., Miller, J. D., … Daley, G. Q. (2010). Telomere elongation in induced pluripotent stem cells from dyskeratosis congenita patients. *Nature*, *464*(7286), 292–296. doi:10.1038/nature08792

99. Lei, F., Haque, R., Weiler, L., Vrana, K. E., & Song, J. (2009). T lineage differentiation from induced pluripotent stem cells. *Cellular immunology*, *260*(1), 1–5. doi:10.1016/j.cellimm.2009.09.005

100. Wu, S. M., & Hochedlinger, K. (2011). Harnessing the potential of induced pluripotent stem cells for regenerative medicine. *Nature cell biology*, *13*(5), 497–505. doi:10.1038/ncb0511-497

101. Ebert, A. D., Liang, P., & Wu, J. C. (2012). Induced pluripotent stem cells as a disease modeling and drug screening platform. *Journal of cardiovascular pharmacology*, *60*(4), 408–416. doi:10.1097/FJC.0b013e318247f642

102. Chun, Y. S., Chaudhari, P., & Jang, Y.-Y. (2010). Applications of patient-specific induced pluripotent stem cells; focused on disease modeling, drug screening and therapeutic potentials for liver disease. *International journal of biological sciences*, *6*(7), 796–805. doi:10.7150/ijbs.6.796

103. Cowan, C. A., Atienza, J., Melton, D. A., & Eggan, K. (2005). Nuclear reprogramming of somatic cells after fusion with human embryonic stem cells. *Science (New York, N.Y.)*, *309*(5739), 1369–1373. doi:10.1126/science.1116447

104. Davis, L., & Maizels, N. (2014). Homology-directed repair of DNA nicks via pathways distinct from canonical double-strand break repair. *Proceedings of the National Academy of Sciences of the United States of America*, *111*(10), E924-32. doi:10.1073/pnas.1400236111

105. Wesselschmidt, R. L. (2011). The teratoma assay: an in vivo assessment of pluripotency. *Methods in molecular biology (Clifton, N.J.)*, *767*, 231–241. doi:10.1007/978-1-61779-201-4_17

106. Potdar, P., & Chaudhary, S. (2017). Current challenges in the therapeutic use of induced pluripotent stem cells (iPSCs) in cancer therapy. *Applied Cancer Research*, *37*(1), 5. doi:10.1186/s41241-017-0015-y

107. Choi, S. M., Liu, H., Chaudhari, P., Kim, Y., Cheng, L., Feng, J., … Jang, Y.-Y. (2011). Reprogramming of EBV-immortalized B-lymphocyte cell lines into induced pluripotent

stem cells. *Blood*, *118*(7), 1801–1805. doi:10.1182/blood-2011-03-340620

108. Maehr, R., Chen, S., Snitow, M., Ludwig, T., Yagasaki, L., Goland, R., … Melton, D. A. (2009). Generation of pluripotent stem cells from patients with type 1 diabetes. *Proceedings of the National Academy of Sciences of the United States of America*, *106*(37), 15768–15773. doi:10.1073/pnas.0906894106
109. Knorr, D. A., Ni, Z., Hermanson, D., Hexum, M. K., Bendzick, L., Cooper, L. J. N., … Kaufman, D. S. (2013). Clinical-scale derivation of natural killer cells from human pluripotent stem cells for cancer therapy. *Stem cells translational medicine*, *2*(4), 274–283. doi:10.5966/sctm.2012-0084
110. Fujii, S.-I., Shimizu, K., Okamoto, Y., Kunii, N., Nakayama, T., Motohashi, S., & Taniguchi, M. (2013). NKT cells as an ideal anti-tumor immunotherapeutic. *Frontiers in immunology*, *4*, 409. doi:10.3389/fimmu.2013.00409
111. Jiang, Z., Han, Y., & Cao, X. (2014). Induced pluripotent stem cell (iPSCs) and their application in immunotherapy. *Cellular & molecular immunology*, *11*(1), 17–24. doi:10.1038/cmi.2013.62
112. Sánchez-Rivera, F. J., & Jacks, T. (2015). Applications of the CRISPR-Cas9 system in cancer biology. *Nature reviews. Cancer*, *15*(7), 387–395. doi:10.1038/nrc3950
113. Wernig, M., Zhao, J.-P., Pruszak, J., Hedlund, E., Fu, D., Soldner, F., … Jaenisch, R. (2008). Neurons derived from reprogrammed fibroblasts functionally integrate into the fetal brain and improve symptoms of rats with Parkinson's disease. *Proceedings of the National Academy of Sciences of the United States of America*, *105*(15), 5856–5861. doi:10.1073/pnas.0801677105
114. Lim, W. F., Inoue-Yokoo, T., Tan, K. S., Lai, M. I., & Sugiyama, D. (2013). Hematopoietic cell differentiation from embryonic and induced pluripotent stem cells. *Stem cell research & therapy*, *4*(3), 71. doi:10.1186/scrt222
115. Kobayashi, T., Yamaguchi, T., Hamanaka, S., Kato-Itoh, M., Yamazaki, Y., Ibata, M., … Nakauchi, H. (2010). Generation of rat pancreas in mouse by interspecific blastocyst injection of pluripotent stem cells. *Cell*, *142*(5), 787–799. doi:10.1016/j.cell.2010.07.039
116. Kooreman, N. G., Kim, Y., de Almeida, P. E., Termglinchan, V., Diecke, S., Shao, N.-Y., … Wu, J. C. (2018). Autologous iPSC-Based Vaccines Elicit Anti-tumor Responses In Vivo. *Cell stem cell*, *22*(4), 501-513.e7. doi:10.1016/j.stem.2018.01.016

117. Liang, G., & Zhang, Y. (2013). Genetic and epigenetic variations in iPSCs: potential causes and implications for application. *Cell stem cell*, *13*(2), 149–159. doi:10.1016/j.stem.2013.07.001

118. Jang, T. H., Park, S. C., Yang, J. H., Kim, J. Y., Seok, J. H., Park, U. S., … Han, J. (2017). Cryopreservation and its clinical applications. *Integrative Medicine Research*, *6*(1), 12–18. doi:10.1016/j.imr.2016.12.001

119. Yuan, Y., Yang, Y., Tian, Y., Park, J., Dai, A., Roberts, R. M., … Han, X. (2016). Efficient long-term cryopreservation of pluripotent stem cells at −80 °C. *Scientific Reports*, *6*(1), 34476. doi:10.1038/srep34476

120. Gstraunthaler, G., Lindl, T., & van der Valk, J. (2013). A plea to reduce or replace fetal bovine serum in cell culture media. *Cytotechnology*, *65*(5), 791–793. doi:10.1007/s10616-013-9633-8

121. Heger, J. I., Froehlich, K., Pastuschek, J., Schmidt, A., Baer, C., Mrowka, R., … Schmidt, A. (2018). Human serum alters cell culture behavior and improves spheroid formation in comparison to fetal bovine serum. *Experimental Cell Research*, *365*(1), 57–65. doi:https://doi.org/10.1016/j.yexcr.2018.02.017

122. Jayme, D., Watanabe, T., & Shimada, T. (1997). Basal medium development for serum-free culture: a historical perspective. *Cytotechnology*, *23*(1–3), 95–101. doi:10.1023/A:1007967602484

123. Jayme, D. W., Epstein, D. A., & Conrad, D. R. (1988). Fetal bovine serum alternatives. *Nature*, *334*(6182), 547–548. doi:10.1038/334547a0

124. Wei, Z., Batagov, A. O., Carter, D. R. F., & Krichevsky, A. M. (2016). Fetal Bovine Serum RNA Interferes with the Cell Culture derived Extracellular RNA. *Scientific Reports*, *6*(1), 31175. doi:10.1038/srep31175

125. Oliver, J. (2013). Standardized solutions for hESC and hiPSC reseach. *Journal of Chemical Information and Modeling*, *53*(9), 1689–1699. doi:10.1017/CBO9781107415324.004

126. Baharvand, H., Totonchi, M., Taei, A., Seifinejad, A., Aghdami, N., & Salekdeh, G. H. (2010). Human-induced pluripotent stem cells: derivation, propagation, and freezing in serum- and feeder layer-free culture conditions. *Methods in molecular biology (Clifton, N.J.)*, *584*, 425–443. doi:10.1007/978-1-60761-369-5_23

127. Lam, R. S., Topfer, F. M., Wood, P. G., Busskamp, V., & Bamberg, E. (2017). Functional Maturation of Human Stem Cell-Derived Neurons in Long-Term Cultures. *PloS one*, *12*(1), e0169506. doi:10.1371/journal.pone.0169506

128. Hansen, S. K., Borland, H., Hasholt, L. F., Tumer, Z., Nielsen, J. E., Rasmussen, M. A., … Hyttel, P. (2016). Generation of spinocerebellar ataxia type 3 patient-derived induced pluripotent stem cell line SCA3.B11. *Stem cell research*, *16*(3), 589–592. doi:10.1016/j.scr.2016.02.042

129. Orellana, M. D., De Santis, G. C., Abraham, K. J., Fontes, A. M., Magalhaes, D. A. R., Oliveira, V. de C., … Covas, D. T. (2015). Efficient recovery of undifferentiated human embryonic stem cell cryopreserved with hydroxyethyl starch, dimethyl sulphoxide and serum replacement. *Cryobiology*, *71*(1), 151–160. doi:10.1016/j.cryobiol.2015.01.005

130. Sato, N., & Brivanlou, A. (2016). Microarray Approach to Identify the Signaling Network Responsible for Self-Renewal of Human Embryonic Stem Cells. *Methods in molecular biology (Clifton, N.J.)*, *1307*, 71–88. doi:10.1007/7651_2015_244

131. Watson, C. L., Mahe, M. M., Munera, J., Howell, J. C., Sundaram, N., Poling, H. M., … Helmrath, M. A. (2014). An in vivo model of human small intestine using pluripotent stem cells. *Nature medicine*, *20*(11), 1310–1314. doi:10.1038/nm.3737

132. Nekrasov, E. D., Vigont, V. A., Klyushnikov, S. A., Lebedeva, O. S., Vassina, E. M., Bogomazova, A. N., … Kiselev, S. L. (2016). Manifestation of Huntington's disease pathology in human induced pluripotent stem cell-derived neurons. *Molecular neurodegeneration*, *11*, 27. doi:10.1186/s13024-016-0092-5

133. M, U. R., K S S, S. D., & V, S. R. (2014). Induced Pleuripotent Stem Cells: a Pioneer in Therapy. *Journal of Evolution of Medical and Dental Sciences*, *3*(71), 15165–15178. doi:10.14260/jemds/2014/4038

134. Miki, T., Wong, W., Zhou, E., Gonzalez, A., Garcia, I., & Grubbs, B. H. (2016). Biological impact of xeno-free chemically defined cryopreservation medium on amniotic epithelial cells. *Stem cell research & therapy*, *7*, 8. doi:10.1186/s13287-015-0258-z

135. Pino, C. J., Yevzlin, A. S., Lee, K., Westover, A. J., Smith, P. L., Buffington, D. A., & Humes, H. D. (2013). Cell-based approaches for the treatment of systemic inflammation. *Nephrology, dialysis, transplantation : official publication of the European Dialysis and Transplant Association - European Renal Association*, *28*(2), 296–302.

doi:10.1093/ndt/gfs503

136. Zhu, W.-Z., Van Biber, B., & Laflamme, M. A. (2011). Methods for the derivation and use of cardiomyocytes from human pluripotent stem cells. *Methods in molecular biology (Clifton, N.J.)*, *767*, 419–431. doi:10.1007/978-1-61779-201-4_31
137. Xu, C., Police, S., Hassanipour, M., Li, Y., Chen, Y., Priest, C., … Gold, J. D. (2011). Efficient generation and cryopreservation of cardiomyocytes derived from human embryonic stem cells. *Regenerative medicine*, *6*(1), 53–66. doi:10.2217/rme.10.91
138. Ginis, I., Grinblat, B., & Shirvan, M. H. (2012). Evaluation of bone marrow-derived mesenchymal stem cells after cryopreservation and hypothermic storage in clinically safe medium. *Tissue engineering. Part C, Methods*, *18*(6), 453–463. doi:10.1089/ten.TEC.2011.0395
139. Thirumala, S., Goebel, W. S., & Woods, E. J. (2009). Clinical grade adult stem cell banking. *Organogenesis*, *5*(3), 143–154. doi:10.4161/org.5.3.9811
140. Sarugaser, R., Ennis, J., Stanford, W. L., & Davies, J. E. (2009). Isolation, propagation, and characterization of human umbilical cord perivascular cells (HUCPVCs). *Methods in molecular biology (Clifton, N.J.)*, *482*, 269–279. doi:10.1007/978-1-59745-060-7_17
141. Stylianou, J., Vowels, M., & Hadfield, K. (2006). Novel cryoprotectant significantly improves the post-thaw recovery and quality of HSC from CB. *Cytotherapy*, *8*(1), 57–61. doi:10.1080/14653240500501021
142. Sosef, M. N., Baust, J. M., Sugimachi, K., Fowler, A., Tompkins, R. G., & Toner, M. (2005). Cryopreservation of isolated primary rat hepatocytes: enhanced survival and long-term hepatospecific function. *Annals of surgery*, *241*(1), 125–133. doi:10.1097/01.sla.0000149303.48692.0f
143. Watanabe, K., Ueno, M., Kamiya, D., Nishiyama, A., Matsumura, M., Wataya, T., … Sasai, Y. (2007). A ROCK inhibitor permits survival of dissociated human embryonic stem cells. *Nature biotechnology*, *25*(6), 681–686. doi:10.1038/nbt1310
144. Muranyi, A., Derkach, D., Erdodi, F., Kiss, A., Ito, M., & Hartshorne, D. J. (2005). Phosphorylation of Thr695 and Thr850 on the myosin phosphatase target subunit: inhibitory effects and occurrence in A7r5 cells. *FEBS letters*, *579*(29), 6611–6615. doi:10.1016/j.febslet.2005.10.055
145. Wang, Y., Zheng, X. R., Riddick, N., Bryden, M., Baur, W., Zhang, X., & Surks, H. K.

(2009). ROCK isoform regulation of myosin phosphatase and contractility in vascular smooth muscle cells. *Circulation research*, *104*(4), 531–540. doi:10.1161/CIRCRESAHA.108.188524

146. Surks, H. K., Richards, C. T., & Mendelsohn, M. E. (2003). Myosin phosphatase-Rho interacting protein. A new member of the myosin phosphatase complex that directly binds RhoA. *The Journal of biological chemistry*, *278*(51), 51484–51493. doi:10.1074/jbc.M305622200
147. Riddick, N., Ohtani, K.-I., & Surks, H. K. (2008). Targeting by myosin phosphatase-RhoA interacting protein mediates RhoA/ROCK regulation of myosin phosphatase. *Journal of cellular biochemistry*, *103*(4), 1158–1170. doi:10.1002/jcb.21488
148. Claassen, D. A., Desler, M. M., & Rizzino, A. (2009). ROCK inhibition enhances the recovery and growth of cryopreserved human embryonic stem cells and human induced pluripotent stem cells. *Molecular reproduction and development*, *76*(8), 722–732. doi:10.1002/mrd.21021
149. Kubota, Y., Noguchi, H., Seita, M., Yuasa, T., Sasamoto, H., Nakaji, S., … Kobayashi, N. (2013). Maintenance of Viability and Function of Rat Islets With the Use of ROCK Inhibitor Y-27632. *Cell medicine*, *6*(1–2), 15–23. doi:10.3727/215517913X674199
150. Kaganman, I. (2007). Throwing a ROCK inhibitor at a problem. *Nature Methods*, *4*(7), 544. doi:10.1038/nmeth0707-544
151. Ribecco-Lutkiewicz, M., Sodja, C., Haukenfrers, J., Haqqani, A. S., Ly, D., Zachar, P., … Bani-Yaghoub, M. (2018). A novel human induced pluripotent stem cell blood-brain barrier model: Applicability to study antibody-triggered receptor-mediated transcytosis. *Scientific Reports*, *8*(1), 1873. doi:10.1038/s41598-018-19522-8
152. Yu, J., Hu, K., Smuga-Otto, K., Tian, S., Stewart, R., Slukvin, I. I., & Thomson, J. A. (2009). Human induced pluripotent stem cells free of vector and transgene sequences. *Science (New York, N.Y.)*, *324*(5928), 797–801. doi:10.1126/science.1172482
153. Briard, J. G., Poisson, J. S., Turner, T. R., Capicciotti, C. J., Acker, J. P., & Ben, R. N. (2016). Small molecule ice recrystallization inhibitors mitigate red blood cell lysis during freezing, transient warming and thawing. *Scientific Reports*, *6*(November 2015), 2–11. doi:10.1038/srep23619
154. Gao, L., Nath, S. C., Jiao, X., Zhou, R., Nishikawa, S., Krawetz, R., … Rancourt, D. E.

(2019). Post-Passage rock inhibition induces cytoskeletal aberrations and apoptosis in Human embryonic stem cells. *Stem Cell Research*, *41*, 101641. doi:https://doi.org/10.1016/j.scr.2019.101641

155. Volpato, V., & Webber, C. (2020). Addressing variability in iPSC-derived models of human disease: guidelines to promote reproducibility. *Disease models & mechanisms*, *13*(1), dmm042317. doi:10.1242/dmm.042317
156. Boatright, K. M., Renatus, M., Scott, F. L., Sperandio, S., Shin, H., Pedersen, I. M., … Salvesen, G. S. (2003). A Unified Model for Apical Caspase Activation. *Molecular Cell*, *11*(2), 529–541. doi:https://doi.org/10.1016/S1097-2765(03)00051-0
157. Muzio, M., Stockwell, B. R., Stennicke, H. R., Salvesen, G. S., & Dixit, V. M. (1998). An induced proximity model for caspase-8 activation. *The Journal of biological chemistry*, *273*(5), 2926–2930. doi:10.1074/jbc.273.5.2926
158. Chang, D. W., Xing, Z., Capacio, V. L., Peter, M. E., & Yang, X. (2003). Interdimer processing mechanism of procaspase-8 activation. *The EMBO journal*, *22*(16), 4132–4142. doi:10.1093/emboj/cdg414
159. Nelakanti, R. V, Kooreman, N. G., & Wu, J. C. (2015). Teratoma formation: a tool for monitoring pluripotency in stem cell research. *Current protocols in stem cell biology*, *32*, 4A.8.1-4A.8.17. doi:10.1002/9780470151808.sc04a08s32
160. Torrent, R., De Angelis Rigotti, F., Dell'Era, P., Memo, M., Raya, A., & Consiglio, A. (2015). Using iPS cells toward the understanding of Parkinson's disease. *Journal of clinical medicine*, *4*(4), 548–566.
161. Poon, A., Zhang, Y., Chandrasekaran, A., Phanthong, P., Schmid, B., Nielsen, T. T., & Freude, K. K. (2017). Modeling neurodegenerative diseases with patient-derived induced pluripotent cells: Possibilities and challenges. *New biotechnology*, *39*, 190–198.
162. Sampaziotis, F., Segeritz, C., & Vallier, L. (2015). Potential of human induced pluripotent stem cells in studies of liver disease. *Hepatology*, *62*(1), 303–311.
163. Rashid, S. T., Corbineau, S., Hannan, N., Marciniak, S. J., Miranda, E., Alexander, G., … Skepper, J. (2010). Modeling inherited metabolic disorders of the liver using human induced pluripotent stem cells. *The Journal of clinical investigation*, *120*(9), 3127–3136.
164. McKinney, C. E. (2017). Using induced pluripotent stem cells derived neurons to model brain diseases. *Neural regeneration research*, *12*(7), 1062.

165. Yang, J., Li, S., He, X.-B., Cheng, C., & Le, W. (2016). Induced pluripotent stem cells in Alzheimer's disease: applications for disease modeling and cell-replacement therapy. *Molecular neurodegeneration*, *11*(1), 39.
166. Muguruma, K. (2018). Self-organized cerebellar tissue from human pluripotent stem cells and disease modeling with patient-derived iPSCs. *The Cerebellum*, *17*(1), 37–41.
167. Giri, S., & Bader, A. (2015). A low-cost, high-quality new drug discovery process using patient-derived induced pluripotent stem cells. *Drug discovery today*, *20*(1), 37–49.
168. Sterneckert, J. L., Reinhardt, P., & Schöler, H. R. (2014). Investigating human disease using stem cell models. *Nature Reviews Genetics*, *15*(9), 625–639.
169. Hornberger, K., Yu, G., McKenna, D., & Hubel, A. (2019). Cryopreservation of Hematopoietic Stem Cells: Emerging Assays, Cryoprotectant Agents, and Technology to Improve Outcomes. *Transfusion Medicine and Hemotherapy*, *46*(3), 188–196. doi:10.1159/000496068
170. Mazur, P. (2004). Principles of cryobiology. *Life in the frozen state*, 3–65.
171. Baust, J. M., Vogel, M. J., Van Buskirk, R., & Baust, J. G. (2001). A molecular basis of cryopreservation failure and its modulation to improve cell survival. *Cell transplantation*, *10*(7), 561–571.
172. Doss, M. X., & Sachinidis, A. (2019). Current Challenges of iPSC-Based Disease Modeling and Therapeutic Implications. *Cells*, *8*(5), 403. doi:10.3390/cells8050403
173. Kusumoto, D., Lachmann, M., Kunihiro, T., Yuasa, S., Kishino, Y., Kimura, M., … Fukuda, K. (2018). Automated Deep Learning-Based System to Identify Endothelial Cells Derived from Induced Pluripotent Stem Cells. *Stem cell reports*, *10*(6), 1687–1695. doi:10.1016/j.stemcr.2018.04.007

Appendix

Copyrights License

Copyright Clearance Center Marketplace™

Elsevier Science & Technology Journals - License Terms and Conditions

This is a License Agreement between Karishma Chopra / University of Ottawa ("You") and Elsevier Science & Technology Journals ("Publisher") provided by Copyright Clearance Center ("CCC"). The license consists of your order details, the terms and conditions provided by Elsevier Science & Technology Journals, and the CCC terms and conditions.

All payments must be made in full to CCC.

Order Date	11-Jun-2020	**Type of Use**	Republish in a thesis/dissertation
Order license ID	1041161-1		
ISSN	0011-2240	**Publisher**	ACADEMIC PRESS
		Portion	Chart/graph/table/figure

LICENSED CONTENT

Publication Title	Cryobiology	**Publication Type**	Journal
Article Title	The role of intracellular freezing in the death of cells cooled at supraoptimal rates.	**Start Page**	251
		End Page	272
		Issue	3
Author/Editor	SOCIETY FOR CRYOBIOLOGY.	**Volume**	14
		URL	http://www.journals.elsevier.com/cryobiology/
Date	01/01/1964		
Language	English		
Country	United States of America		
Rightsholder	Elsevier Science & Technology Journals		

REQUEST DETAILS

Portion Type	Chart/graph/table/figure	**Distribution**	Canada
Number of charts / graphs / tables / figures requested	1	**Translation**	Original language of publication
		Copies for the disabled?	No
Format (select all that apply)	Print, Electronic	**Minor editing privileges?**	Yes
		Incidental promotional use?	No
Who will republish the content?	Academic institution		
		Currency	CAD
Duration of Use	Life of current edition		
Lifetime Unit Quantity	Up to 499		

Rights Requested	Main product, any product related to main product, and other compilations/derivative products

NEW WORK DETAILS

Title	Improved Cryopreservation of Induced Pluripotent Stem Cells Using N-aryl Glyosidic Small Molecule Ice Recrystallization Inhibitors	**Institution name**	University of Ottawa
		Expected presentation date	2020-07-31
Instructor name	Karishma Chopra		

ADDITIONAL DETAILS

Order reference number	N/A	**The requesting person / organization to appear on the license**	Karishma Chopra / University of Ottawa

REUSE CONTENT DETAILS

Title, description or numeric reference of the portion(s)	Figure 2- Schematic of physical events in cells during freezing	**Title of the article/chapter the portion is from**	The role of intracellular freezing in the death of cells cooled at supraoptimal rates.
Editor of portion(s)	Mazur, Peter	**Author of portion(s)**	Mazur, Peter
Volume of serial or monograph	14	**Issue, if republishing an article from a serial**	3
Page or page range of portion	251-272	**Publication date of portion**	1977-01-01

PUBLISHER TERMS AND CONDITIONS

Elsevier publishes Open Access articles in both its Open Access journals and via its Open Access articles option in subscription journals, for which an author selects a user license permitting certain types of reuse without permission. Before proceeding please check if the article is Open Access on http://www.sciencedirect.com and refer to the user license for the individual article. Any reuse not included in the user license terms will require permission. You must always fully and appropriately credit the author and source. If any part of the material to be used (for example, figures) has appeared in the Elsevier publication for which you are seeking permission, with credit or acknowledgement to another source it is the responsibility of the user to ensure their reuse complies with the terms and conditions determined by the rights holder. Please contact permissions@elsevier.com with any queries.

CCC Republication Terms and Conditions

1. Description of Service; Defined Terms. This Republication License enables the User to obtain licenses for

Copyright Clearance Center Marketplace™

Royal Society of Chemistry - License Terms and Conditions

This is a License Agreement between Karishma Chopra / University of Ottawa ("You") and Royal Society of Chemistry ("Publisher") provided by Copyright Clearance Center ("CCC"). The license consists of your order details, the terms and conditions provided by Royal Society of Chemistry, and the CCC terms and conditions.

All payments must be made in full to CCC.

Order Date	11-Jun-2020	**Type of Use**	Republish in a thesis/dissertation
Order license ID	1041161-2		
ISSN	2046-2069	**Publisher**	RSC Publishing
		Portion	Chart/graph/table/figure

LICENSED CONTENT

Publication Title	RSC advances	**Publication Type**	e-Journal
Article Title	Designing ice recrystallization inhibitors: from antifreeze (glyco)proteins to small molecules	**Start Page**	42682
		End Page	42696
		Issue	80
		Volume	4
Date	01/01/2011	**URL**	http://pubs.rsc.org/en/Journals/JournalIssues/RA
Language	English		
Country	United Kingdom of Great Britain and Northern Ireland		
Rightsholder	Royal Society of Chemistry		

REQUEST DETAILS

Portion Type	Chart/graph/table/figure	**Distribution**	Canada
Number of charts / graphs / tables / figures requested	2	**Translation**	Original language of publication
		Copies for the disabled?	No
Format (select all that apply)	Print, Electronic	**Minor editing privileges?**	No
Who will republish the content?	Academic institution	**Incidental promotional use?**	No
Duration of Use	Current edition and up to 5 years	**Currency**	CAD
Lifetime Unit Quantity	Up to 499		

Rights Requested	Main product, any product related to main product, and other compilations/derivative products

NEW WORK DETAILS

Title	Improved Cryopreservation of Induced Pluripotent Stem Cells Using N-aryl Glyosidic Small Molecule Ice Recrystallization Inhibitors	**Institution name**	University of Ottawa
		Expected presentation date	2020-07-31
Instructor name	Karishma Chopra		

ADDITIONAL DETAILS

Order reference number	N/A	**The requesting person / organization to appear on the license**	Karishma Chopra / University of Ottawa

REUSE CONTENT DETAILS

Title, description or numeric reference of the portion(s)	Fig. 6 Illustration of the proposed mechanism by which carbohydrates and C-AFGP analgoues inhibit ice recrystallization. A solute will reside at the QLL–bulk water interface between two adjacent ice crystals. and Figure	**Title of the article/chapter the portion is from**	Designing ice recrystallization inhibitors: from antifreeze (glyco)proteins to small molecules
		Author of portion(s)	Balcerzak, Anna K.; Capicciotti, Chantelle J.; Briard, Jennie G.; Ben, Robert N.
Editor of portion(s)	Balcerzak, Anna K.; Capicciotti, Chantelle J.; Briard, Jennie G.; Ben, Robert N.	**Issue, if republishing an article from a serial**	80
		Publication date of portion	2014-09-11
Volume of serial or monograph	4		
Page or page range of portion	42682-42696		

CCC Republication Terms and Conditions

1. Description of Service; Defined Terms. This Republication License enables the User to obtain licenses for republication of one or more copyrighted works as described in detail on the relevant Order Confirmation (the "Work(s)"). Copyright Clearance Center, Inc. ("CCC") grants licenses through the Service on behalf of the